Co-optimisation of the sizing and control of an urban microgrid

Fadi Agha Kassab

Par **Fadi AGHA KASSAB**

Co-optimisation of the sizing and control of an urban microgrid

Thèse présentée
pour l'obtention du grade
de Docteur de l'UTC

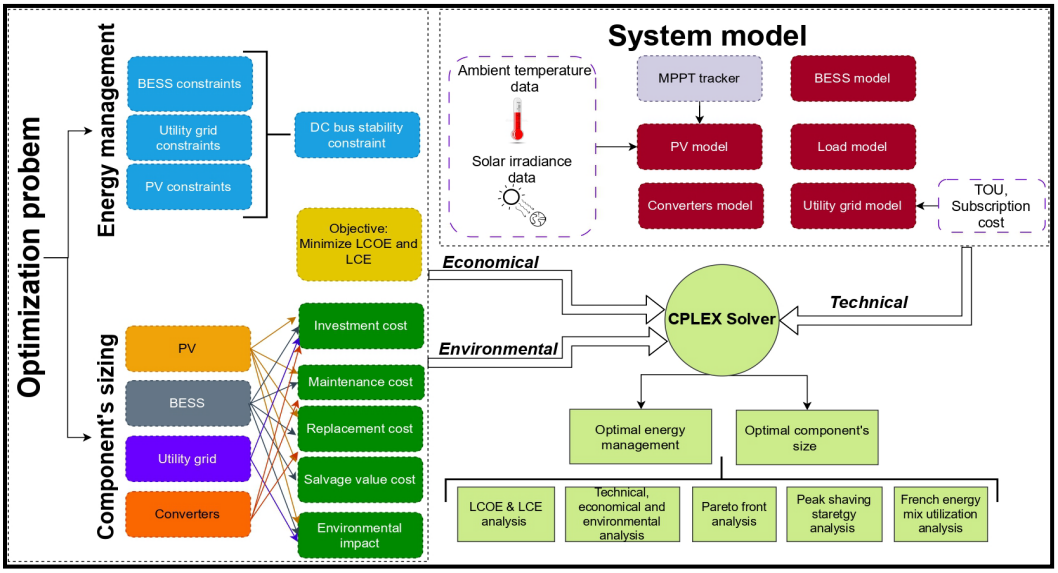

Soutenue le 4 octobre 2024
Spécialité : Génie Électrique : Laboratoire Avenues - GSU (EA-7284)

D2822

UNIVERSITÉ DE TECHNOLOGIE DE COMPIÈGNE

THESE

Pour obtenir le grade de

DOCTEUR

Spécialité : Génie Électrique

Par **Fadi AGHA KASSAB**

Co-optimisation of the sizing and control of an urban microgrid

Laboratoire Avenues, EA 7284

Soutenance le 04 Octobre 2024 devant le jury composé de :

Rapporteurs	Jean-Paul GAUBERT	LIAS, Université de Poitiers
	Robin ROCHE	FEMTO-ST, Université Bourgogne Franche-Comté
Examinateurs	Dimitri LEFEBVRE	GREAH, Université Le Havre Normandie
	Marc PETIT	GeePs, CentraleSupélec
	Christine PRELLE	Roberval, Université de Technologie de Compiègne
	Delphine RIU	G2ELab, Grenoble INP - Ense3
Invité	Timothy M. HANSEN	EECS, South Dakota State University
Directeur	Fabrice LOCMENT	Avenues, Université de Technologie de Compiègne
Co-directeur	Berk CELIK	Avenues, Université de Technologie de Compiègne

Université de Technologie de Compiègne – Avenues

Rue du docteur Schweitzer, 60200 Compiègne, France

Abstract

The modernization of the electricity grid (EG) through the implementation of microgrids offers significant potential for enhancing energy resilience, sustainability, and efficiency. However, this transition involves navigating a complex web of technical, economic, and environmental challenges. Microgrids require meticulous planning and optimization to balance energy generation, storage, and consumption while minimizing costs and carbon emissions. Achieving this balance calls for advanced optimization strategies, which are capable of addressing the intricacies of system components and operational dynamics.

The objective of this research is to enhance the decision-making capabilities of microgrid designers by providing a comprehensive approach for microgrid planning. The study offers an in-depth analysis of the project's lifetime from technical, economic, and environmental perspectives. Implemented in Python and solved using CPLEX, the optimization process aims to minimize both the levelized cost of energy (LCOE) and the levelized cost of emissions (LCE). The study utilizes real economic and environmental data considering load growth as well as actual solar irradiation, ambient temperature, and wind speed data. The load for the university building is based on data from the Université de Technologie de Compiègne, France with the electric vehicle (EV) load modeled using probabilistic modeling.

The study introduces a joint multi-objective optimization strategy using Mixed-Integer Linear Programming (MILP) to ensure globally optimal solutions, thereby that facilitates obtaining more informed and effective design choices. These choices involve evaluating various proposed solutions to balance cost and carbon emissions while addressing the complexities and technical constraints of the energy management (EM) problem. A novel aspect of this work is the integration of EM and component sizing into a unified optimization problem, aiming for an optimality gap of 0% with reduced computation time compared to existing literature. The proposed method evaluates the inherent trade-offs among various solutions by identifying the Pareto front and allowing for an optimal balance between economic and environmental objectives. The results indicate a significant reduction in LCOE and LCE in the GCMG compared to the IMG. The study reveals that Battery Energy Storage System (BESS) capacity increases as the LCE decreases, and the number of Photovoltaic (PV) systems is higher when the LCOE is lower for both operation modes. This occurs because the BESS has a slightly lower LCE compared to PV, and the LCOE of PV is also lower than that of BESS. Furthermore, as the limit of the EG increases, the Pareto fronts become lower and steeper.

Additionally, the same MILP algorithm is applied to optimize microgrids from a tertiary university campus across various cities. The study further integrates wind turbines (WT) and EV loads into the microgrid. The study provides a comparative analysis of three scenarios (PV/BESS, WT/BESS, and PV/WT/BESS) across different cities for evaluating the impacts of seasonal fluctuations on LCOE and LCE, and for assessing how microgrid component technologies influence LCOE and LCE outcomes. The results indicate that scenarios including PV/WT/BESS yield the lowest LCOE and LCE values, while the WT/BESS scenario results in the highest LCOE and LCE. It is also observed that the order of cities based on average solar irradiation or wind speed does not necessarily correspond to the order of LCOE and LCE. Monthly and daily fluctuations in solar irradiation and wind speed significantly impact these results. Regarding the technologies, locally produced PV panels contribute positively to the overall LCE of the microgrid, with PV panels incorporating phase changing material showing

higher LCE.

The research also compares two distinct algorithms. Algorithm 1 employs a cascaded MILP approach to optimize microgrid sizing and EM without EV flexibility over a year, then focuses on daily EV flexibility. Algorithm 2 integrates APSO with MILP to determine the sizes of microgrid components and perform daily EM with EV flexibility. It examines battery degradation and load shedding, excluding critical loads in a university building, while focusing on the flexibility of EV loads within the microgrid's EM system. Both algorithms address battery degradation through a kWh throughput model and aim to minimize the LCOE and LCE. Loads are segregated between EVs and a university building. The findings reveal that the Embedded APSO-MILP algorithm (Algorithm 2) ensures no load shedding under all scenarios, unlike the cascaded MILP approach (Algorithm 1), which exhibits marginal load shedding in scenarios where load shedding is explicitly prohibited. Moreover, in terms of LCOE and LCE, no EV flexibility, and no load shedding scenario of Algorithm 2 performs the worst, while the scenario of incorporating EV flexibility and load shedding of the same algorithm demonstrates the best outcomes for both metrics.

Overall, this research presents a holistic approach for optimizing microgrid design and operation by unifying component sizing and EM strategies, integrating advanced optimization techniques, and addressing both economic and environmental objectives throughout the project lifespan. Furthermore, the proposed method contributes to the reduction of carbon dioxide emissions and energy costs by increasing the utilization of renewable energy sources.

Keywords: microgrid, multi-objective optimization, optimal sizing, energy management, renewable energy integration, electric vehicle.

Résumé

La modernisation du réseau électrique (RE) par la mise en œuvre de micro-réseaux offre un potentiel significatif pour améliorer la résilience énergétique, la durabilité et l'efficacité. Cependant, cette transition implique de naviguer dans un ensemble complexe de défis techniques, économiques et environnementaux. Les micro-réseaux nécessitent une planification et une optimisation méticuleuses pour équilibrer la génération, le stockage et la consommation d'énergie tout en minimisant les coûts et les émissions de carbone. Atteindre cet équilibre nécessite des stratégies d'optimisation avancées capables de traiter les subtilités des composants du système et des dynamiques opérationnelles.

L'objectif de cette recherche est d'améliorer les capacités de prise de décision des concepteurs de micro-réseaux en fournissant une approche globale pour la planification des micro-réseaux. L'étude offre une analyse approfondie du projet sur toute sa durée de vie, du point de vue technique, économique et environnemental. Implémenté en Python et résolu à l'aide de CPLEX, le processus d'optimisation vise à minimiser à la fois le *levelized cost of energy* (LCOE) et le *life cycle emission* (LCE). L'étude utilise des données économiques et environnementales réelles, en tenant compte de la croissance de la charge ainsi que des données réelles d'irradiation solaire, de température ambiante et de vitesse du vent. La charge pour le bâtiment universitaire est basée sur des données de l'Université de Technologie de Compiègne, France, avec la charge des véhicules électriques (VE) modélisée à l'aide d'une modélisation probabiliste.

L'étude introduit une stratégie d'optimisation multi-objectifs conjointe utilisant le *mixed integer linear programming* (MILP) pour garantir des solutions globalement optimales, facilitant ainsi des choix de conception plus informés et efficaces. Ces choix impliquent l'évaluation de diverses solutions proposées pour équilibrer les coûts et les émissions de carbone tout en abordant les complexités et les contraintes techniques du problème de gestion de l'énergie. Un aspect novateur de ce travail est l'intégration de la gestion d'énergie (GE) et du dimensionnement des composants dans un problème d'optimisation unifié, visant un écart d'optimalité de 0 % avec un temps de calcul réduit par rapport à la littérature existante. La méthode proposée évalue les compromis inhérents entre diverses solutions, identifiant le front de Pareto et permettant un équilibre optimal entre les objectifs économiques et environnementaux. Les résultats indiquent une réduction significative du LCOE et du LCE dans le GCMG par rapport à l'IMG. L'étude révèle que la capacité du système de stockage d'énergie par batterie (BESS) augmente à mesure que le LCE diminue, et que le nombre de systèmes photovoltaïques est plus élevé lorsque le LCOE est plus bas pour les deux modes de fonctionnement. Cela se produit parce que le BESS a un LCE légèrement inférieur à celui du PV, et que le LCOE du PV est également inférieur à celui du BESS. De plus, à mesure que la limite du RE augmente, les fronts de Pareto deviennent plus bas et plus raides.

En outre, le même algorithme MILP est appliqué pour optimiser les micro-réseaux d'un campus universitaire tertiaire dans diverses villes. L'étude intègre également des éoliennes (WT) et des charges de VE dans le micro-réseau. L'étude fournit une analyse comparative de trois scénarios (PV/BESS, WT/BESS et PV/WT/BESS) dans différentes villes, évalue les impacts des fluctuations saisonnières sur le LCOE et le LCE, et évalue comment les technologies des composants des micro-réseaux influencent les résultats du LCOE et du LCE. Les résultats indiquent que les scénarios incluant PV/WT/BESS produisent les valeurs de LCOE et de LCE

les plus basses, tandis que le scénario WT/BESS aboutit aux valeurs de LCOE et de LCE les plus élevées. Il est également observé que l'ordre des villes en fonction de l'irradiation solaire moyenne ou de la vitesse du vent ne correspond pas nécessairement à l'ordre du LCOE et du LCE. Les fluctuations mensuelles et quotidiennes de l'irradiation solaire et de la vitesse du vent influencent de manière significative ces résultats. En ce qui concerne les technologies, les panneaux photovoltaïques produits localement contribuent positivement au LCE global du micro-réseau, avec des panneaux PV intégrant un matériau à changement de phase montrant un LCE plus élevé.

La recherche compare également deux algorithmes distincts. L'algorithme 1 utilise une approche MILP en cascade pour optimiser le dimensionnement des micro-réseaux et la GE sans flexibilité des VE sur une année, puis se concentre sur la flexibilité quotidienne des VE. L'algorithme 2 intègre APSO avec MILP pour déterminer les tailles des composants du micro-réseau et effectuer la GE quotidienne avec flexibilité des VE. Il examine la dégradation des batteries et la délestage de charge, en excluant les charges critiques dans un bâtiment universitaire, tout en se concentrant sur la flexibilité des charges VE dans le système de GE du micro-réseau. Les deux algorithmes abordent la dégradation des batteries par un modèle de débit en kWh et visent à minimiser le LCOE et le LCE. Les charges sont réparties entre les VE et un bâtiment universitaire. Les résultats révèlent que l'algorithme APSO-MILP intégré (algorithme 2) garantit qu'il n'y a pas de délestage de charge dans tous les scénarios, contrairement à l'approche MILP en cascade (algorithme 1), qui présente un délestage de charge marginal dans les scénarios où le délestage de charge est explicitement interdit. De plus, en termes de LCOE et de LCE, le scénario sans flexibilité des VE et sans délestage de charge de l'algorithme 2 est le moins performant, tandis que le scénario intégrant la flexibilité des VE et le délestage de charge du même algorithme montre les meilleurs résultats pour les deux métriques.

Dans l'ensemble, cette recherche présente une approche holistique pour optimiser la conception et l'exploitation des micro-réseaux en unifiant les stratégies de dimensionnement des composants et de GE, en intégrant des techniques d'optimisation avancées et en abordant à la fois les objectifs économiques et environnementaux tout au long de la durée de vie du projet. De plus, la méthode proposée contribue à la réduction des émissions de dioxyde de carbone et des coûts énergétiques en augmentant l'utilisation des sources d'énergie renouvelables.

Mots-clés : Micro-réseau, optimisation multi-objective, dimensionnement optimal, gestion de l'énergie, intégration des énergies renouvelables, véhicule électrique.

Acknowledgments

I would like to express my deepest gratitude to my thesis director, Fabrice Locment, for the unwavering support and guidance throughout this journey. Fabrice, your positive outlook, encouragement, and joyful presence have been invaluable. Your fun and light-hearted nature brought joy to this challenging process. I am also immensely grateful to my co-director, Berk Celik. Berk, your scientific expertise and assistance have been instrumental in the completion of this thesis. Your insights and support have greatly enhanced my work, providing a solid foundation for my research.

My heartfelt thanks go to the jury members for their time and effort in reviewing my work. Special thanks to the reporters, Jean-Paul Gaubert and Robin Roche. I also extend my gratitude to the examiners, Dimitri Lefebvre, Marc Petit, Christine Prelle, Delphine Riu, and Timothy M. Hansen. Additionally, I am grateful to Arnaud Hubert and Philippe Trigano for believing in my capacity to teach at UTC. Your confidence in me has been a significant encouragement.

I would also like to acknowledge my former colleagues, Saleh Cheikh Mohamad, for your assistance with my integration into the lab and for your help in the beginning when I came to Compiègne. Nathanael Dougier, who brought energy and enthusiasm to the office and helped me mentally to surpass the difficulties in my thesis. Amalie Al Chami, for your invaluable help in overcoming difficult challenges. A special thank you to Bashar Al Mohammad, Constant Brncic, Saray Chavez, Mohamad Zeyad, Rusber Octavio Rodriguez, and Jamila Aourir, who have contributed significantly to my research environment. I would also like to thank Sheroze Liaquat for the mutual collaboration during our PhDs. Thanks to Eduard Antaluca and Fabien Lamarque, my laboratory members, for the cool discussions during breaks.

To my friends, Wiaam, Chawki, Georges, and Khaled, thank you for the memorable moments and companionship during this thesis. Wiaam, your unwavering support and cheerful spirit have been a constant source of motivation. Chawki, your wisdom and encouragement have always provided me with clarity during challenging times. Georges, your positive energy have made the tough days easier to bear. Khaled, your loyalty and friendship have been a pillar of strength for me. I also want to extend my gratitude to my childhood friends Akram, Jad, Joud, Nour, and Alaa, whose lasting friendship and encouragement have been a great source of strength. Nawal, although you came nearly at the end of this journey, I am grateful for your presence in my life. You have been there when needed, and your support has been invaluable. I am grateful to everyone who has crossed my path during this thesis. Each interaction has been a learning experience and has contributed to this achievement.

I want to express my deepest thanks to my family. To my brothers, Samer and Rami, my father, and my mother, your love and support have been my foundation throughout this process. Your belief in me and your encouragement have been a constant source of strength. I hope I have made you proud and that this accomplishment reflects the values and perseverance you have instilled in me. I could not have done this without you.

Acronyms

AC Alternating Current

AHA Artificial Hummingbird Algorithm

APSO Accelerated Particle Swarm Optimization

BESS Battery Energy Storage System

CV Converter

DC Direct Current

DER Distributed Energy Resource

DOD Depth of Discharge

EG Electricity Grid

EM Energy Management

ESS Energy Storage System

EV Electric Vehicle

EVCS Electric Vehicle Charging Station

GA Genetic Algorithm

GCMG Grid Connected Microgrid

GEV Generalized Extreme Value

GOA Grasshopper Optimization Algorithm

GWO Grey Wolf Optimizer

HHO Harris Hawks Optimization

IMG Isolated Microgrid

LCC Life Cycle Cost

LCE Life Cycle Emission

LCOE Levelized Cost of Energy

LOPS Loss of Power Supply

LPSP Loss of Power Supply Probability

MILP Mixed Integer Linear Programming

MINLP Mixed Integer Non-Linear Programming

MOEA Multi-Objective Evolutionary Algorithm

MOGOA Multi-objective Grasshopper Optimization Algorithm

MPPT Maximum Power Point Tracking

NPC Net Present Value

P2P Peer to Peer

PCC Point of common coupling

PCM Phase-Changing Material

PDF Probability Density Function

PHEV Plug-in Hybrid Electric Vehicle

PSO Particle Swarm Optimization

PV Photovoltaic

SOC State of Charge

STC Standard Test Conditions

TIC Total Investment Cost

TOC Total Operation Cost

TOU Time-of-Use

VoLL Value of Lost Load

WE Wasted Energy

WT Wind Turbine

Contents

List of Figures

List of Tables

Chapter I

Introduction

I.1 Context

Energy is crucial for survival, economic progress, and improving life quality. It powers factories, moves vehicles, and provides vital services like healthcare and education. Energy also supports technological advances that connect and update the world. In the past, the reliance on fossil fuels such as coal, oil, and natural gas was predominant. These resources kickstarted the Industrial Revolution, boosted economies, and led to the growth of cities and modern infrastructure. However, using these fossil fuels has caused major environmental problems like air pollution and climate change, leading to a reconsideration of energy usage and the selection of energy sources. As a result, there has been a growing interest in sustainable energy alternatives, including the development of microgrids.

I.2 Climate Change

Climate change describes significant alterations in global temperature and weather patterns over time [1]. Although natural processes can induce these changes, current trends are primarily attributed to human-induced factors, such as the emission of greenhouse gases (e.g. carbon dioxide) [2]. These shifts are evident in several key phenomena: rising temperatures across global land and oceans , higher sea levels [3], diminishing ice across polar regions and mountain glaciers. There is also a marked increase in the frequency and intensity of extreme weather events [4], including hurricanes, heatwaves, wildfires, droughts, and floods, as well as variations in precipitation. Furthermore, changes in cloud and vegetation cover are occurring, significantly affecting ecosystems globally.

Human activities have raised Earth's average global temperature by approximately 1℃ since the pre-industrial era with current rates of increase exceeding 0.2℃ each decade. This current warming trend, driven by human activity primarily since the 1950s, is occurring at a rate unprecedented over thousands of years [5]. Climate change indicators such as carbon dioxide (CO_2) levels, global temperatures, sea level, and ocean heat content are evaluated in [5]. Fig. 1(a) presents the atmospheric CO_2 concentrations recorded at the Mauna Loa Observatory in Hawaii since 1958. The data demonstrates noticeable seasonal variations with peaks in spring and troughs in autumn due largely to plant life cycles. Remarkably, human activities have increased atmospheric CO_2 by 50% within the past two centuries [5]. Fig. 1(b) illustrates deviations in global surface temperatures from the average recorded between 1951 and 1980, highlighting that the most recent decade contains the hottest years on record. Fig. 1(c) displays the increase in sea level, showing a rise of approximately 103.3 mm since 1993. Fig. 1(d) depicts the warming of the oceans, where 90% of the global warming is absorbed, indicating an increase in internal heat content in the top 2000 meters of ocean since 1955 with 95% data confidence represented via the shaded blue area [5].

Over the past two centuries, various industrial revolutions have evolved the sources of energy supply. However, new production sources have not replaced the old ones; instead, they have overlapped to keep pace with the growth in consumption, as can be observed in Fig. 2. Thus, the main sources for energy production remain coal, oil, and natural gas, accounting

for 81% of global energy production in 2019. These energy sources are called fossil fuels because they result from the fossilization of organic matter in the soil over millions of years. This dependency is problematic for three reasons. First, the combustion of fossil fuels emits CO_2, which is a greenhouse gas responsible for climate change. Second, the reserves of fossil resources are finite and their renewal occurs on a scale far greater than a human lifespan. They are thus destined to be depleted, raising concerns about a potential shortage in the medium term. Finally, the reserves are unevenly distributed across the planet. Supply is ensured by a small number of countries, which creates geopolitical tensions. Thus, diversifying sources of production would allow for greater territorial autonomy, anticipate the decline of fossil fuel extraction, and limit climate change [6].

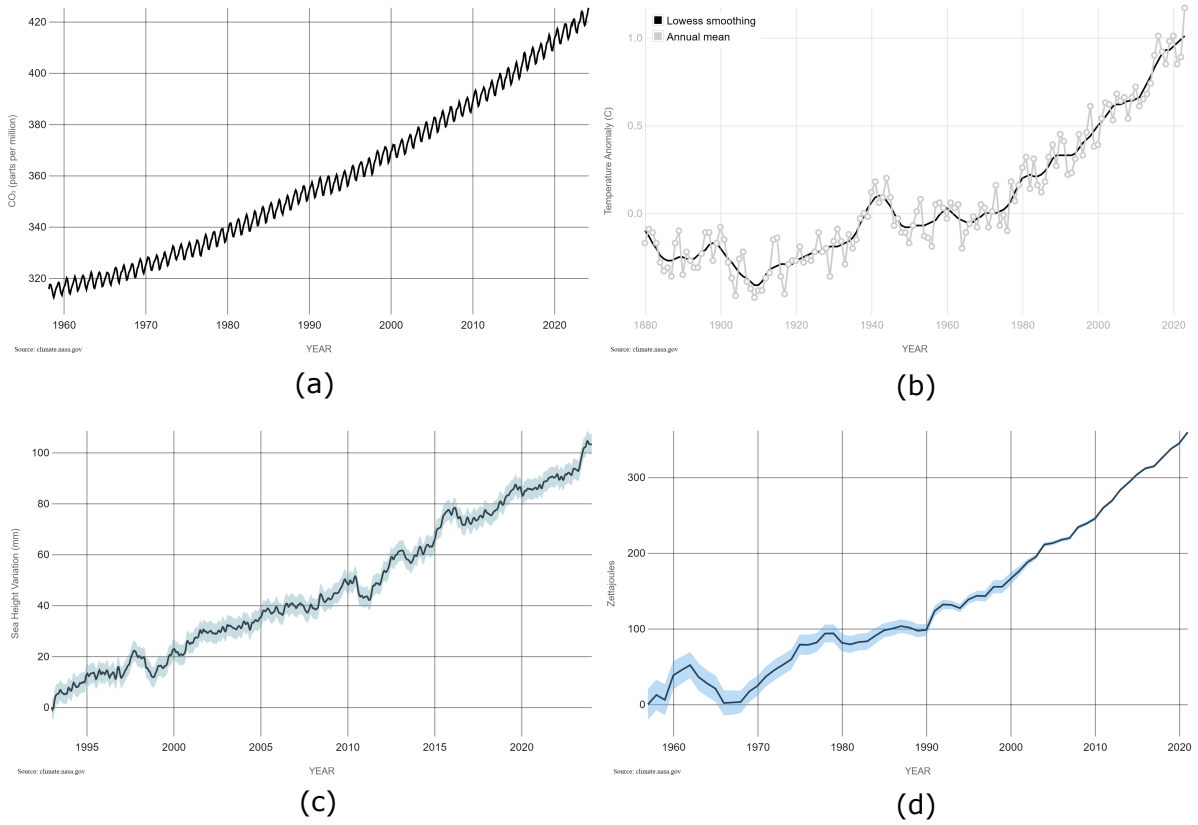

Figure 1: Variations over time in (a) CO_2, (b) global temperature, (c) sea level, and (d) ocean warming [5].

I.3 Renewable Energy Integration

The Paris Agreement is committed to maintaining global temperature increases under 2°C above pre-industrial levels by decreasing dependence on fossil fuels for electricity production and enhancing the use of renewable energy sources such as solar, wind, hydropower, biomass, geothermal, ocean energy, and biofuels [8]. According to recent data, renewable electricity capacity saw a significant boost of approximately 507 GW in 2023, marking an increase of nearly 50% from 2022 [9]. This represents the most rapid expansion observed in the last two

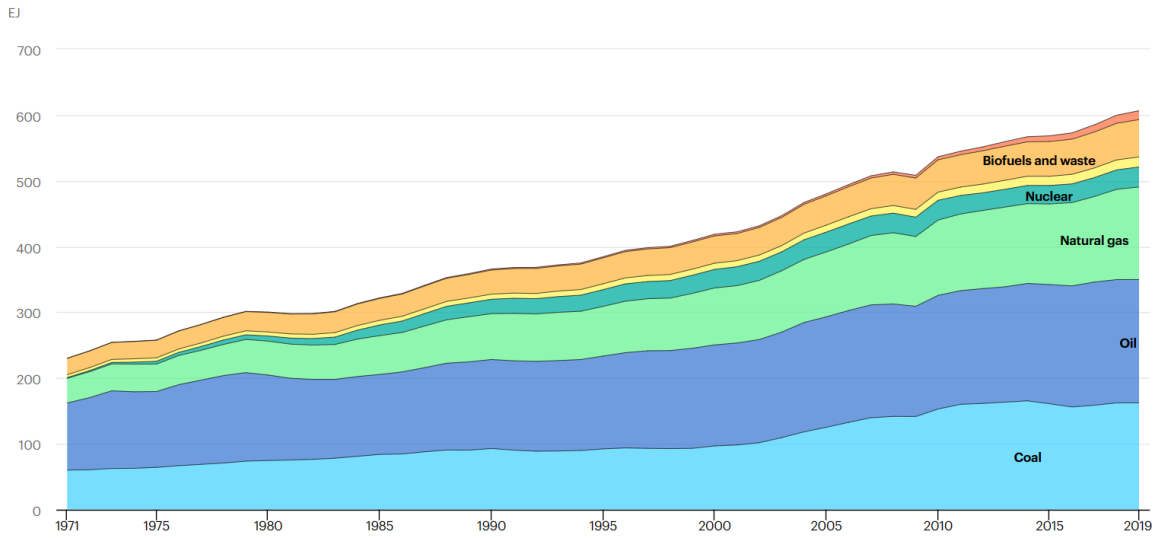

Figure 2: World total energy supply by source between 1971 and 2019 [7].

decades. Record highs in renewable capacity were achieved in 2023 across Europe, the United States, and Brazil. As depicted in Fig. 3, projections indicate that renewable power capacity will continue to rise over the next five years with solar PV and wind energy expected to contribute an unprecedented 96% of this growth. The projections forecast that by 2028, the additions for solar PV and wind energy will be more than double compared to 2022 levels, setting new records annually and potentially reaching nearly 710 GW. Conversely, hydropower and bioenergy are anticipated to see reduced growth in the coming years due to slowed development in emerging markets. By 2028, renewable energy is projected to produce 42% of global electricity with WT and solar PV combined accounting for 25% of this generation [9].

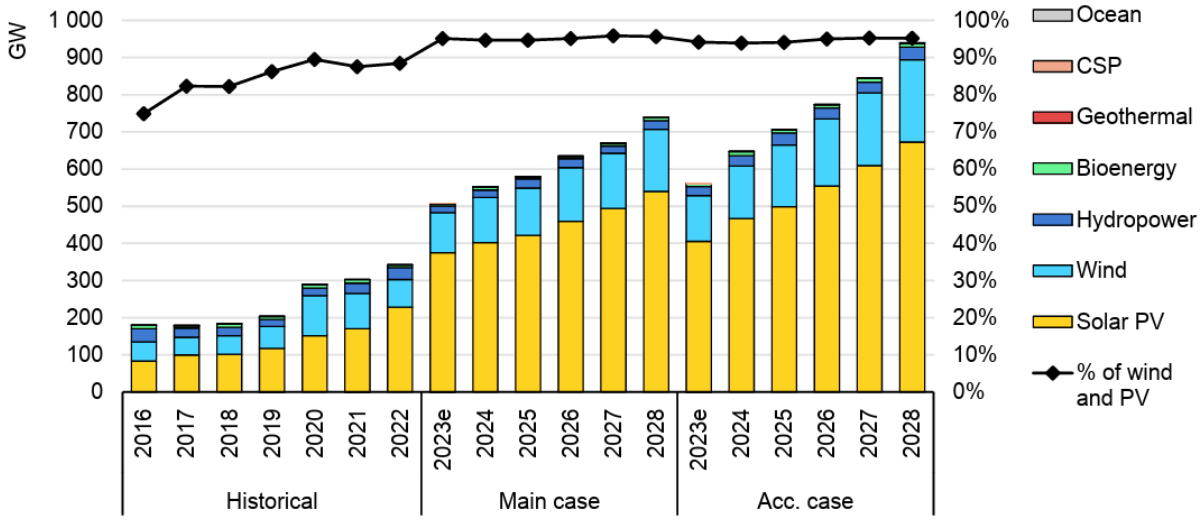

Figure 3: Renewable electricity capacity additions by technology and segment, 2016-2028 [9].

Renewable energy capacity expansion in Europe is expected to be more than double in the period from 2023 to 2028 compared to the previous six years with projected additions of 532 GW. Solar PV is set to drive over 70% of this growth, predominantly through distributed systems, which surpass utility-scale installations by one-third. Wind energy contributes an

additional 26%, primarily from onshore projects. In July 2023, the European Union officially resolved to elevate the proportion of renewable energy in final energy consumption from 32% to 42.5% by 2030 in order to hasten decarbonisation. Consequently, EU member states are currently revising their National Energy and Climate Plans (NECPs) to align with the new EU mandate and establish revised national objectives as required. As of this writing, 21 out of the 27 member states have submitted draft plans and yet only 14 have explicitly defined renewable electricity targets. Fig. 4 displays the proportion of renewable electricity production in Europe for the years 2022 and 2028, alongside the targets from the 2019 and 2023 NECP drafts [9]. Notably, Denmark and Luxembourg presently boast the highest shares of renewable electricity. Estonia is projected to witness a significant surge in renewable electricity by 2028, while Lithuania has set the most ambitious goal in the 2030 NECP draft by aiming for 100% renewable electricity by 2023.

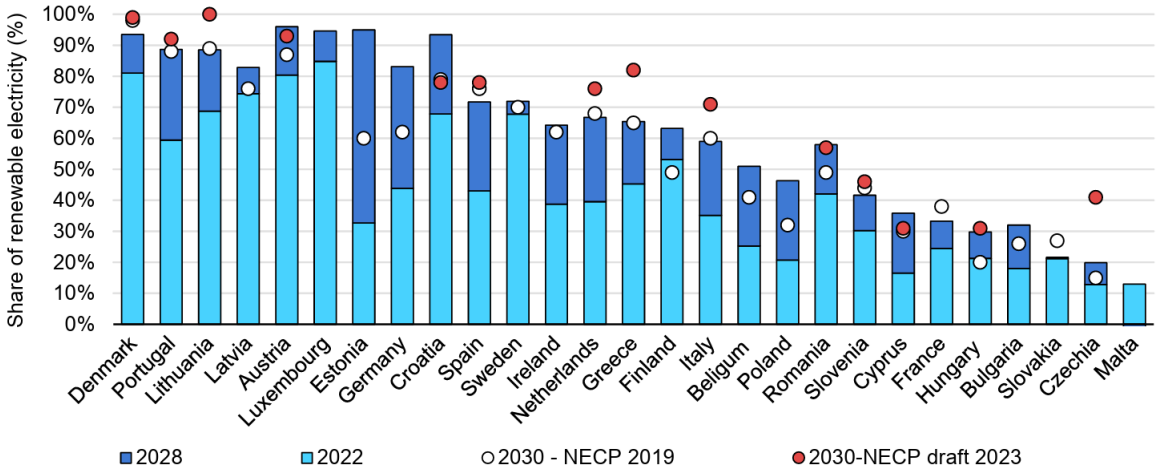

Figure 4: European Union renewable energy share in electricity generation by country, 2022 and 2028, and NECP targets (2019 and 2023 draft) [9].

In France, renewable energy contributes approximately 26.2% to the total electricity production, while the country's share of global emissions stands at 0.9% [10]. Despite the relatively modest share of renewables in its energy mix, France maintains low emission levels due to high nuclear power utilisation, which accounts for 36.5% of its energy mix. Nuclear energy is recognized as one of the low carbon emission sources, which significantly aids France in its efforts to reduce greenhouse gas emissions.

I.4 Energy Storage System

ESSs play a crucial role in mitigating the inherent variability of power output from renewable energy sources. ESSs maintain equilibrium between energy generation and load demands. Broadly, ESSs are categorized into three types:

1. **Chemical ESSs**, which include technologies such as batteries, hydrogen storage, and flow batteries.

2. **Mechanical ESSs**, encompassing flywheels, compressed air energy storage, and pumped hydroelectric storage.

3. **Electrical ESSs**, notably supercapacitors and superconductors.

These various forms of ESSs exhibit differing characteristics in terms of power density and energy density, as depicted in Fig. 5.

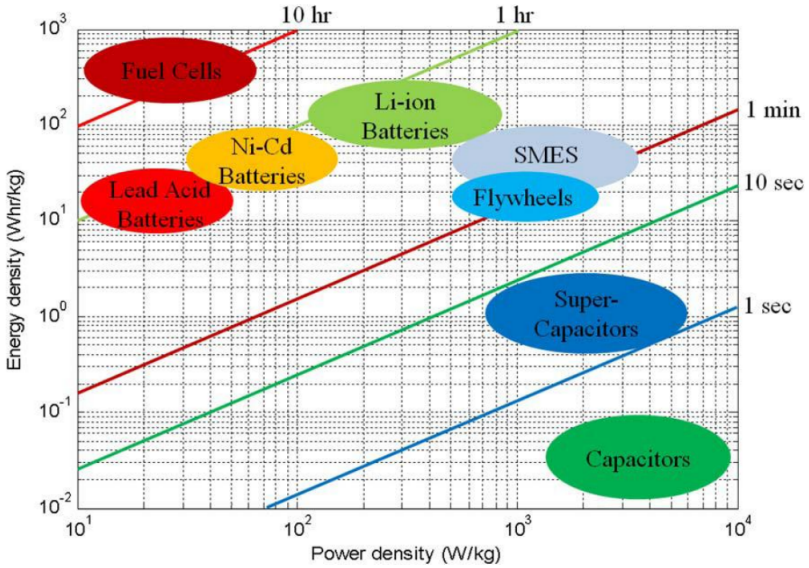

Figure 5: Power and energy densities of different ESSs [11].

Pumped-storage hydropower remains the most extensively utilized storage technology [12], but grid-scale batteries are rapidly advancing. As of 2021, the total installed capacity of pumped-storage hydropower was approximately 160 GW [12]. In 2020, the global capability was about 8500 GWh, representing over 90% of the world's total electricity storage capacity. The United States has the largest capacity worldwide. Most of the currently operating plants are used for daily balancing purposes. However, grid-scale batteries are quickly gaining ground. Although their capacity is still significantly smaller than that of pumped-storage hydropower, grid-scale batteries are expected to lead the majority of future storage capacity growth globally. By the end of 2022, the total installed capacity of grid-scale batteries was nearly 28 GW, with most of this capacity being added in the previous six years [12]. In comparison to 2021, installations saw a substantial increase of over 75% in 2022, with around 11 GW of new storage capacity added [12].

I.5 Electric Vehicles

EVs are categorized into several types, each with distinct features and benefits. Battery EVs are fully electric and depend entirely on batteries for power that need to be charged from external sources. Notable examples include the Tesla Model S and Nissan Leaf [13, 14]. PHEVs combine a battery-powered electric motor with an internal combustion engine. Examples of

PHEVs include the Chevrolet Volt and Toyota Prius Prime [15, 16]. Hybrid EVs, such as the Toyota Prius, also use both an electric motor and an internal combustion engine, but they cannot be plugged in to charge. Instead, they rely on regenerative braking and the engine to recharge the battery [17]. Extended-range EVs, like the BMW i3 REx, operate primarily as EVs but include a gasoline generator to extend their range when the battery is low [18]. Lastly, fuel cell EVs use hydrogen gas to power an electric motor, emitting only water vapor and heat. The Toyota Mirai and Hyundai Nexo are prominent examples of fuel cell EVs [19, 20]. Each EV type provides unique advantages tailored to different driving requirements, infrastructure availability, and environmental impacts.

EVs are pivotal for decarbonizing road transport, which is a sector contributing over 15% to global energy-related emissions [21]. In 2022, EV sales surpassed 10 million units, and the number is increased to approximately 14 million by 2023 [21]. The majority of global EV sales are concentrated in China, Europe, and the United States. Specifically, China represented nearly 60% of all new electric car registrations worldwide. In Europe, EV sales in 2022 increased by more than 15% compared to 2021, reaching 2.7 million units. While sales growth was more pronounced in previous years (exceeding 65% in 2021 and averaging 40% between 2017 and 2019), Europe maintained its position as the world's second-largest EV market after China in 2022, accounting for 25% of annual sales and 30% of the global EV stock [21]. In the United States, EV sales grew by 55% in 2022 compared to the previous year, predominantly driven by battery EVs. The U.S. contributed to 10% of the global increase in sales, with the total stock of electric cars reaching 3 million, marking a 40% rise from 2021 and representing 10% of the global total. Despite these advances, EV adoption is not yet widespread globally. In developing and emerging economies, EV uptake remains slow, hindered by the relatively high cost of EVs and insufficient charging infrastructure availability [22]. To achieve a net-zero emissions scenario by 2030, it is projected that the number of EVs globally needs to reach approximately 59.25 million. This amount represents about 67% of the total vehicle worldwide.

I.6 Microgrid

Microgrids are essential for modern power systems due to their ability to enhance energy reliability, efficiency, and resilience. They represent a cohesive and compact network that integrates various DERs like PV panels, WTs, and ESSs with local energy demands [23]. DERs are small-scale units of local generation connected to the EG at the distribution level. They are important because they decentralize power generation, which reduce dependency on centralized power plants, and increase the use of renewable energy sources. This integration underscores the pivotal role of microgrids in harmonizing DERs with local ESS resources, thereby enhancing their utility and compatibility [24]. Additionally, microgrids mitigate the variability of DER outputs, such as those from solar and wind, by combining them with ESS, demand response strategies, and traditional power generation methods. They enable the EG to function in both GCMG and IMG configurations without compromising system reliability or stability. Furthermore, microgrids promote the adoption of renewable energy sources [25] and facilitate cost-effective operations of local electrical networks [26].

Microgrids are categorized into three types: AC, DC, and hybrid AC/DC systems. The architecture of the DC and AC microgrids are illustrated in Fig. 6. AC microgrids readily integrate a variety of power sources. Hybrid AC/DC microgrids cater to both AC and DC loads, merging multiple power sources for enhanced flexibility. DC microgrids, particularly those incorporating PV systems and ESSs, offer distinct benefits over their AC counterparts by minimizing energy losses associated with DC power generation from these components. Crucially, these systems require only voltage amplitude regulation, eliminating the need for synchronization. The absence of reactive power in the DC bus allows for the connection of AC sources to a common DC bus that operates on active power only, thus it will boost power efficiency and transfer capacity. Further benefits of this configuration are detailed in [27].

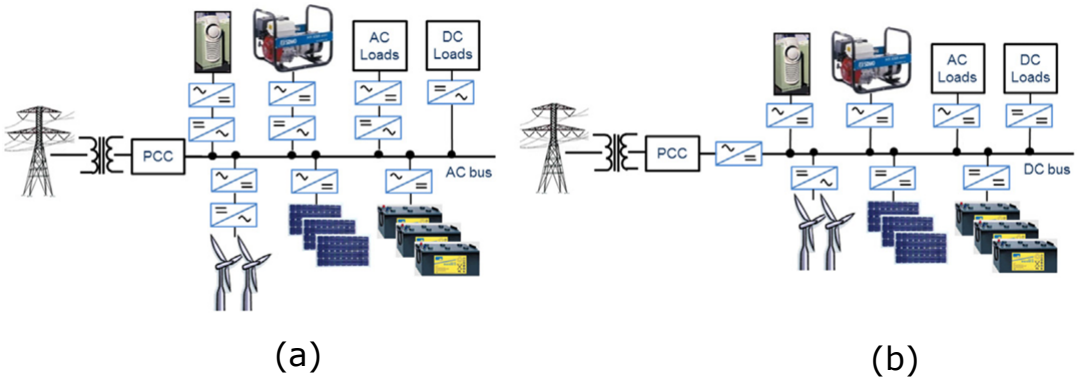

Figure 6: The architecture of (a) AC and (b) DC microgrid [27] (PCC: point of common coupling) .

Fig. 7 depicts the progression from traditional EGs to contemporary setups and towards futuristic configurations, known as microgrids. Traditional EGs rely heavily on fossil fuels, with energy primarily sourced from utility providers. Power plants are often sited close to fuel sources, which adds complexity to the transmission infrastructure. This arrangement leads to considerable transmission losses and has a substantial environmental footprint [28]. Additionally, these conventional systems feature a unidirectional flow of electricity from utilities to consumers, limiting interaction and preventing consumers from contributing electricity back to the EG. Such systems, reliant on centralized sources, are prone to significant disruptions from faults at generation sites or transmission issues caused by environmental events, technical failures, or maintenance needs. To mitigate these issues, the current EG incorporates DERs and EM techniques, allowing for the return of excess generated power to the EG. This approach focuses on local power consumption to reduce transmission losses and enhance system resilience. Nonetheless, a notable limitation of this model is the absence of direct interaction among individual households, restricting the ability to share or trade surplus energy locally if it cannot be returned to the EG due to technical constraints. Future EG designs are aimed at overcoming these challenges by introducing local energy utilization capabilities, allowing households to buy and sell electricity directly from one another. This feature enhances the EG's flexibility and supports autonomous operations, particularly useful in IMG scenarios where local energy solutions become crucial.

In late 2022, the European Commission unveiled the "Digitalisation of the Energy System"

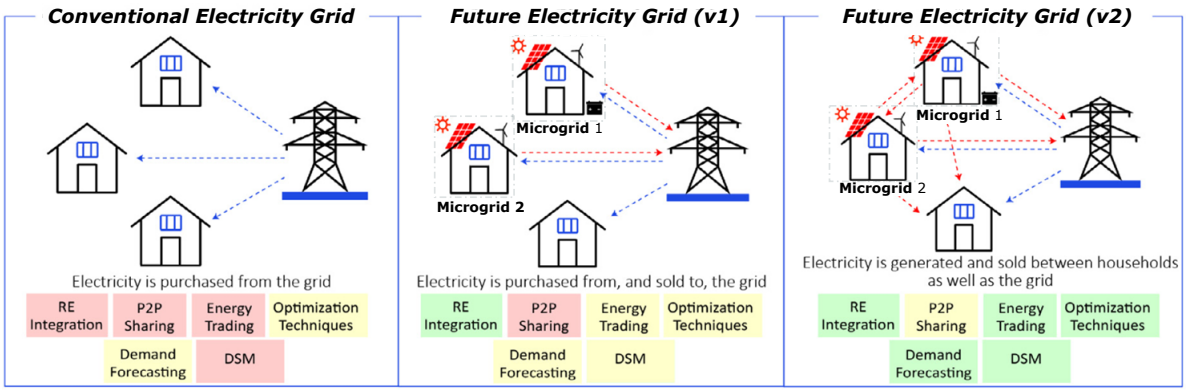

Figure 7: Evolution of the EG infrastructure with slight modifications [28] (DSM: Demand Side Management, P2P, RE: Renewable Energy).

action plan for the EU, with a significant focus on microgrid development. The Commission anticipates investments totaling approximately €584 billion in the European EG by 2030. Of this investment, €170 billion is earmarked specifically for digitalization efforts, including the deployment of smart meters, the automation of EG management, and the integration of advanced digital technologies to enhance metering and field operations [29]. Moreover, the capacity for EM in the French market was approximately 2.4 GW in 2022 and grew up by 12% in 2023 [29].

I.7 Research Problematic

In microgrid systems, achieving optimal sizing of components and EM is essential for maintaining both efficiency and reliability. As discussed in the previous section, microgrids play a critical role in decentralized power generation and distribution. Optimal component sizing ensures that economic and environmental objectives are balanced over the extended project lifetime, while effective EM guarantees proper system functioning, preventing issues such as overcharging or overdischarging of ESS and ensuring power injections into the EG are within prescribed limits. This contributes to the proper management of energy flows within the microgrid.

However, the economic and environmental objectives often conflict; minimizing environmental impacts typically incurs higher costs. For instance, using more eco-friendly but expensive materials or technologies can drive up initial investment and operational costs. This dichotomy necessitates the development of solutions that represent compromises between these conflicting objectives. Optimization algorithms are pivotal in this context, as they are formulated to identify the most effective compromise, achieving the best possible balance between technical, economic, and environmental factors.

This leads to the central research question of the thesis: **"Can an optimization algorithm be developed that simultaneously addresses the optimal sizing and EM of a microgrid by integrating technical, economic, and environmental dimensions over the project's lifes-**

pan?" This research aims to explore and develop such an algorithm, contributing to more sustainable and cost-effective microgrid solutions.

I.8 Objectives

The primary goal of this research is to enhance the decision-making capabilities of microgrid designers by offering a comprehensive methodology for system planning. This study aims to empower designers to make more informed and effective decisions by:

- **Evaluating Various Proposed Solutions:** Implementing a systematic approach to assess different design configurations and technologies for microgrid components, including RESs, ESSs, and EM strategies.
- **Balancing Economic and Environmental Aspects:** Creating criteria and metrics to achieve an equilibrium between cost minimization and environmental impact reduction, ensuring that both objectives are addressed without compromising the technical viability of the system.
- **Addressing Technical Constraints:** Integrating the technical constraints associated with the EM problem, such as ensuring the reliability, stability, and efficiency of energy flows within the microgrid.

By tackling the complexities and trade-offs inherent in microgrid design, this research seeks to provide a robust framework that guides designers toward achieving optimal configurations that meet technical, economic, and environmental criteria. The development of this decision-making tool requires the modeling of DERs and ESSs, formulation of constraints and objective functions for the optimization problem, and the acquisition of real-world data to construct realistic scenarios. This tool is designed to be driven by data, meaning that variations in input data can lead to different outcomes. Additionally, it is adaptable to changes in the configuration of microgrid components, allowing for the addition or removal of components as needed to suit different scenarios and requirements.

I.9 Thesis Outline

This thesis is organized into five chapters:

- Chapter II *"State of the Art"* discusses various approaches to microgrid sizing and energy EM, the integration of these two aspects, and highlights the existing challenges and research gaps.
- Chapter III *"Optimal Microgrid Sizing and Energy Management: A Combined MILP Approach for Reducing Energy Costs and Carbon Emissions"* elaborates on combining the

optimal sizing and EM into a unified multi-objective optimization problem, that aims to minimize the economic and environmental impacts over the microgrid's project lifetime. This chapter presents the system modeling, formulation of the optimization problem, and includes discussions on IMG and GCMG, Pareto front analysis, peak shaving strategies, scalability analysis, and an examination of the energy sources utilized in the French EG.

- Chapter IV *"Cost and Emission Minimization in University Building: A Multi-Objective MILP Study with Renewable Energy and EV Integration including Geographic and Technology Analysis"* provides a comparative analysis between several French and international cities while focusing on different as PV, WT, and BESS technologies. This chapter also includes a section on EVs with their demand modeled through probabilistic approaches.

- Chapter V *"Comparative Analysis of Cascaded MILP and Embedded APSO-MILP Algorithms for Multi-objective Microgrid Sizing with EV Demand Flexibility"* assesses a microgrid's performance by minimizing the economic and environmental impacts throughout the project lifetime. It includes the flexibility of EVs within the optimization framework. The chapter outlines two optimization algorithms: a cascaded MILP approach and an embedded MILP-APSO algorithm. Detailed equations of both algorithms and results including LCOE, LCE analyses, microgrid component performance, power profiles, and comprehensive economic and environmental impacts are discussed.

- Chapter VI *"Conclusions and Future Perspectives"* presents the main conclusions of the thesis and discusses potential future research directions stemming from this work.

Chapter II

State of the Art

Optimal sizing is crucial in developing microgrids, serving as a cornerstone for both their economic, environmental viability and operational success [6]. It involves strategically configuring components such as RESs, ESSs, and consumption loads to balance minimizing initial investments against ongoing operational costs such as maintenance and replacement costs [30]. The importance of accurate sizing stems from its ability to reduce inefficiencies, eliminate unnecessary financial and spatial investment in infrastructure, and prevent energy shortages that could compromise the microgrid's ability to meet energy demands. Additionally, as the use of variable RESs increases, expert sizing becomes essential for integrating these unpredictable energy sources into microgrids to ensure a stable and reliable power supply. This balance is crucial not just for the autonomy of IMGs but also for GCMGs, which must efficiently manage the exchange of surplus energy and grid-supplied additional power [31]. Beyond operational considerations, the importance of microgrid sizing extends to its impact on the system's carbon footprint, reliability, and economic viability. It marks a key element in designing sustainable energy infrastructure [32].

The planning of a microgrid encompasses selecting the appropriate optimization sizing approach, devising an EM strategy, and coordinating both microgrid sizing and EM effectively. Furthermore, it is crucial to conduct precise load modeling and choose suitable models for the RES and the BESS including its degradation model. Each component has a significant role in achieving operational efficiency and sustainability of the microgrid.

This chapter gives a systematic review of relevant literature to microgrid planning. It includes an elaborate study of planning methodologies, EM strategies, and objective functions used for microgrids design and operation.

II.1 Microgrid EM Approaches

The integrating of DERs into microgrids is beneficial for sustainability but brings challenges related to reliability and stability because of the unpredictable nature of renewable energy. To mitigate these drawbacks in microgrid, the implementation of an efficient EM system is essential [28]. Numerous studies have explored EM within microgrids by employing diverse methodologies. Some of these studies have utilized a rule-based approach, which relies on predefined rules for managing RESs and ESSs. On the other hand, various studies have adopted optimization-based methods, which seek to find the most efficient solution by optimizing specific objectives, such as minimizing costs or maximizing energy efficiency. The diversity and application of these optimization-based methods within the context of microgrid EM are illustrated in Fig. 8.

II.1.1 Commercial Software

As with microgrid sizing, commercial software is used to plan the EM within the microgrid, such as HOMER, DER-CAM, EPLANopt, etc. In [33], the EPLANopt software is utilized alongside a MOEA to optimize the energy system of Favignana Island for sustainability by the

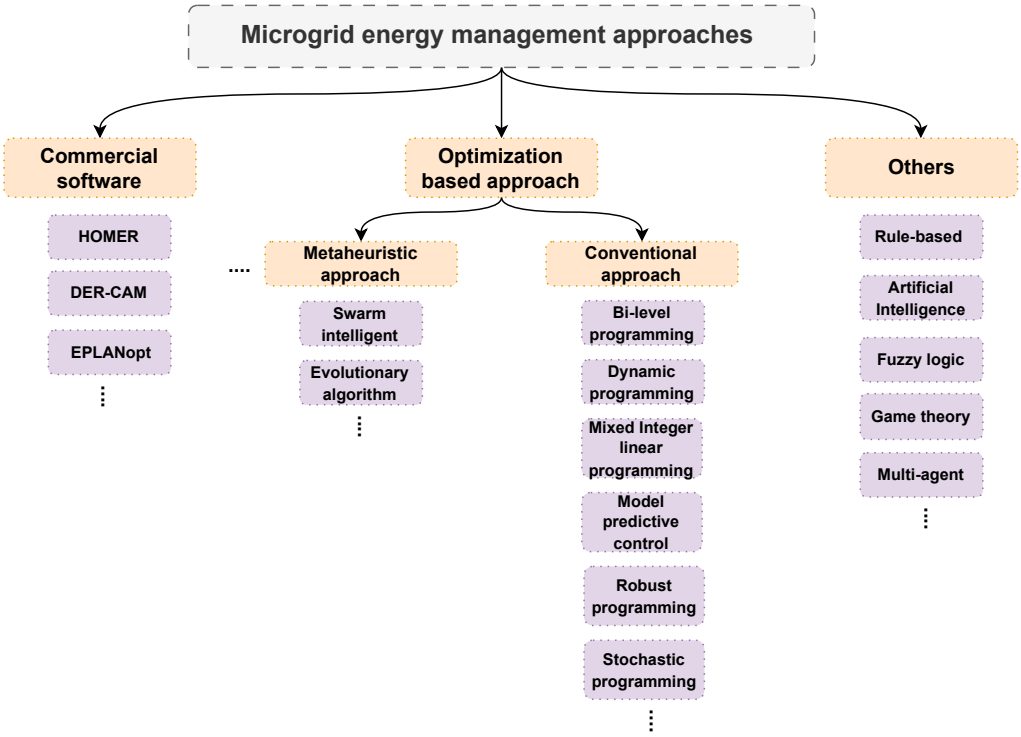

Figure 8: Microgrid EM approaches.

year 2050. EPLANopt is used to model and to simulate various energy system configurations incorporating data such as energy demand and renewable energy potential. The MOEA then analyzes these configurations, and it evolves a set of solutions through processes like mutation and selection. While EPLANopt provides detailed simulations, the MOEA identifies the most efficient and sustainable solutions by balancing objectives such as cost, emissions, and renewable energy usage. In [34], the RETScreen Expert software is used to examine a GCMG wind farm in Ghana, evaluating its technical, financial and environmental benefits. It investigates the NPC, the Internal Rate of Return, the cost of electricity production, and the emission savings to gauge the project's feasibility and its role in sustainable energy progress. RETScreen Expert software is also used in [35, 36, 37, 38]. In [39], a comprehensive study is presented on integrating DERs into healthcare systems, focusing on a hospital case study in Azad Jammu and Kashmir. Utilizing HOMER Pro and RETScreen Expert software for analysis, the study compares a proposed hybrid renewable energy system against the current energy setup. Main results indicate that both HOMER Pro and RETScreen Expert predict the increased energy output with the proposed system, though RETScreen Expert tends to give more optimistic projections. The study highlights the efficiency and sustainability of integrating renewable energy into healthcare while demonstrating significant potential for enhancing infrastructure resilience and reducing costs. HOMER is the most used software in the literature for the EM. In [40], the research details an optimal microgrid design for Basco Island in the Philippines by employing HOMER software. It integrates PV, WT, diesel generators, and BESS to boost power reliability and sustainability. By evaluating technical and economic factors, the study identifies the most efficient, and cost-effective system setup. HOMER's simulations, optimizations, and sensitivity analyses are crucial for balancing energy demand, resource availability, and operational cost reduction. In [41], the article explores the best configuration for a hybrid microgrid

at a desalination facility in Sfax, Tunisia by employing HOMER software for simulations, and FAHP-PROMETHEE for evaluating multiple criteria. Results show a dramatic 50.2% cut in the cost of energy for producing desalinated water, which illustrates the significant role of hybrid microgrids that can play in making desalination processes more sustainable and economically viable, especially in areas with inconsistent conventional energy supplies.

II.1.2 Optimization Based Approach

Fig. 8 illustrates that the optimization-based strategy for EM in microgrids. Two categories of EM optimization based approach are defined and analyzed in detail.

II.1.2.1 Metaheurstic Approach

Metaheuristic method-based EM used in microgrids is mainly categorized into three major groups: evolutionary algorithms, swarm optimization and other metaheuristic algorithms, such as GA, simulated annealing, etc. Evolutionary algorithms, inspired by biological evolution processes such as mutation, recombination, selection, and reproduction, which have found extensive application in computational research. An innovative approach was introduced by the study in [42], which proposed a Niching Evolutionary Algorithm to optimize the allocation of RESs and ESS within IMG systems. The research presented in [43] proposed an Enhanced Memetic Algorithm for demand-side management in microgrids. The research presented in [43] proposed an Enhanced Memetic Algorithm for EM in microgrids. Another noteworthy contribution is detailed in [44], where the Water Cycle Algorithm is applied to the EM of microgrid systems. This approach focuses on minimizing both operational costs and emissions by efficiently coordinating distributed generation units alongside ESS. Lastly, the study in [45] explores the use of a GA, the most commonly encountered evolutionary algorithm in literature, for optimizing day-ahead demand scheduling under uncertainty. This research highlights the algorithm's robustness in dealing with the stochastic nature of microgrid EM, further underlining the critical role of evolutionary algorithms in advancing smart city initiatives.

Swarm intelligence draws inspiration from the natural world's social living creatures, which exhibit coordinated behaviors in groups without central control. These phenomena, observable in entities such as ant colonies engaging in foraging, birds moving in unison, animals grouping together for migration, hawks coordinating in pursuit of prey, and fish swimming in schools, serve as the foundation for algorithms designed to tackle intricate challenges through collective effort. Among these, the PSO algorithm stands out for its widespread application. This algorithm mimics the social behavior of birds and fish to navigate toward optimal solutions in a multidimensional space, which effectively addresses various computational and optimization problems. The study in [46] presents a probabilistic approach methodology for the enhancement of EM in microgrids equipped with DERs and ESSs. The study introduces a self-adaptive modified q-PSO algorithm optimizing the EM process by adapting to changes dynamically, thus it ensures efficient and reliable microgrid operations under diverse conditions. In [47], the study introduces an innovative approach for EM in IMGs by employing a multi-layer ant colony optimization algorithm. This algorithm is designed to minimize electricity production costs by

optimizing both day-ahead and real-time scheduling. In [48], the Adaptive Modified Firefly Algorithm is introduced for a scenario-based stochastic optimization framework for a microgrid including WT, PV, micro-turbines, fuel cells, and ESS. The GWO, which is considered as a swarm intelligence algorithm, is considered for optimizing the EM in [49, 50].

Beyond swarm optimization and evolutionary algorithm-based metaheuristic techniques, several other metaheuristic algorithms have been employed to enhance the EM of the microgrid. In [51], The Gravitational Search Algorithm is employed to identify the optimal approach for managing energy within the MG using a probabilistic method focused on resolving the challenges related to energy and operational management within the microgrid. The same algorithm is also applied in [52] for achieving optimal EM and design of an IMG. The study in [53] examines a microgrid located in Oshawa (Ontario, Canada) by employing variable load models, which utilizes the Interior Search Algorithm to optimize the hour-by-hour scheduling for day-ahead power scheduling issues. The two-stage Scenario-Based optimization approach is employed for forecasting within a coordinated scheduling model, as detailed in [54].

II.1.2.2 Conventional Approach

Conventional approaches has six categories as illustrated in Fig. 8. In [55], a bilevel optimization model is employed where the Karush-Kuhn-Tucker approach for problem reformulation into a single-level optimization in employed with a combination of binary PSO and quadratic programming. In [56], a dynamic programming solution was implemented to address a convex optimization problem aimed at reducing the microgrid's TOC. An energy cost optimization using MILP is introduced in [57, 58, 59]. In [60], MILP is utilized to manage energy production and demand, incorporating rolling horizon-based forecasting of load. In the context of model predictive control, a receding horizon control-based model for the optimal scheduling of batteries was introduced in [61]. The study in [62] presents a robust counterpart formulation designed to manage peak demand and smooth out load variations amid uncertainties in energy generation and demand within a microgrid by employing a robust programming strategy. In [63], a stochastic energy scheduling system for a microgrid with DERs was assessed, including a case study on a modified IEEE-37 bus test feeder setup. Findings from this research underscored the efficiency and precision of the proposed stochastic programming-based algorithm for microgrid energy scheduling.

II.1.2.3 Other Optimization Based Approach

In addition to metaheuristic, conventional, and AI approaches, other methods are also discussed in the literature. Some of these alternative approaches are cited here. In [64], the deployment of an EM strategy within a standalone microgrid is explored. Utilizing a probabilistic framework grounded in Bayesian networks coupled with Monte Carlo simulations, the study effectively captures the unpredictable aspects of electricity demand, which enhances system profitability. Conducting a simulation over the span of a year, the findings reveal that the EM strategy contributes to a reduction in energy expenses by 11.3% while elevating the utilization of solar energy to 54%. In [65], the study focuses on enhancing the operation and design of

microgrids that incorporate DERs using a holistic strategy that aims minimizing energy costs and emissions. This is achieved through the commitment and dispatch of distributed devices. The uncertainties associated with PV generation are captured through a Markovian process, while a branch-and-cut method is applied to address the optimization challenges. In [66], the study presents a methodology employing Hong's Two-Point Estimate method for day-ahead scheduling taking into account the uncertainties in load consumption and WT generation. The primary goal is to reduce operational costs while maintaining system reliability.

II.1.3 Other EM Approach

Rule-based, artificial intelligence, fuzzy logic, game theory, and multi-agent approaches are also utilized for EM in microgrids. Rule-based approaches, characterized by predefined "if-else" strategies, are extensively explored in the literature for EM within microgrids. These methodologies often involve establishing a hierarchy among different energy sources and storage systems based on various factors, such as user preference or the availability of energy. A representative rule-based decision making in microgrid EM is presented in Fig. 9, which is widely used in the literature [31, 57, 58]. If the solar and wind output are sufficient, the power is distributed to the load and any excess power is stored in the BESS. If the renewable energy output is insufficient, power is drawn from the BESS if the battery level is adequate. If the BESS level is low, load shedding is implemented or power is purchased from the EG. Optionally, the battery discharge can be prioritized to ensure that critical loads are powered during nighttime or periods without RES generation. In [67], a priority sequence is determined allowing PV systems, BESS, or biomass to be selected as the primary energy source contingent upon the user's selection. Similarly, [68] details a rule-based method wherein surplus energy from PV panels is initially stored in the BESS before being dispatched to the EG. This illustrates how rule-based strategies can be adapted to manage diverse configurations of microgrid components including PV-WT-BESS, PV-Hydrogen, PV-Pumped Hydroelectric, WT-BESS, and PV-BESS systems. Another exemplary implementation of rule-based EM is showcased in [69], which proposes a model for an IMG integrating PV panels, WTs, an EG, and a diesel generator.

The study in [70] introduces a multi-objective EM system tailored for microgrids, focusing on minimizing overall operational expenses and carbon emissions. Utilizing a fuzzy logic approach, this system enhances the BESS management process by managing uncertainties in microgrid operations. It determines the optimal timing and rate for charging or discharging the BESS considering variables such as RES production, demand load, and electricity costs. The method employs input membership functions to steer the inference engine in assessing the rules. Furthermore, the study in [71] presents an EM system that utilizes a fuzzy logic controller, which is developed and monitored using LabVIEW, for the regulation of a DC microgrid system. This EM system employs fuzzy logic to manage the SOC of lithium-ion batteries, thereby enhancing their life cycle. In [72], a game theory-based multi-objective optimization approach for EM is presented. This method effectively balances load demand while simultaneously minimizing the operational costs and emissions associated with microgrid operations. The game theory approach considers each objective, such as cost and emissions, as a

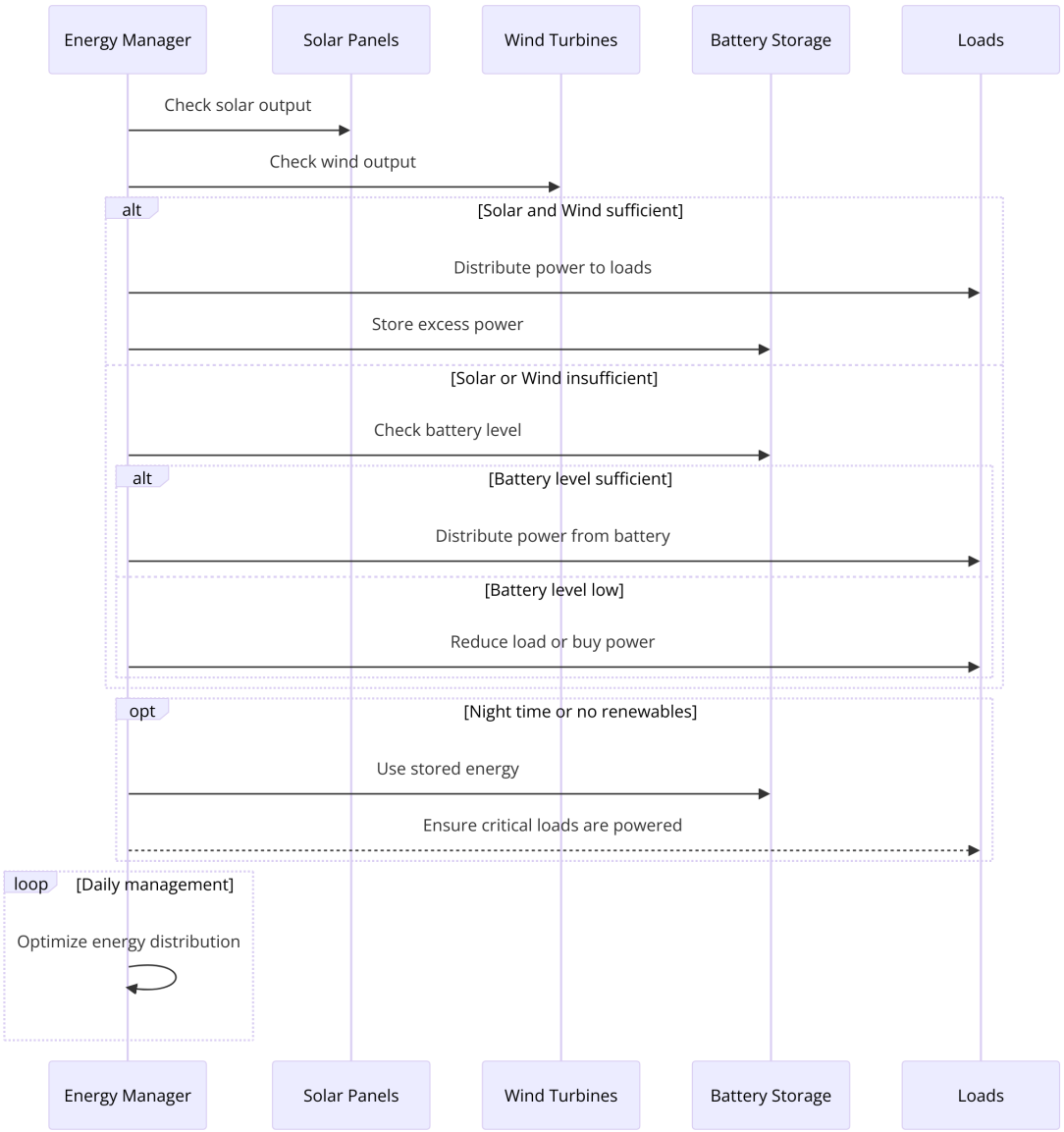

Figure 9: Rule-based decision making in microgrid EM (alt: alternative, opt: optional).

player in a game. Each player aims to optimize their own outcome while negotiating to reach a compromise solution. The study in [73] introduces a strategy for a real-time decentralized demand-side management system in a GCMG. Within this system, every client linked to the microgrid predicts their daily load demand. Utilizing these predictions, the EM system partakes in a mixed-strategy noncooperative game, proceeding until a Nash equilibrium is achieved. At this equilibrium, consumption forecasts are modified to aim for the lowest possible electricity cost. In [74], the study proposes a hierarchical control strategy for an IMG based on a multi-agent system, which focuses on maintaining stable voltage levels while optimizing economic and environmental aspects of the system. In [75], an EM model is presented for an isolated hybrid microgrid system. This model utilizes the PSO in combination with Artificial Neural Networks to enhance EM strategies. In [76], the authors introduce an EM system powered by Recurrent Neural Networks and complement it with a multi-agent-based weather forecasting method. In [77], a reinforcement learning algorithm, leveraging a Markov chain model, is introduced for planning ESS scheduling within a microgrid taking into account the anticipated

wind power production. Additionally, this reinforcement learning approach has been applied to enhance the coordination among various ESS in a microgrid as discussed in [78].

II.2 Microgrid Sizing Approaches

The sizing of microgrids is a complex optimization problem that is typically addressed through a variety of methodologies, as illustrated in Fig. 10. These methodologies include commercial software (e.g., HOMER, DER-CAM), heuristic algorithms such as GA, PSO, mathematical programming techniques (MILP, Quadratic Programming), and hybrid approaches combining the strengths of different methods (e.g., JAYA & GWO, Simulated Annealing & Tabu Search). These methodologies are selected for their efficiency in exploring and exploiting the solution space. They balance the trade-offs between computational time, accuracy, and the challenges of handling the multi-dimensional and multi-objective aspects of microgrid sizing. The selection of a specific approach over others depends on the specific requirements of the microgrid project, including but not limited to cost minimization, reliability maximization, and environmental impact reduction. The advantages and disadvantages of each approach are presented in Table 1.

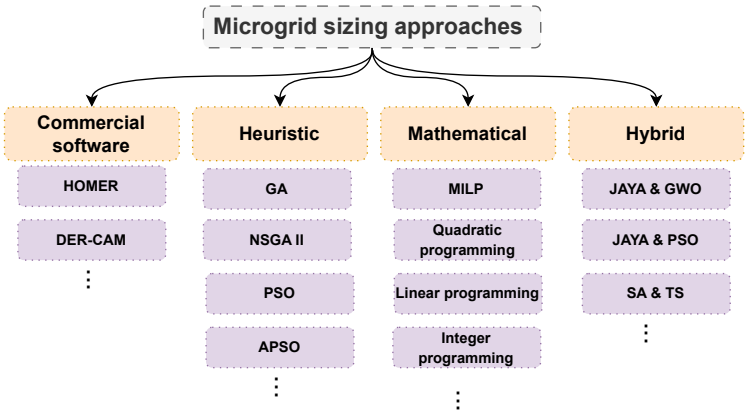

Figure 10: Microgrid sizing approaches.

II.2.1 Commercial Software

Commercial software tools play a crucial role in the optimal sizing of microgrids with the Optimization Model for Electric Renewables (HOMER) standing out as a particularly prominent example. Developed by the National Renewable Energy Laboratory (NREL) in the United States, HOMER is distinguished by its comprehensive economic evaluation capabilities [79]. Alongside HOMER, there are several other notable tools, including the Hybrid Power System Simulation Model (HYBRID2) by the Renewable Energy Research Laboratory (RERL), the General Algebraic Modeling System (GAMS), and the Optimization of Renewable Intermittent Energies with Hydrogen for Autonomous Electrification (ORIENTE), among others [80].

These tools offer diverse approaches and functionalities for sizing microgrids, highlighting the rich landscape of available resources for researchers and practitioners in the field.

HOMER software is essential in both designing and economically evaluating microgrids, whether or not they are connected to the EG. It operates through a three-phase process of simulation, optimization, and sensitivity analysis. This process utilizes weather data, demand forecasting, economic and technical considerations, among other inputs, to help identify the optimal sizes of DERs for achieving the minimum overall NPC [6]. This optimization strategy is crucial for the design and evaluation of sustainable and efficient energy systems. A notable application of HOMER is in the optimization of PV-fuel cell microgrids, as discussed in [81]. The study aimed to enhance system efficiency and sustainability through the optimal integration of DERs, fuel cells, and ESSs. The results demonstrated the potential of the proposed microgrid configuration to reduce reliance on conventional energy sources. This configuration also showcased significant improvements in EM and a reduction in the overall system cost. Similarly, the study in [82] employs HOMER software to optimize a microgrid configuration consisting of PV panels, WT, and BESS. The focus of the optimization was to minimize the microgrid's NPC. The reliability of the system was also assessed through a sensitivity analysis on the LPSP for evaluating the impact of variations in the microgrid's size and cost. In another study [83], a GCMC comprising PV panels, BESS, fuel cells, microturbines, and WT was optimally sized using HOMER. The methodology aimed at determining the optimal size for the microgrid to achieve efficient management of DERs and ESS, with an emphasis on load satisfaction and minimizing dependency on fossil fuels. Research conducted in [84] explored the integration and optimization of multi-microgrids utilizing HOMER Grid software in Goma, DRC. The objective was to minimize the NPC over a 12.5-year horizon considering both technical and economic aspects. The study highlighted the feasibility of a system configuration without PV, which achieved nearly the same NPC with a significantly lower initial capital cost, albeit with higher operational and maintenance costs affecting the LCOE. Furthermore, the study in [85] utilized HOMER to determine the optimal configurations for PV/Diesel/Pump-hydro and PV/Diesel/BESS systems. This study emphasized the calculation of payback periods, while identifying cost-effective solutions for energy systems. The study in [86] developed a techno-economic methodology for standalone, renewable energy-based EVCS in Qatar by employing HOMER for optimization. The aim was to minimize installation and lifetime operating costs among all technically feasible configurations that meet the daily EVCS demand. The optimal configuration's NPC was found to range between \$2.53M to \$2.92M, with electricity costs varying from \$0.285 to \$0.329 per kWh. In Vietnam, the optimization of EVCS in major cities was the focus of [87] using HOMER Grid for analysis. The study aimed to reduce NPC and enhance efficiency by considering local solar conditions and economic factors. It proposed optimal system configurations for Hanoi, Da Nang, and Ho Chi Minh City, highlighting the impact of solar irradiation on investment and operational performance.

Additionally, the study in [88] optimizes an IMG for rural electrification in India using GA and HOMER. The study aimed to minimize the NPC and the LCOE by comparing various hybrid configurations. The GA optimization yielded an optimal solution with the lowest LCOE at \$0.163 per kWh. The potential of DR in off-grid micro-grid optimization was explored in [89] using MILP and HOMER. The study aimed to minimize the total NPC, while highlighting

significant cost savings and efficiency improvements from implementing DR. Lastly, HOMER Pro, an advanced version of HOMER [90], was used in [91] for optimizing hybrid microgrids for green hydrogen production in Fiji. The study focused on achieving the most cost-effective configuration for hydrogen production, which is critical for powering fuel cell buses, aiming to minimize the NPC. The economic viability of microgrids across various geographic locations and with different DERs combinations has been assessed using the HOMER software. Notably, analyses have been conducted on a solar-wind hybrid system in Indonesia [92], a comprehensive PV-WT-hydro-biodiesel hybrid system in India [93], a PV-WT-diesel system in Sri Lanka [94], and a WT-biogas hybrid system in Canada [95].

These studies highlight the adaptability and effectiveness of HOMER in optimizing microgrid configurations to improve sustainability, cost-efficiency, and energy reliability. The advantages of HOMER software include:

- User-friendly interface [79]
- Comprehensive financial analysis capabilities, including cash flow analysis and payback period calculations
- Integration capability with Geographic Information Systems for enhanced project planning and site selection [96]
- Advanced sensitivity analysis to evaluate the impact of variable parameters on project outcomes
- The ability to process hourly data for detailed and accurate modeling of energy systems [79]

However, HOMER also has certain limitations:

- Utilizes a ”black box” approach to its code, which can limit transparency and customizability [79]
- Lacks the functionality to formulate multi-objective optimization problems, which limits its applicability in scenarios requiring the balancing of multiple goals
- Does not account for intra-hour variability, which could affect the accuracy of simulations for systems sensitive to short-term fluctuations
- It omits the consideration of the DOD BESS, potentially overlooking an important factor in the lifespan and efficiency of ESSs, suggesting a need for a more customized and detailed battery degradation model.

II.2.2 Heuristic Approaches

In the domain of heuristic optimization for microgrid configurations, several studies have employed a variety of algorithms to optimize their design and operational efficiencies. For instance, the work in [68] demonstrated the use of GA to size both GCMC and IMG, aiming to

optimize the LCOE with configurations including PV panels and BESS. In a similar study presented in [97], GA is applied to optimize a microgrid comprising PV, WTs, BESS, and loads. The primary objectives of this optimization are to minimize greenhouse gas emissions, reduce the LCC, and decrease non-renewable energy consumption. Further research [67] explored multiple microgrid configurations to find a balance between various factors such as greenhouse gas emissions versus global cost and microgrid autonomy versus global cost. The study in [98] targeted the sizing of an autonomous AC microgrid to minimize energy and installation costs while enhancing reliability by reducing the probability of loss of supply. In addition, [99] aimed at minimizing energy and installation costs and maximizing reliability through GA for determining the capacity of BESS, PV, and other components. Lastly, the research presented in [100] discussed integrating life cycle analysis into the hybrid microgrid design process to optimize design and minimize environmental impact while ensuring the technical and economic feasibility. The study in [101] critically evaluated a range of metaheuristic algorithms for reducing the NPC of a microgrid system that incorporates residential, commercial, and EV loads, in addition to PV panels, WTs, and BESS. Among these algorithms, the Moth-Flame Optimization Algorithm stood out for its superior performance, while the Equilibrium Optimizer was noted for its relatively lower efficiency. Another research [102] applied the Multi-Objective PSO technique to size the microgrid with the goal of minimizing both the dependency on non-renewable energy imports and the system's annualized cost. The outcomes were illustrated via a Pareto front by highlighting the trade-offs between the two objectives. Furthermore, in [103], a two-step methodology was employed for the optimization and analysis of a standalone hybrid system consisting of PV, WT, BESS, and diesel generator, which is specifically designed to fulfill the electricity demands of a remote village Fanisau in northern Nigeria. This approach, executed in the MATLAB environment using a GA solver, aimed to efficiently and economically cater to the unique energy needs of the region. The optimized hybrid renewable energy system proposed for Fanisau includes 273 PV modules, 148 batteries, and a 100.31-W diesel generator, capable of producing 200,792 kWh annually at a total annualized cost of $43,807 USD with a cost of energy $0.25 USD/kWh. In [104], the study applies the Non-Dominated Sorting GA II (NSGA-II) for microgrid sizing, aiming to minimize annualized costs, emissions, and energy imports from the EG. The study elucidates optimal configurations via the Pareto Front and employs the Topsis method for decision analysis. The study in [105] outlines the development of a hybrid renewable energy system optimization using the PSO Algorithm-based Monte Carlo Simulation to minimize total annual costs, accounting for resource and load uncertainties. It focuses on microgrid components such as WTs, PV panels, and BESS. The findings demonstrate the algorithm's efficiency in enhancing system reliability and cost-effectiveness for off-grid energy solutions. The PSO algorithm is praised for its computational simplicity, swift convergence, ease of implementation, and accuracy [106, 107]. In [108], the GOA is used to optimize an autonomous microgrid comprising PV panels, WTs, BESS, and a diesel generator. The objective function aimed at minimizing the LPSP and the LCOE. The main numerical results demonstrate GOA's efficiency over PSO and Cuckoo Search algorithms. GOA achieves a reduction in system capital cost by 14% and 19.3%, respectively. The optimal configuration includes 26 PV panels, 4 WTs, and a 40 kW BESS. In [109], the article explores microgrid optimization using the Fuzzified GWO to minimize costs and maximize renewable energy use. It covers PV panels, WTs, BESS, and generators, achieving notable cost reductions and efficiency

gains. This demonstrates significant advancements in sustainable EM through the application of heuristic algorithms. In the domain of microgrid optimization through meta-heuristic techniques, the review paper [110] revealed that approximately 25% of the research in this field employs the PSO method. Additionally, GA and GWO are used by nearly 10% and 5% of the studies analyzed in the paper to enhance the performance of microgrids, respectively.

II.2.3 Mathematical Approaches

Within the realm of mathematical approaches, MILP has a significant role [111]. This technique is selected for its capacity to secure a globally optimal solution to the optimization problem. In [112], a convex optimization approach was used to determine the optimal sizing and EM of an island microgrid while taking into account the battery degradation. In [113], the study focuses on the optimal sizing, placement, and daily charge/discharge scheduling of a battery within the distribution network. In [114], the paper focuses on utilizing a two-stage stochastic programming. The model addresses uncertainties in DERs power and load demand by ensuring a reliable PV power supply for essential services. In [115], an investigation is conducted on a microgrid system in an island territory, which incorporated multiple technologies such as PV, WT, biomass, and geothermal sources, among others, with the objective function of minimizing the overall costs of the system. The authors in [116] conducted a temporal decomposition using Benders' algorithm to determine the optimal sizing and operation of a hybrid railway power substation annually. In [117], the study explores multi-year economic energy planning optimization in microgrids by employing a MILP method. The authors in [118] utilized linear programming to minimize costs or emissions. They explored the effects of policy on generation investment choices. Similarly, the study in [119] implements a multi-objective MILP approach while focusing on renewable energy investment decisions under various cost and emissions scenarios.

Non-linear approaches play a significant role in optimizing microgrid systems, as seen in the literature where various complex problem formulations are addressed using advanced mathematical models. A mixed integer non-linear program (MINLP) is notably applied to tackle multi-objective optimization problems, such as the one from [120], which focuses on minimizing both the system cost (related to equipment sizing) and emissions. This highlights the capability of MINLP to address multiple aspects of microgrid optimization simultaneously. It provides solutions that balance economic and environmental concerns. In [121], the authors present a non-linear constrained model to identify the optimal mix of microgrid components (hydro, WT, PV, diesel, and BESS) through an iterative approach by employing a Quasi-Newton algorithm. Furthermore, a single objective function is presented in [122] to minimize the system's costs through a non-linear problem formulation. This study extends the application of non-linear optimization to the management of multiple microgrids with incorporating probabilistic modeling of energy resources and load demand. By doing so, it accounts for the inherent uncertainties in energy production and consumption. This enhances the decision-making process for microgrid operation and planning. These non-linear approaches underline the complexity and multidimensional nature of optimizing microgrid systems. They reflect the ongoing advancements in mathematical modeling techniques to achieve more sustainable and

cost-effective energy solutions.

II.2.4 Hybrid Approaches

Hybrid approaches, which involve the integration of multiple algorithms, are increasingly utilized to improve various aspects of microgrid efficiency. The research presented in [111] employs a synergistic application of the JAYA and GWO algorithms to simultaneously minimize annualized costs, carbon emissions, and improve the microgrid's reliability. This approach is recognized for its swift convergence and high accuracy. Conversely, in [123], the authors explore a hybrid model that merges Simulated Annealing and Tabu Search techniques, aimed at achieving optimal sizing for autonomous systems, thereby streamlining computational efficiency. Another significant contribution is reported in [124], where a combination of JAYA, PSO, and Harmony Search algorithms is used in designing hybrid DERs. This configuration, comprising PV systems, biomass, WT, and ESS, is tailored to meet consumer demand in an efficient, cost-effective, and reliable manner. Additionally, in [125], a hybrid strategy combining NSGA-II and MOPSO is implemented to reduce carbon dioxide emissions and the total cost associated with an IMG configuration simultaneously. Furthermore, [126] shows the application of Ant Colony Optimization with Continuous Domain Integer Programming, achieving remarkable accuracy and rapid convergence.

II.3 Microgrid Sizing vs EM Optimization

Optimal sizing of microgrid components and the EM within the system represent pivotal areas of focus in current research. The optimization of these two crucial aspects of microgrid functionality can be undertaken through either a multi-stage or a single-stage methodology.

In the multi-stage optimization paradigm, two primary methodologies are predominantly discussed in the literature. The foremost strategy entails addressing the component sizing dilemma in an initial phase, followed by resolving the EM challenge in a subsequent phase. This sequential methodology leverages optimization-based methods, commercial software solutions, or rule-based strategies for problem formulation. This approach is extensively recognized and prevalent in academic discussions with its general framework depicted in Fig.11. The second form of multi-stage optimization utilizes decomposition algorithms, notably the Dantzig-Wolfe decomposition [128]. This method entails an iterative process that includes several subproblems and a master problem. In each iteration, a new variable is introduced to the master problem, facilitating a gradual convergence towards the solution. Another key decomposition algorithm is the Alternating Direction Method of Multipliers [129], which segments the optimization challenge into multiple subproblems, without incorporating a master problem. Here, each subproblem iteratively shares its solution with the others, aiding in convergence to a global solution. Prominently, Benders' decomposition [130], proposed by Benders [131], is designed to solve mixed-variable optimization problems, with Geoffrion later extending the approach to address nonlinear convex problems [132]. Benders' decomposition effectively bifurcates the target problem into two simpler components: the master problem and one or more

Approach	Advantage	Disadvantage
Commercial software (HOMER)	User-friendly graphical interface and updated to the latest technologies and improvements	Lacks support for multi-objective problems, does not accommodate intra-hour variability. Additionally, it exhibits extended computational times for intricate problem scenarios
Heuristic	Heuristic algorithms efficiently address complex optimization problems including sizing problems within a reduced computation time. Moreover, they exhibit the capability to handle nonlinear equations	It does not guarantee a global optimum [112] and may get stuck in a local optimum. Additionally, each algorithm has specific parameters that require expert knowledge to be adjusted properly, preventing high computation time and infeasible solutions
Mathematical	An effective technique to ensure a global optimal solution in the search space [127]	It cannot solve very complex optimization problems due to the substantial computation time, thereby limiting server capabilities. Additionally, it has limitations in handling stochastic environments and is not suitable for highly complex and nonlinear problems
Hybrid	It exhibits faster convergence compared to heuristic approaches and leverages the advantages of each employed algorithm. This approach is generally used to solve multi-dimensional optimization problem	Coordinating the tuning of parameters for each heuristic algorithm poses a challenge. Additionally, there is a risk of becoming trapped in a local optimum

Table 1: Advantage and disadvantage of each microgrid sizing approach.

subproblems [133]. The master problem, a simplified model, includes a subset of the original variables and constraints, representing a relaxed version of the problem [134]. Conversely, the subproblem(s) mirror the original problem's complexity, conditioned on the premise that the variables derived from the master problem are fixed. The general framework of Benders' decomposition is illustrated in Fig.12. In the context of an optimization problem involving EM and component sizing, the master problem involves to the EM within the microgrid, while the subproblem addresses the sizing of the components. The capacity of each microgrid component is adjusted according to the EM constraints imposed by the optimization algorithm.

The single-stage optimization approach, addressing both sizing and EM in microgrids, presents a substantial challenge in the field. This approach is particularly difficult due to the vast array of constraints and decision variables that must be navigated by optimization solvers. The complexity increases due to the long-term optimization horizon, which ranges from 1 year to the project's lifetime. This period can potentially extend up to 30 years, surpassing the

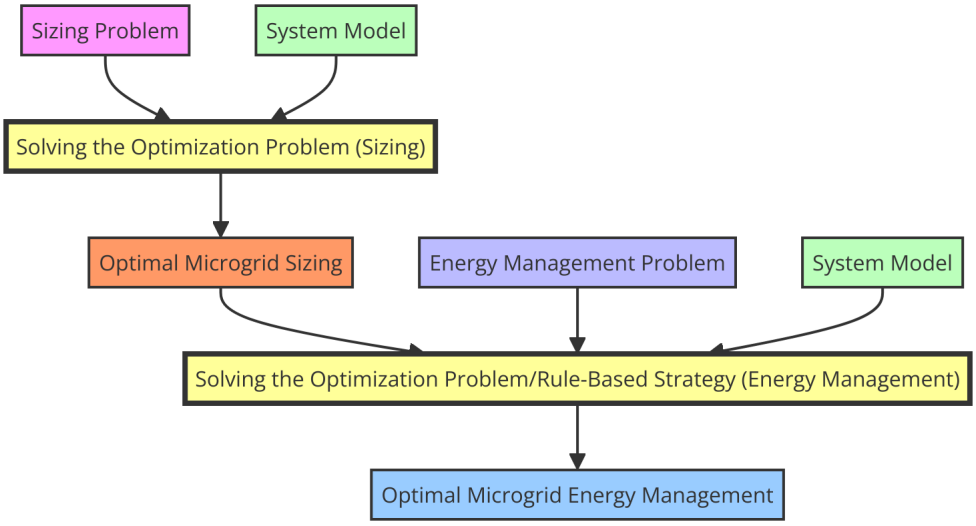

Figure 11: General framework of the multi-stage optimization problem.

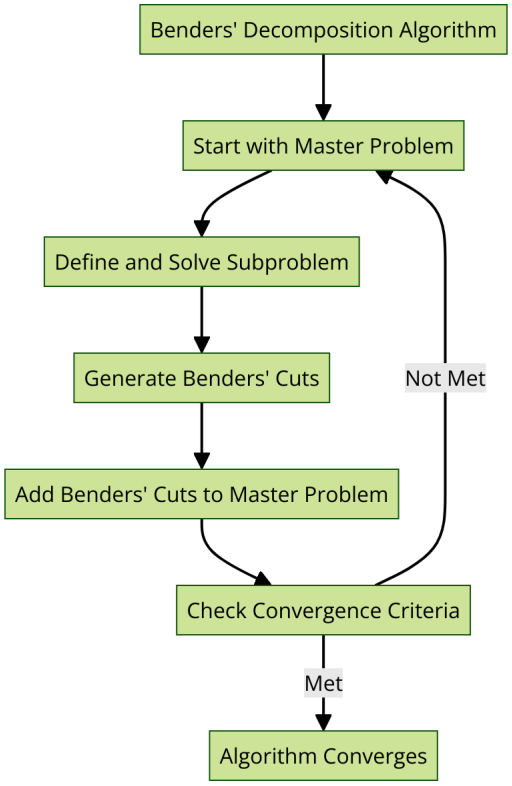

Figure 12: General framework of the Benders' decomposition algorithm.

computational capabilities of conventional computing systems [135]. [135]. Nevertheless, the single-stage methodology is valued for its potential to deliver a global optimal solution because the optimization problem is solved one time instead of several times. The general framework of the single-stage optimization problem is illustrated in Fig.13.

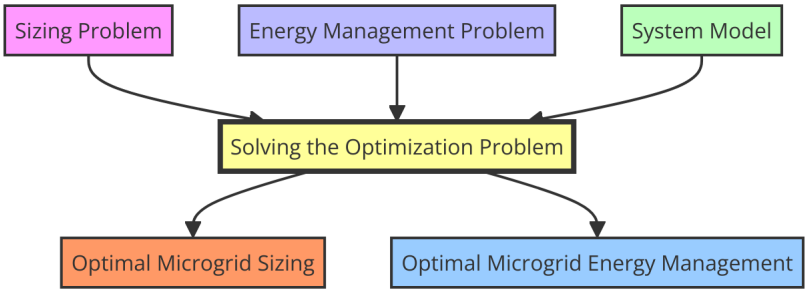

Figure 13: General framework of the single stage problem.

II.3.1 Multi-Stage Co-optimization of Microgrid Sizing and EM

The multi-stage approach illustrated in Fig.11 is widely used in the literature. In [136], the study contrasts hydrogen and BESS in PV systems by employing a GA for optimal sizing and a rule-based strategy. It focuses on self-sufficiency, NPC, and the impact on the EG. In [69], the multi-stage methodology is also applied. The Stochastic Fractal Search (SFS) and the Symbiotic Organisms Search (SOS) algorithms are used for sizing, while the EM is conducted using a rule-based strategy. Another example can be found in [68, 97], where GA is used for sizing and rule-based for EM. The NSGA-II with several rule-based options is presented [67]. The same approach is also presented [102] with the PSO algorithm used for sizing the GCMG. The PSO algorithm is also used in [137] to size the microgrid components where the EM is conducted using simple rules.

Shifting from heuristic approaches for sizing and rules based for EM, some studies implemented optimization algorithms for both stages. In [55], the model uses the Karush – Kuhn – Tucker approach to simplify the bi-level problem into a single-level one. A mix of binary PSO and quadratic programming finds the optimal BESS size and operation schedule in order to enhance microgrid design and reliability. In [138], the methodology applies the two-stage methodology where the first stage focuses on determining the size of the microgrid, while the second stage addresses the daily EM considerations. This study implements MILP optimization techniques in both stages. In [135], the first stage employs an evolutionary algorithm to handle the sizing task, exploring a vast solution space to identify viable configurations. In the second stage, MILP fine-tunes these configurations by meticulously scheduling microgrid assets to balance demand fulfillment with the dual objectives of cost minimization and reliability maximization. A similar approach is found in [139], where the study uses a GA to identify optimal sizing solutions that concurrently lower the lifecycle CO_2 emissions and total costs of the microgrid. Moreover, An EM strategy is developed, employing a MILP algorithm to efficiently distribute power flow while also reducing CO_2 emissions. In [140], a stochastic two-stage model is presented for optimizing microgrid design by addressing the uncertainties in DERs. The initial stage focuses on setting capacities for PV, WT, diesel generation, and ESS, while the second stage targets operational decisions, such as diesel and ESS usage. The study in [141] introduces a method for optimizing microgrid components in 'El Espino' community. It uses linear programming firstly to minimize costs while meeting energy needs, and secondly to incorporate operational and reliability constraints. In [142], the paper applies a two-stage stochastic optimization approach to minimize both capital and operational costs taking into

account uncertainties in demand.

Benders decomposition algorithm is used in [143], showcases a multi-stage optimization process for microgrid sizing and EM using the iterative Benders decomposition algorithm. In [144], the optimization is decomposed into two principal components: the investment decision-making as a master problem and the EM as a sub-problem. By distinguishing between design decision variables and EM variables, this strategy enhances the efficiency of solving the planning problem. It iteratively addresses these interconnected components, thereby optimizing both the investment and operational phases of microgrid management. In [145], the paper tackles the intermittency of DERs using Benders' decomposition, which breaks down the optimization problem into smaller and manageable sub-problems. This approach facilitates sizing and scheduling by treating PV generation as a stochastic input, showing how Benders' decomposition aids in determining the appropriate size and operation schedule for storage and microturbine units. The study in [146] outlines a two-stage stochastic MILP model for optimizing investments in renewable energy within DERs. Its goal is to lower costs associated with investments in PV and WT, as well as operational and total substation expenses, which include energy purchases and losses. The innovative aspect of this study is the use of Benders' decomposition, which simplifies the complex problem by separating investment from operational decisions. In [147], the study presents a parallel multi-period optimal scheduling algorithm for microgrids incorporating ESSs and addressing the challenges of DERs integration. It optimizes microgrid operations by decomposing inter-temporal constraints. Utilizing both generalized Benders' decomposition and optimality condition decomposition.

II.3.2 Single-stage Co-optimization of Microgrid Sizing and EM

The single-stage optimization approach is rarely utilized in literature due to computational challenges. Within this approach, MILP is commonly used to solve single-stage optimization problems to find the optimal configuration for the sizing and EM of the microgrid. In [115], a MILP framework integrates sizing and EM into one optimization problem by analyzing scenarios for Reunion Island's transition to renewable energy by 2030 and 2050. Another example can be found in [148], where the optimization problem addresses the optimal sizing and energy dispatch of a residential microgrid incorporating PV, a WT, EG connection. In [149], the paper demonstrates a cost optimization approach that incorporates hourly dispatch and load demand within an IMG. In the study by [150], cost minimization is realized through MILP, complemented by an additional sensitivity analysis conducted over the LPSP. Similarly, in [151], a multi-objective function is formulated using MILP and a trade off constraint approach, aiming to simultaneously minimize both costs and emissions. Concentrating on minimizing the LCOE, the research presented in [127] also formulates the optimization problem using MILP. The results highlight that a microgrid composed of WT, PV, diesel, and BESS exhibits the lowest LCOE compared to alternative combinations. In [152], MILP is similarly employed where authors explore scenarios where a PV-fuel cell-BESS system is employed to fulfill residential energy requirements within a GCMG environment. The study in [153] introduces a multi-objective optimization approach for the planning and operation of GCMGs, incorporating various energy sources. It focuses on achieving economic efficiency and enhancing customer

satisfaction by implementing demand side management and employing a fuzzy logic-based method to maximize satisfaction.

II.3.3 Multi-objective Functions

The objectives of optimization within the framework of sizing and EM can be realized through various forms. Some studies focus on minimizing the annual costs [154] and the cost per kilowatt-hour produced (LCOE) [155], or the NPC [101]. Others aim at enhancing the autonomy of the microgrid [102] or reducing the CO_2 emissions [100], among other objectives (e.g., decreasing the nuclear consumption from the EG). While certain investigations consider a single objective function, there are studies that address multiple objective functions simultaneously. In the context of multi-objective optimization problems, a variety of approaches can be employed to address these complexities such as the weighted sum approach, hierarchical optimization method, trade-off method, global criterion method, and goal programming method [156].

Weighted Sum Approach

- **Advantage**: The Weighted Sum Approach is appreciated for its simplicity due to its straightforward implementation and understanding. It allows the adjustment of weights according to the significance of each objective, providing a clear way to prioritize among different goals. By transforming multiple objectives into a single composite objective using weights, this method simplifies the optimization process. This consolidation renders the multi-objective problem compatible with traditional optimization techniques and tools, which makes the solution process more manageable.
- **Disadvantage**: The effectiveness of the Weighted Sum Approach significantly relies on the selection of weights for each objective. Consequently, the solution's quality and acceptability depend on these chosen weights. With different sets of weights leading to vastly different solutions, identifying the optimal weights to balance the importance of each objective is both critical and challenging. Moreover, when objectives are on substantially different scales, assigning weights that accurately reflect each objective's relative importance becomes complicated. This often necessitates the normalization of objectives to a common scale, which introduces additional complexity to the optimization process.

Hierarchical Optimization Method

- **Advantage**: This method's prioritization strategy guarantees that the most critical objectives are addressed firstly, which is paramount in scenarios where failing to meet primary objectives could negate the relevance of secondary objectives. In environments where some objectives cannot be compromised, such as safety-critical systems, environmental conservation, or healthcare, prioritizing these ensures alignment with the scenario's overarching goals and ethical considerations. This ensures that the optimization process respects the most critical requirements.

- **Disadvantage**: There exists a substantial risk that lower-priority objectives might not receive sufficient consideration if high-priority objectives significantly consume resources. This situation could yield solutions that, albeit satisfying primary goals, are sub-optimal in the context of the broader problem. The potential depletion of resources on high-priority objectives might marginalize secondary goals, undermining the comprehensive quality of the solution. Furthermore, optimizing objectives sequentially by importance can introduce challenges when objectives are highly interdependent. Enhancing one objective might impair another, especially if improvements in one domain lead to regressions in another. This complicates the pursuit of a balanced and globally optimal solution.

Trade-off method

- **Advantage**: Trade-off analysis aids in identifying Pareto optimal solutions, where improving any objective would lead to the detriment of at least one other objective. This approach is crucial for ensuring that chosen solutions are efficient from a multi-objective standpoint.
- **Disadvantage**: The process of analyzing trade-offs can become increasingly complex as the number of objectives grows. This complexity necessitates the use of advanced tools and expertise.

Global Criterion Method

- **Advantage**: Targets the identification of a solution that optimizes all objectives concurrently, potentially yielding more balanced and universally acceptable outcomes. Moreover, concentrating on a singular, global criterion enhances efficiency in discovering a solution that moderately satisfies all objectives, diminishing the necessity for iterative or repeated optimization processes.
- **Disadvantage**: Developing a global criterion that accurately encapsulates the significance of all objectives poses a challenge, particularly in scenarios where the objectives significantly conflict or are difficult to quantify. Furthermore, a singular focus on a global criterion may result in missing some Pareto optimal solutions, especially those poorly represented by the selected global criterion.

Goal Programming Method

- **Advantage**: Goal programming enables the concurrent consideration of various goals, with the possibility of assigning different priorities to each. This adaptability proves advantageous in intricate decision-making contexts, where it is essential to navigate trade-offs among conflicting objectives.
- **Disadvantage**: This approach depends significantly on the decision-maker's capacity to precisely establish and rank goals. Such reliance can inject subjectivity into the process, potentially skewing the results.

A core principle in the study of multi-objective optimization is the concept of the Pareto front, which is alternatively referred to as the Pareto set or Pareto frontier. This concept encapsulates a collection of dominated and non-dominated solutions within the framework of multi-objective optimization. It highlights the essential compromises that must be made between conflicting objectives. The Pareto front serves as a visual representation of these trade-offs.

II.4 Challenges and Research Gaps

The co-optimization of microgrid sizing and EM presents significant challenges due to complex mathematical equations and extensive computational time, often exceeding the capabilities of standard computers. Additionally, the design and implementation of the EM model, including factors like time resolution and simulation length, can greatly impact the results. Therefore, the requirements and capacities of EM are crucial in the sizing process. This is particularly evident in MILP-formulated optimization problems, where maintaining problem linearity while managing a vast array of constraints and decision variables is demanding. Techniques such as the "Big M" method, which introduces a binary decision variable, add further complexity to the optimization process. Several studies have formulated their sizing and EM problems using MILP. For instance, the study in [127] established stopping criteria—either a maximum CPU time of 10,800 seconds or an optimality gap of 5%—to manage computational complexity. Additionally, a study referenced in [151] employed representative days as a strategy to mitigate computational demands. The study in [150] used MILP for sizing and EM in IMGs, but their approach lacks formulation for GCMG optimization and overlooks CO_2 emission considerations. Furthermore, comparative analyses of different approaches are scarce in the literature. In [101], the study compared metaheuristic approaches for EM sizing, and [85] contrasted heuristic approaches with commercial software solutions. However, comparisons between heuristic and mathematical approaches or between single-stage and multi-stage optimization processes are notably absent. Additionally, the choice of technologies for microgrid components, such as PV, WT, and BESS, significantly influences planning results due to varying costs and CO_2 emissions. Research comparing different microgrid components to enhance decision-making capabilities for planners is rare. Comparing the performance of microgrids under identical conditions across different geographical locations could provide valuable insights into optimal microgrid placement, both nationally and internationally. Yet, this type of analysis is uncommon in current literature. Installing GCMG in France presents unique considerations due to the country's low CO_2 emissions from the EG, which are attributed to its reliance on nuclear energy. Moreover, the dynamic nature of greenhouse gas emissions is not adequately addressed in existing studies, potentially affecting EM outcomes if emissions are considered within the optimization objective. This oversight represents another gap in the literature. Table 2 gives a summary of different studies that treat the sizing and EM of the microgrid.

Table 2: Literature review on the optimal sizing of microgrids.

Ref	Methodology	Loads considerations		System EV load	Analysis			GCMG	Optimized components				Objective function
		EV load	Building load		Tech	Econ	Env		WT	PV	ESS	CV	
[157]	MILP	√	√	Deterministic	√	√		√		√	√		LCOE
[158]	MILP	√	√	Deterministic	√	√		√	√	√	√		Total cost
[138]	MILP	√	√	Probabilistic	√	√			√	√	√		LCC & reliability
[159]	HOMER(PDFA,OGSA)	√	√	Probabilistic	√	√	√	√		√	√	√	LCOE/NPC
[160]	Mixed PSO	√		Deterministic	√	√		√			√		Daily cost
[139]	GA& MILP		√		√	√	√			√	√		Hourly cost & emissions
[161]	AHA,PSO,GA	√	√	Probabilistic	√	√			√	√	√	√	NPC
[162]	MOPSO, MOGOA	√	√	Probabilistic	√	√	√	√	√	√	√		LOPS & cost & CO_2 emissions
[88]	GA & HOMER	√	√	Probabilistic	√	√	√	√	√	√	√		LCOE
[89]	GAMS & HOMER		√		√	√			√	√	√		NPC
[163]	PSO & MINLP		√		√	√				√	√		TOC & TIC
[164]	GA	√		Deterministic	√					√	√		Hourly charge demand
[165]	NSGA-II	√	√	Probabilistic	√	√	√	√		√	√		Total cost, LPSP, WE, Load matching variance
[135]	GA & MILP		√		√	√				√	√		Total cost
[69]	SFS, SOS, PSO		√		√	√			√	√	√	√	LCOE, LPSP
[143]	MILP (Benders' algorithm)		√		√	√				√	√		LCC
[67]	NSGA-II		√		√	√	√		√	√	√		LCOE
[148]	MILP	√	√	Deterministic	√	√			√	√	√		Annual cost
[68]	GA		√		√	√	√	√		√	√		LCOE
[102]	PSO		√		√	√	√	√	√	√	√		LCOE & autonomy
[86]	HOMER	√	√	Probabilistic	√	√		√	√	√	√		LCOE
[139]	GA & MILP		√		√	√	√		√	√	√		Emissions, capital & maintenance costs
[100]	Matlab toolbox		√		√	√	√		√	√	√		LCA & NPC
[98]	HHO		√		√	√		√	√	√	√	√	LCOE & LPSP
[84]	HOMER		√		√	√		√	√	√	√		NPC
[85]	HOMER & GA		√		√	√	√			√	√		NPC
[103]	HOMER		√		√	√	√		√	√	√		NPC
[108]	GOA & PSO		√		√	√			√	√	√		LCOE & LPSP

Chapter III

Optimal Microgrid Sizing and Energy Management: A Combined MILP Approach for Reducing Energy Costs and Carbon Emissions

The objective of this research is to enhance the decision-making capabilities of microgrid designers by providing them with a comprehensive approach for system planning for both IMG and GCMG operation modes. This research uses a joint multi-objective optimization strategy with MILP, ensuring a globally optimal solution [127]. It enables designers to make more informed and effective design choices. These choices involve evaluating various proposed solutions and balancing cost and carbon emissions while considering the technical constraints of the EM problem. This approach addresses the complexities and trade-offs fundamental to microgrid design.

One of the key novel aspects of this work is the integration of EM and component sizing into a unified optimization problem while ensuring an optimality gap of 0 % with a decreased computation time in comparison with the existing literature. Implemented in Python and solved using CPLEX, the optimization process aims to minimize both the LCOE and the LCE. The proposed method allows to perform a comprehensive analysis by evaluating the interdependence among components and their collective influence on the overall system performance in terms of emission and cost over the project lifetime. Additionally, by identifying the Pareto front —a set of optimal trade-off solutions— the chapter provides valuable insights by proposing the range of feasible solutions and the associated compromises between economic and environmental objectives.

The overall structure of the study, as depicted in Fig. 14, encompasses a comprehensive set of inputs, including electrical load data, ambient temperature data, solar irradiation data, TOU tariffs with EG subscription costs, and economic and environmental data for each microgrid component. These inputs form the foundation for the system model, which incorporates the physical models of PV systems, BESS, EG, and the associated converters. By unifying EM and component sizing within a single framework, the optimization problem yields the optimal EM strategy and optimal component sizes for the microgrid system. The main contributions of this study are:

- integrating the sizing and EM challenges within a DC microgrid framework, with due consideration to a project lifespan spanning 20 years. The focus extends to achieving hourly optimal EM within the microgrid;
- encompassing technical, economic, and environmental dimensions in the microgrid context through the formulation of a unified multi-objective MILP algorithm. The algorithm's primary objective is to find an optimal solution, minimizing both the LCOE and the LCE of the microgrid, all while optimizing computational efficiency;
- varying the LCE constraint value to analyze and compare the Pareto front and the variation in BESS and PV capacities of the GCMG and IMG operation modes;
- evaluating the influence of peak shaving on the LCOE and LCE of the microgrid by calculating the average variation for each EG limit;
- assessing the impact of load increase on the LCOE and LCE for both IMG and GCMG operation modes;

- analyzing the energy sources utilized in the French EG under different LCOE and LCE scenarios where this assessment involves examining the proportional contribution of each energy source and exploring seasonal trends; and
- maximizing the consumption of renewable energy within the microgrid to enhance sustainability, reduce reliance on non-renewable sources, and improve overall energy efficiency.

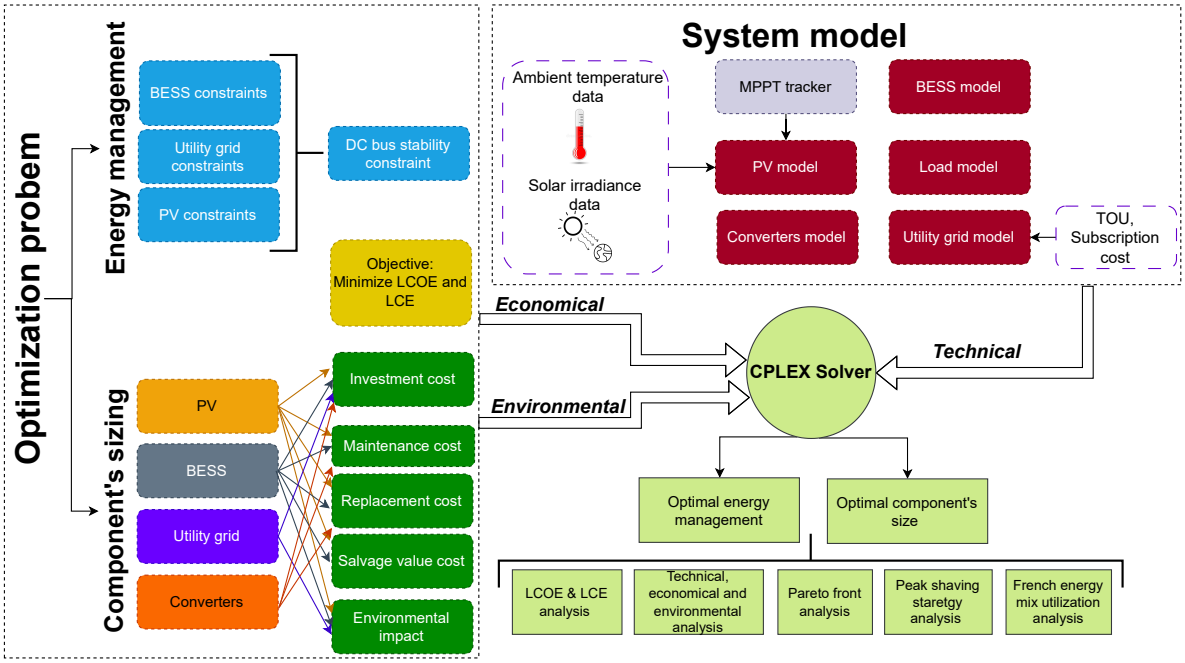

Figure 14: General framework of the proposed multi-objective joint optimization algorithm.

This chapter is organized as follows: Section III.1 presents the system modeling. The formulation of the optimization is detailed in Section III.2. Section III.3 discusses the results and analysis. A discussion on the findings is provided in Section III.4, while the conclusions are summarized in Section III.5.

III.1 System Modeling

This chapter analyzes a university campus DC microgrid, which includes a DC bus, PV system, BESS, a connection to the EG, two DC/DC converters, an AC/DC converter, and a DC/AC converter. The architecture of the microgrid is shown in Fig. 15, which is designed to operate with and without the EG connection. Excess power generated from the PV system is curtailed if the load demand is met, the BESS is fully charged, and the EG has reached its maximum injection limit (GCMG mode). Each component is formulated prior to determining the optimal sizing and the EM strategy of the DC microgrid in the rest of this section. The MPPT mode of the PV system is accomplished through the associated converter. The efficiency of all converters is assumed to be constant for simplicity in this study.

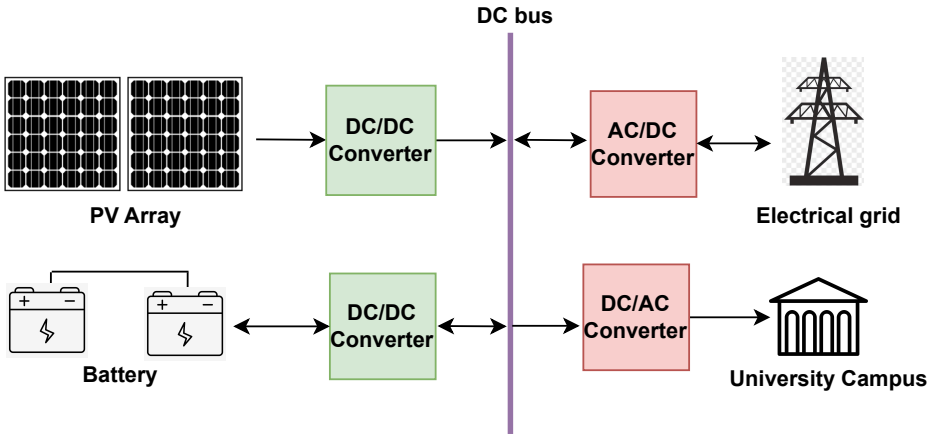

Figure 15: The architecture of the studied microgrid.

III.1.1 PV System Modeling

In this study, Eq. (1) is used to calculate the PV output power $p_{PV}^{MPPT}(t)$ at each time instant t, which depends on the solar irradiation and ambient temperature data. It is assumed that the PV system operates in MPPT mode and its power output is determined by [166] :

$$p_{PV}^{MPPT}(t) = p_{PV\_STC} \cdot \frac{irr(t)}{1000} \cdot (1 + \gamma \cdot (T_{PV}(t) - 25)) \cdot N_{PV} \tag{1}$$

$$\text{with } t = \{t_0, t_0 + \Delta t, ..., t_f\}$$

where p_{PV_STC} is the PV panel rated power at standard test conditions (STC). The STC stands for conditions to standardize the performance characteristics of PV panels. It typically refers to a solar irradiation of 1000 W/m^2, solar spectrum of air mass 1.5, and PV cell temperature at 25 ℃ [167]. irr is the measured solar irradiation, γ is the power temperature coefficient of the PV panel, T_{PV} is the PV cell temperature, N_{PV} is the number of PV panels, and t, t_0, Δt, and t_f are the continuous time, initial time, time step, and simulation time, respectively. In Eq. (2), the PV cell temperature is calculated as follow [166]:

$$T_{PV}(t) = T_{amb}(t) + g(t) \cdot \frac{NOCT - 20}{800} \tag{2}$$

where T_{amb} is the ambient temperature, and $NOCT$ is the nominal operating cell temperature.

III.1.2 Battery System Modeling

The battery is utilized as the energy storage system in the microgrid to fulfill the energy requirements in the absence of enough renewable production using stored excess PV production at high renewable production times. The energy transfer between the EG and the battery is prohibited in this study, hence the battery can only be charged by PV production and discharged for local load.

The battery models can be summarized in three models: the first is the charge model, which consists of modeling the state of charge (SOC) of the battery [168], the second is the voltage

model, which focuses on modeling the terminal voltage for more detailed losses calculation [169], and the third is the lifetime model which assesses the impact of the operations on the battery lifetime [170]. These models could be independent or interdependent from each other. In this study, the charge model is considered as follows:

$$e_b(t) = e_b(t-1) + (p_b^c(t) + p_b^d(t)) \cdot \Delta t \tag{3}$$

where $e_b(t)$ is the quantity of energy at each instant; and $p_b^c(t)$, and $p_b^d(t)$ are the charging and discharging powers of the battery, respectively. Eq. (3) represents the charge model for the battery, despite not considering the SOC. The reason for this choice is to maintain the linearity of the optimization problem, as the calculation of SOC involves dividing two decision variables (charge/discharge powers and BESS capacity), which makes the problem formulation nonlinear.

III.2 Formulation of the Joint Multi-Objective Optimization Problem

The optimization problem considers both economic and environmental objectives and aims to find a trade-off between them. By balancing the competing objectives, the joint multi-objective optimization problem enables the design of a microgrid that integrates cost-effective solutions while reducing CO_2 emissions. While the constraints for both IMG and GCMG are almost similar, the IMG excludes constraints related to the EG. The constraints and objective functions are discussed in the following sections.

III.2.1 Constraints

In the optimization problem, constraints play a crucial role in defining the feasible solution space. Firstly, the quantity of BESS energy $e_b(t)$ is restricted by the maximum and the minimum allowed SOC as follows:

$$SOC_{min} \cdot E_b \leq e_b(t) \leq SOC_{max} \cdot E_b \tag{4}$$

where E_b is the installed capacity of the BESS in kWh; and SOC_{min} and SOC_{max} are the minimum and maximum SOC of BESS, respectively. Ensuring a dependable energy supply for the subsequent year is of paramount importance, necessitating that the stored energy within the BESS at the end of the one-year simulation equals or surpasses the initial battery energy (taken as 50% of the storage capacity in this study). This strategic choice is implemented to guarantee a sufficiently robust BESS energy reserve capable of meeting the anticipated load demands in the forthcoming year. Omitting this constraint from the optimization algorithm could result in the BESS SOC settling at the minimum SOC level, potentially leading to load shedding in the subsequent year due to inadequate stored energy in the BESS. This constraint is formulated as follows:

$$e_b(t_f) \geq 0.5 \cdot E_b \tag{5}$$

where $e_b(t_f)$ is the BESS energy at the end of the one-year simulation.

To specify the power flow of the BESS and the EG powers, the constraints on BESS charge/discharge powers ($p_b^c(t)/p_b^d(t)$) and the utility supply/inject powers ($p_{EG}^{in}(t)/p_{EG}^{in}(t)$) are established as follows:

$$p_b^c(t) \geq 0,\ p_b^d(t) \leq 0 \tag{6}$$

$$-p_{EG}^{max} \leq p_{EG}^{s}(t) \leq 0 \tag{7}$$

$$0 \leq p_{EG}^{in}(t) \leq p_{EG}^{max} \tag{8}$$

where p_{EG}^{max} is the maximum limit that can be supplied/injected by/into the EG. The convention of representing injection as positive and supply as negative is to reflect the direction of power flow. The constraints for maximum charge/discharge powers of the BESS are not included into the formulation due to the conflicting need of determining the optimal capacity of the BESS-associated converter in the sizing optimization problem. Therefore, to determine converter capacities, the nominal power value of the associated converters of the PV, BESS, building load, and EG is considered to be equal or greater than electric power that flows through them as stated below:

$$p_{PV}^{MPPT}(t) \leq M_{PV}^{DC/DC} \tag{9}$$

$$-p_b^d(t) \cdot \mu_d + p_b^c(t)/\mu_c/\gamma_b^{DC/DC} \leq M_b^{DC/DC} \tag{10}$$

$$-p_{EG}^{s}(t) + p_{EG}^{in}(t)/\gamma_{EG}^{DC/AC} \leq M_{EG}^{AC/DC} \tag{11}$$

$$p_{buil}(t)/\gamma_{buil}^{DC/AC} \leq M_{buil}^{DC/AC} \tag{12}$$

where $M_{PV}^{DC/DC}$, $M_b^{DC/DC}$, $M_{EG}^{AC/DC}$, and $M_{buil}^{DC/AC}$ are the nominal power capacity of the PV, the BESS, the EG, and the building converters, respectively; and $\gamma_b^{DC/DC}$, $\gamma_{EG}^{DC/AC}$, and $\gamma_{buil}^{DC/AC}$ are the efficiency of the BESS, EG, and building converters, respectively.

If the load power surpasses the PV power, the BESS should discharge and/or the EG should provide power. Conversely, the BESS must be charged and/or the surplus power should be fed into the EG. Therefore, the EM within the microgrid typically requires the use of "if-else" conditions to control the power flow among each microgrid component. The "if-else" statements are used in programming to make decisions based on certain conditions; however, they cannot be expressed as linear equations or inequalities, hence it cannot be used directly in linear programming (LP). However, some formulations of certain problems may require the use of binary variables for the "if-else" statement, and in such cases alternative techniques may be used to model the optimization problem. As a solution in this study, the "Big M" method is employed that introduces a large constant value M (typically set to 10^4) and a binary decision variable $x_{aux}(t)$. The Big M method works by defining constraints that represent the conditions in "if-else" statements. The binary decision variable takes on either the value of 1 or 0, and the large constant value is used to penalize the objective function if the conditions are not met. When $x_{aux}(t) = 1$, the constraints corresponding to the "if" part of the "if-else" statement are active, otherwise if $x_{aux}(t) = 0$ the "else" constraints are active. This allows to consider the different scenarios represented by the "if-else" conditions, while the optimization problem remains linear [171].

Therefore, to determine whether the load power is greater than or less than the PV power, constraints in Eqs. (13) and (14) are introduced using Big M method as follows:

$$M \cdot x_{aux}(t) - (p_{buil}(t)/\gamma_{buil}^{DC/AC} - \gamma_{PV}^{co} \cdot p_{PV}^{MPPT}(t)) \geq 0 \tag{13}$$

$$M \cdot (1 - x_{aux}(t)) - (\gamma_{PV}^{co} \cdot p_{PV}^{MPPT}(t) - p_{buil}(t)/\gamma_{buil}^{DC/AC}) \geq 0 \tag{14}$$

where γ_{PV}^{co} is the PV converter efficiency, and $p_{buil}(t)$ is the load demand. In Eqs. (13) and (14), $x_{aux}(t) = 0$ when $p_{PV}^{MPPT}(t) - p_{buil}(t) \geq 0$ and $x_{aux}(t) = 1$ when $p_{buil}(t) - p_{PV}^{MPPT} \geq 0$. Once $x_{aux}(t)$ is determined, the "if-else" conditions are implemented using constraints to control the BESS and EG powers as follows:

$$p_{EG}^{s}(t) \cdot \gamma_{EG}^{DC/AC}, p_b^d(t) \cdot \gamma_b^{DC/DC} \cdot \mu_d \geq -M \cdot x_{aux}(t) \tag{15}$$

$$p_{EG}^{in}(t)/\gamma_{EG}^{DC/AC}, p_b^c(t)/\mu_c/\gamma_b^{DC/DC} \leq M \cdot (1 - x_{aux}(t)) \tag{16}$$

where $\gamma_b^{DC/DC}$ represents the efficiency of the BESS converter, and μ_c and μ_d represent the charging and discharging efficiencies of the battery, respectively. In Eqs. (13) and (14), the algorithm determines $p_{EG}^{s}(t) = 0$, $p_b^d(t) = 0$ when $x_{aux}(t) = 0$ and $p_{EG}^{in}(t) = 0$, $p_b^c(t) = 0$ when $x_{aux}(t) = 1$. The control of the battery discharge and the EG supply in order to not exceed the load power within the system is formulated as follows:

$$p_{EG}^{s}(t) \cdot \gamma_{EG}^{DC/AC} + p_b^d(t) \cdot \gamma_b^{DC/DC} \cdot \mu_d + M \cdot (1 - x_{aux}(t)) \geq -(p_{buil}(t)/\gamma_{buil}^{DC/AC} - \gamma_{PV}^{co} \cdot p_{PV}^{MPPT}(t)) \tag{17}$$

In the absence of Eq.(17), there is a possibility that the battery can over-discharge beyond the required load demand. This situation arises due to the conditions described in Eqs. (15) and (16), when $x_{aux}(t) = 1$, the optimization algorithm might discharge the BESS more than the load demand (avoid selling energy to EG). Additionally, it's important to note that in convex optimization, multiple optimal solutions can exist, but Eq.(17) serves the critical purpose of eliminating solutions where the battery is discharged beyond the load demand, ensuring the appropriate power balance.

Lastly, the DC bus net power $p_{bus}(t)$ of the system is determined by summing the entering/leaving powers on the DC bus of the microgrid as in Eq. (18):

$$\begin{aligned} p_{bus}(t) = {} & p_{buil}(t)/\gamma_{buil}^{DC/AC} - \gamma_{PV}^{co} \cdot p_{PV}^{MPPT}(t) + p_b^c(t)/\mu_c/\gamma_b^{DC/DC} \\ & + p_b^d(t) \cdot \gamma_b^{DC/DC} \cdot \mu_d + p_{EG}^{s}(t) \cdot \gamma_{EG}^{DC/AC} + p_{EG}^{in}(t)/\gamma_{EG}^{DC/AC} \leq 0 \end{aligned} \tag{18}$$

According to Eq. (18), when $p_{bus}(t) < 0$, the produced PV power exceeds the total consumption power, battery charging, and grid selling powers, hence the surplus generation should be curtailed. On the other hand, when $p_{bus}(t) = 0$, the generation and consumption powers are equal, thus there is no surplus generation in the DC microgrid. However, it should be noted that if $p_{bus}(t)$ was chosen to be strictly equal to zero in Eq. (18), the algorithm would be forced to utilize all the PV power, which means that the excess power should be either injected into the EG or stored in the BESS. Therefore, the algorithm in this case increases the capacity of the BESS and reduces the capacity of the PV system to obtain $p_{bus}(t) = 0$ for all times. However, this will not be the most cost-effective solution (if the cost of the PV system is lower than BESS), because the algorithm will force increasing the BESS capacity in order to reduce curtailment. To avoid that situation, PV curtailment is allowed by enabling $p_{bus}(t) \leq 0$ in Eq. (18).

III.2.2 Objective Functions

The multi-objective optimization problem is formulated to obtain the system's minimal annual LCOE and LCE while ensuring an optimized EM. The LCOE is the average cost per unit of producing electricity over the lifetime of a power plant, while LCE is the total amount of CO_2 emissions produced over the entire life cycle of a product. The LCOE is calculated as in [68]:

$$LCOE = \frac{TC \cdot CRF}{\sum_{t_0}^{t_f} (p_{buil}(t)/\gamma_{buil}^{DC/AC}) \cdot \Delta t} \tag{19}$$

where TC is the total cost over the project lifetime, CRF is the capital recovery factor. The CRF is a financial metric used to determine the annual capital cost from the project lifetime cost [172]. The TC and the CRF are calculated as follows:

$$TC = C_{inv} + C_{mtn} + C_{rep} + C_{EG} - C_{sv} \tag{20}$$

$$CRF = \frac{d \cdot (1+d)^Q}{(1+d)^Q - 1} \tag{21}$$

where d is the discount rate, Q is the project lifetime, and C_{inv}, C_{mtn}, C_{rep}, C_{EG}, C_{sv}, are the investment, maintenance, replacement, grid, and salvage value, respectively, which are calculated as [68]:

$$C_{inv} = \sum_{k=1}^{K} C_{inv}^k \cdot N^k + C_{dep} \tag{22}$$

$$C_{mtn} = \sum_{k=1}^{K} C_{mtn}^k \cdot N^k \cdot \sum_{q=1}^{Q} \left(\frac{1+\varepsilon}{1+d}\right)^q \tag{23}$$

$$C_{rep} = \sum_{k=1}^{K} C_{rep}^k \cdot N^k \cdot \sum_{r=1}^{NOR} \left(\frac{1+\varepsilon}{1+d}\right)^r \tag{24}$$

$$C_{EG} = \left(C_{sub} - \Delta t \cdot \left(\sum_{t_0}^{t_f} p_{EG}^s(t) \cdot \lambda^s(t) + p_{EG}^{in}(t) \cdot \lambda^{in}\right)\right) \cdot \sum_{q=1}^{Q} \left(\frac{1+\varepsilon}{1+d}\right)^q \tag{25}$$

where N^k is the total number of the k^{th} microgrid component (PV, BESS, etc.), K is the total number of microgrid components, and C_{inv}^k and C_{dep} are the k^{th} component investment cost and the microgrid deployment cost, respectively.

The microgrid deployment cost includes the installation of the microgrid components (such as wiring, concrete, steel, wood, and electrical connections), as well as labor costs and indirect costs associated with the microgrid installation. For the k^{th} microgrid component, C_{mtn}^k is the operation and maintenance; ε is the escalation rate; C_{rep}^k is the replacement cost; NOR is the number of r^{th} component replacement over the project lifetime; q and r are the year and replacement indices, respectively; and λ^s and λ^{in} are the grid tariffs for power supply (buying from grid) and injection (selling to grid), respectively. Finally, C_{sub} represents the fixed subscription cost for the EG which is a fixed annual fee imposed by the French EG companies [173] and is paid by customers to maintain their connection to the grid, covering infrastructure upkeep and operational expenses. The subscription cost is determined by the utility companies, and its value is taken differently based on the registered maximum power rating (allowed peak

consumption) of the grid connection. The salvage value is considered to be 10% of the PV investment cost and 20% of the battery investment cost [68].

The second objective function is formulated to obtain the system's minimal annual LCE given in Eq. (26) as follows:

$$LCE = \frac{LCE_{PV} + LCE_{BESS} + LCE_{EG} + LCE_{cables}}{\sum_{t_0}^{t_f} (p_{buil}(t)/\gamma_{buil}^{DC/AC}) \cdot \Delta t} \tag{26}$$

$$LCE_{PV} = \frac{\alpha_{PV} \cdot p_{PV}^{MPPT}}{Q} \tag{27}$$

$$LCE_{BESS} = \frac{\alpha_b \cdot E_b \cdot (NOR + 1)}{Q} \tag{28}$$

$$LCE_{EG} = \sum_{t=t_0}^{t_f} p_{EG}^{s}(t) \cdot \alpha_g(t) \cdot \Delta t \tag{29}$$

$$LCE_{cables} = \frac{\alpha_{cables} \cdot \varsigma_{cables}}{Q} \tag{30}$$

where LCE_{PV}, LCE_{BESS}, LCE_{EG}, and LCE_{cables} are the LCE of the PV system, BESS, the EG, and the cables respectively; α_{PV} is the equivalent CO_2 emissions of the PV system per kWp; α_b is the equivalent CO_2 emissions of the BESS per kWh installed; and $\alpha_g(t)$ is the dynamic emissions from the EG per kWh.

The optimization problem aims to minimize two objective functions, which are LCE and LCOE. Several approaches are used to solve a multi-objective optimization problem such as weighted-sum, trade-off constraint, hierarchical, goal programming, and global criterion methods [156]. In this study, the trade-off constraint approach is used as follows:

$$\min\{LCOE\} \tag{31}$$

$$LCE \leq \varepsilon \tag{32}$$

where ε represents predetermined value that the objective functions are not allowed to surpass. The trade-off methodology, a widely adopted strategy in multi-objective optimization, involves the transformation of one of the two objective functions into an inequality constraint with an upper bound represented by ε. By manipulating the parameter ε, multiple solutions for the LCOE can be derived. This method effectively converts the original multi-objective optimization problem into a mono-objective form. The motivation for adopting this approach arises from the distinct units of measurement associated with LCOE and LCE. However, this method eliminates the need to convert the units of the two separate objective functions.

The optimization problem in Eq. (31) is solved by determining the following decision variables under the constraints in Eq. (4) to Eq. (18) with the Eq.(32): the BESS capacity (E_b), the number of PV panels (N_{PV}), the BESS charge/discharge powers ($p_b^c(t)/p_b^d(t)$), the EG supply/inject powers ($p_{EG}^s(t)/p_{EG}^{in}(t)$), and the auxiliary variables ($x_{aux}(t)$); and the capacity of PV, BESS, and the EG associated converters ($M_{PV}^{DC/DC}$, $M_b^{DC/DC}$, $M_{EG}^{AC/DC}$).

III.3 Results and Analysis

The meteorological data for Compiègne, a city located in northern France (latitude: 49.41° North, longitude: 2.82° East), serves as the primary case study for conducting simulations. The solar irradiation and ambient temperature data, presented in Fig 16a, are acquired through sensors strategically positioned in the study area. The solar irradiation sensor is equipped with a monocrystalline silicon sensor, featuring a permissible tolerance of ±5%. Functioning within an extensive temperature range from -40 °C to 85 °C, this sensor ensures reliable operation across diverse environmental conditions. The ambient temperature sensor can operate within the temperature range of -40 °C to +180 °C with a nominal tolerance of ±0.8 °C. Together, these sensors provide indispensable meteorological data, and enhances significantly the predictive accuracy of our model. The electrical load shown in Fig. 16b is derived from empirical data by capturing the typical energy consumption patterns exhibited by the building of a university building, affiliated with the Université de Technologie de Compiègne. The EG's CO_2 emissions, a dynamic factor, are sourced from the French transmission system operator, as depicted in Fig.16c [10]. The technical, economic, and environmental data used in this study are presented in Table 3. The optimization horizon spans one year (8760 hours) with an hourly time step with the consideration of the economic lifespan of the project, set at 20 years. The

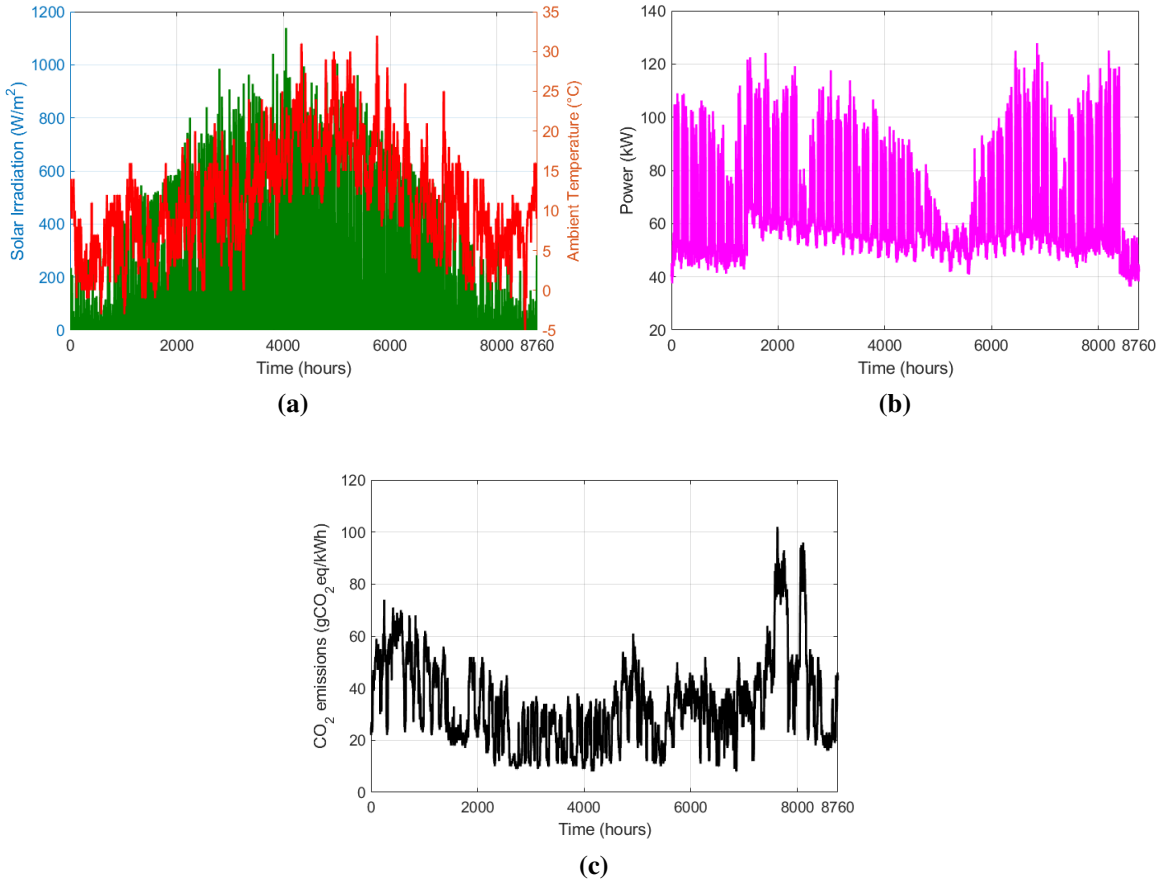

Figure 16: Hourly input data: (a) Solar irradiation and ambient temperature, (b) the electrical load, and (c) EG CO_2 emissions.

Parameter	Value	Unit	Parameter	Value	Unit
JinkoSolar PV			**DC/DC & AC/DC & DC/AC Converters**		
NOCT	40	°C	Efficiency	95	%
PV module-rated power	335	Wp	Lifetime	10	years
Power temperature coefficient	-0.328	%/°C	Investment cost	80	€/kW
Lifetime	25	years	Maintenance cost	2	% of conv inv cost/year
Investment cost	400	€	Replacement cost	80	€/kW
Maintenance cost	1	% of PV inv cost/year	**System**		
CO_2 emissions	1447	$kgCO_2$,eq/kWp	Cable CO_2 emissions	17680	$kgCO_2$,eq
Li-ion Battery			Project Lifetime	20	years
Charging efficiency	90	%	Discount rate	7	%
Discharging efficiency	90	%	Escalation rate	3	%
Max lifetime	10	years	Installation cost	40	% of PV inv cost
Unit capacity	2.55	kWh	**Electricity grid**		
SOC initial	0.5	pu	Grid power limit	120	kVA
SOC min	0.2	pu	Inject tariff	0.07878	€/kWh
SOC max	1	pu	Fixed subscription cost	800	€/year
Investment cost	1084	€	Peak hour supply tariff	0.2460	€/kWh
Maintenance cost	3	% of BESS inv cost/year	Off-Peak hour supply tariff	0.1824	€/kWh
Replacement cost	1084	€			
CO_2 emissions	102	$kgCO_2$,eq/kWh			

Table 3: PV, BESS, EG, DC/DC & AC/DC & DC/AC CVs and system parameters data [174, 102, 175, 173, 176, 171].

optimization problem is structured and solved using Python 3.8 with the CPLEX optimization solver. Computation tasks are executed on a high-performance supercomputer equipped with robust hardware specifications including an AMD EPYC 7763 64-Core Processor, 256 cores, and 1510GB of RAM. The entire system operates on the *"Rocky Linux 9.1"* operating system.

III.3.1 Technical, Economic, and Environmental Results

The economic and environmental results for $LCE \leq 0.75$ $kgCO_2$,eq/kWh in IMG operating mode and GCMG operations mode are displayed in Table 4. The system LCE is computed as the LCE sum of the PV, BESS, and EG. The results in Table 4 show that the system's LCOE and LCE are higher in IMG mode compared to GCMG mode. One reason is that the French EG is heavily dominated by the nuclear power plants which provides cost-efficient and low-carbon electricity services for the end-users. Therefore, the EG provides already a clean and cost-efficient solution in GCMG case, where the BESS capacity is mostly determined to provide electricity when the load demand passes the subscribed grid power limit. Additionally, the specific characteristics of the PV technology, fabricated in China, Shangrao city, make the PV system the primary contributor to the overall system's LCE in both operational modes because of the emissions that are emitted from the transportation of these PV panels from China. It should be noted that the CO_2 emissions of the chosen PV panel consider the maintenance of the product over the project lifetime. The microgrid components' sizes and technical results under identical conditions (where $LCE \leq 0.75$ $kgCO_2$,eq/kWh in IMG operating mode and GCMG operations mode) are presented in Table 5. The size of BESS and PV for IMG is higher than that of GCMG, with a percentage difference of 828.57% for the PV and a difference of 571% for the BESS. Larger PV and BESS capacities translate to increased capacities for their associated converters, as illustrated in Table 5 for the IMG case in comparison with GCMG operation mode. CPLEX computation time for IMG is lower than that of GCMG because the IMG operation mode is based on LP, requiring fewer decision variables and constraints. In contrast, the GCMG operation mode is a MILP with the addition of a binary decision variable and deci-

Parameter	IMG	GCMG	Unit
System LCOE	2.33	0.42	€/kWh
System LCE	0.75	0.10	$kgCO_2$,eq/kWh
PV LCE	0.69	0.074	$kgCO_2$,eq/kWh
BESS LCE	0.062	0.01	$kgCO_2$,eq/kWh
Cables LCE	0.001	0.001	$kgCO_2$,eq/kWh
EG LCE	-	0.018	$kgCO_2$,eq/kWh

Table 4: Economic and environmental results in IMG and GCMG operation modes.

Parameter	IMG	GCMG	Unit
Components size			
PV system capacity	6.5	0.7	MWp
BESS capacity	4.2	0.7	MWh
PV converter capacity	6.9	0.7	MW
BESS converter capacity	6.7	0.1	MW
EG converter capacity	-	0.1	MW
Building converter capacity	0.1	0.1	MW
Technical results			
PV output energy	7116	770	MWh/year
PV curtailed energy	5919	87	MWh/year
Battery energy	360	142	MWh/year
EG supplied energy	-	327	MWh/year
EG injected energy	-	174	MWh/year
BESS complete cycles	103	211	cycles/year
CPLEX computation time	1651	4320	seconds

Table 5: Components size and technical results for IMG and GCMG operation modes.

sion variables related to the EG. The outcomes from Table 4 and Table 5 are comprehensively analyzed in the following section.

III.3.1.1 Isolated Microgrid

Another reason of high LCOE and LCE in the IMG mode is that load shedding is not allowed, as stated in Eq. (18). This means that the optimization problem must be able to meet the load demand even during periods of low solar irradiation, such as the winter season. Fig. 17(a) depicts the energy profiles throughout a year, indicating a significant amount of curtailed power generated by the PV system, particularly during the summer season. Specifically, the curtailed PV energy amounts to about 83% of the total PV output energy. Even though the PV curtailed power is high, the PV contribution to the system still reaches around 60%, with the remaining contribution coming from the BESS. Fig. 18 shows simulation results for August 19-20 and November 13-14, which are the dates with the highest and lowest solar irradiation levels, respectively. As solar irradiation is typically high during the summer, the battery is not always charging during this period as there is an excess PV generation throughout this time. However, the BESS is configured to maintain its maximum SOC between November 13 and 14 to ensure a continuous supply of power to meet the load demand. The IMG is sized to match the energy needs between November 13 and 14, which demands significant capacities for both the PV

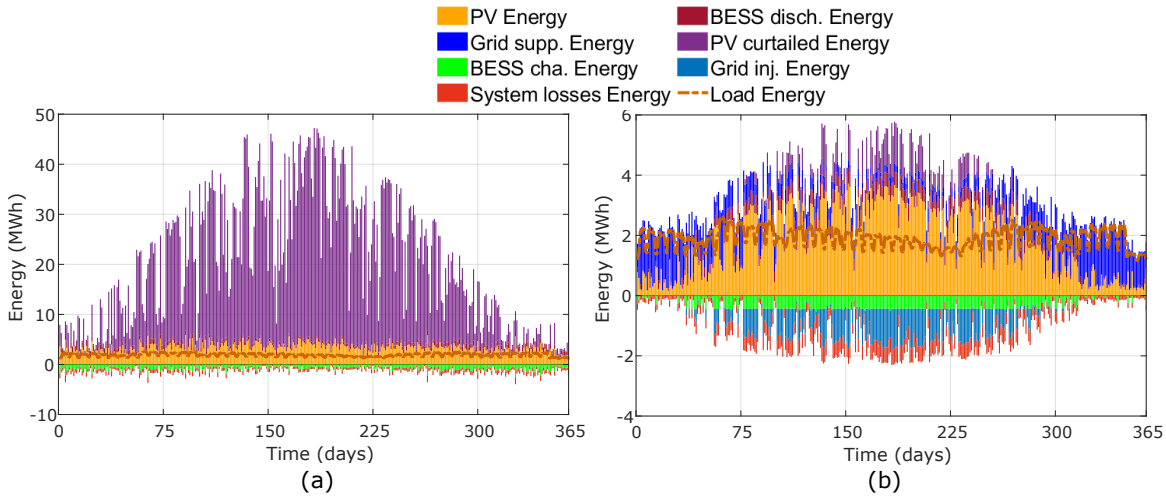

Figure 17: Annual energy profiles for (a) IMG operation mode and (b) GCMG operation mode.

system and BESS. As a result, there is a high amount of energy from the PV system that is being curtailed during the period of 19 to 20 August. This high level of energy curtailment (see Table 5 and Fig. 18(a) also affects the size of the PV associated converter, as it needs to be able to handle the incoming energy from the PV system. It can be seen in Table 5 that the BESS has a maximum charging/discharging power that is low in comparison to its capacity, this indicates that the BESS does not overcharge or discharge as the charging C-rate equals 0.102 and the discharging C-rate equals to 0.033. Avoiding high BESS C-rates is recommended for better safety and the improved lifespan of the battery [177]. Furthermore, the relatively low number of complete BESS cycles is a result of the BESS's substantial capacity. In simpler terms, because the BESS can store a lot of energy, it doesn't need to cycle through charging and discharging as frequently as a smaller BESS would. Additionally, this demonstrates that the assumption of a fixed battery replacement every five years guarantees a well-operating BESS, as 103 BESS cycles per year won't exceed the cycles to failure in the fifth year for the chosen battery.

III.3.1.2 Grid Connected Microgrid

The LCOE and LCE have significantly decreased in the GCMG operation mode compared to the IMG mode (see Table 4). This decrease can be attributed to the lower cost of purchasing power from the EG as opposed to increasing the capacity of BESS. Fig.17(b) demonstrates the power profiles over a simulated year, revealing a noteworthy reduction in curtailed power generated by the PV system compared to the IMG mode. Additionally, the graph highlights the significance of grid injection and battery charging during the summer season. The load is served directly from the EG during periods of low solar irradiation (November 13-14, see Fig. 18d), rather than relying on an increased PV and BESS capacities. This results in a decreased capacity for PV and BESS capacities and their associated converters in the GCMG mode compared to the IMG mode. Hence, during periods of high solar irradiation (August 19-20), as illustrated in Fig. 18b, there is a reduction in curtailed power. Overall, the curtailed power decreased to 6710% in this operation mode with a PV contribution of 57 %. During the summer months,

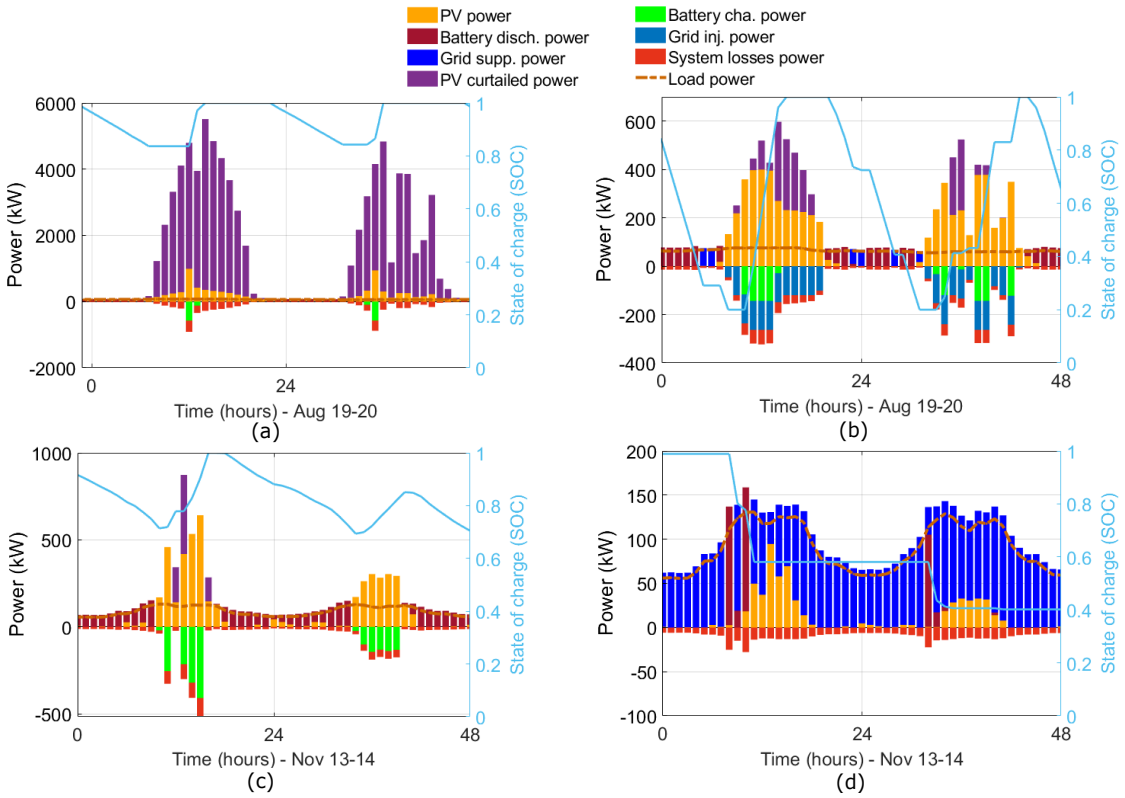

Figure 18: Power profiles for August 19-20: (a) IMG operation mode, (b) GCMG operation mode; and for November 13-14: (c) IMG operation mode, (d) GCMG operation mode.

when solar irradiation is abundant, the SOC of BESS is experiencing complete cycles because it is guaranteed that the BESS would be recharged the next day. Conversely, the SOC of BESS is kept at a certain level during the period of 13 to 14 November to maintain a sufficient power supply for the load. The charging/discharging C-rates of the BESS are approximately 0.14 and 0.11, respectively. Although these rates are higher than those of the IMG operation mode, they are still considered low, thus it ensures that the battery does not overcharge or overdischarge. Similar to the IMG operation mode, the BESS cycles of 211 per year guarantees a well-operating BESS during the five years considered in this study.

III.3.2 Analysis of Pareto Fronts

A key idea in multi-objective optimization is the Pareto front, sometimes referred to as the Pareto set or Pareto frontier. It describes a group of solutions to a problem area that cannot be enhanced for one target without degrading the effectiveness of another objective. In other words, it symbolizes the trade-offs among multiple competing aims. In this paper, the Pareto front is determined by manipulating ε (see Eq. (32)) where the trade-off between the objectives can be altered, which leads to have different solutions on the Pareto front. Fig. 19 illustrates the Pareto front along with the variations observed in BESS and PV panels for both IMG and GCMG operation modes. In the instance of the IMG, there's an approximate 20% difference in both LCOE and LCE between various solutions. For the GCMG mode, these differences amount to about 22% for LCOE and 16% for LCE. It can be seen that reducing the LCE would

necessitate an increase in LCOE and vice versa. This can be explained by the fact that reducing one objective requires sacrificing some of the other objective. Additionally, reducing the LCE of the system can be achieved by increasing the proportion of BESS in the overall system and decreasing the number of PV panels. This finding is consistent with the observation that the LCE of the PV system is slightly greater than that of the BESS in this study. For the GCMG operation mode, the Pareto front exhibits a generally downward slope from left to right, indicating that it is typically possible to reduce the LCE without substantially increasing the LCOE. However, decreasing LCOE often necessitates accepting higher levels of LCE. The variation of the BESS and PV panels is the same for both operation modes, where the BESS increases and the PV decreases whenever the LCE decreases. It should be noted that in the Fig. 19 dominated and non dominated solutions are presented in both IMG and GCMG operations mode as the non dominated solutions form the Pareto frontier. Fig. 20 shows a radar plot that compares

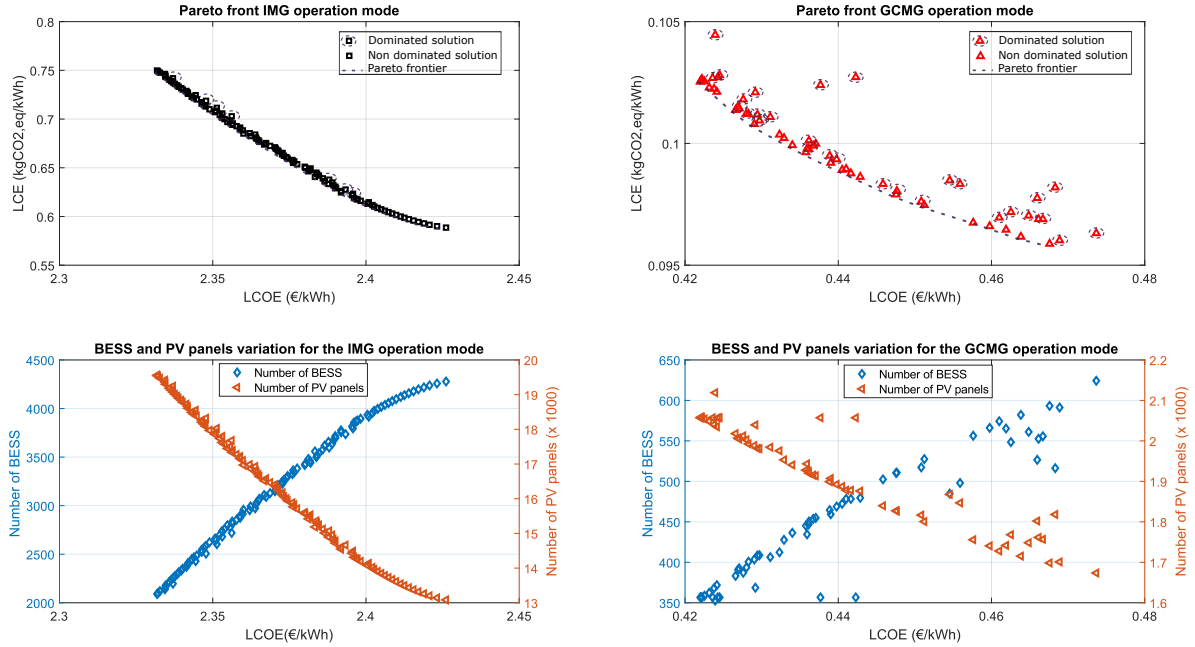

Figure 19: Pareto front and the variation of BESS and PV panels for the IMG and GCMG operation modes.

the economic indicators such as investment, maintenance, replacement, salvage value, and EG costs (for GCMG operation mode). It can be inferred that when LCOE is the lowest, the investment cost is the highest for both operation modes. This is because the algorithm suggests a microgrid that relies on PV panels, which have a larger investment cost than that of BESS. On the other hand, when LCE is the lowest, the maintenance, replacement, and EG costs are larger compared to the case where LCOE is the lowest. This is because in this case, the algorithm suggests a solution that is more reliant on BESS, which is a only replaced component several times during the project lifetime, in this study.

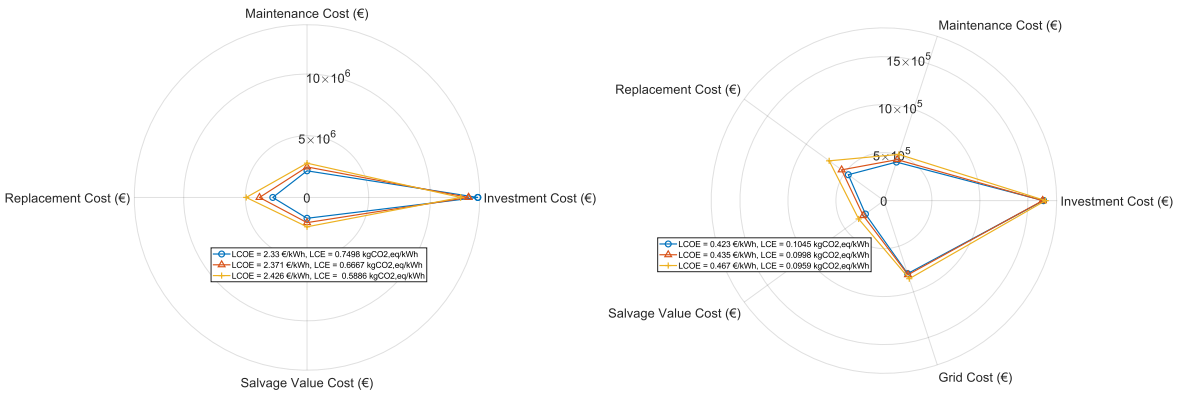

Figure 20: Radar plot for economic analysis for (a) IMG (b) GCMG operation modes.

III.3.3 Peak Shaving Strategy Impact

Peak shaving is achieved by varying the maximum subscription limit from 140 kVA to lower limits of 120 kVA, 100 kVA, 80 kVA, 60 kVA, and 40 kVA by updating the subscription cost C_{sub} for each power level [173]. Fig. 21 displays the Pareto fronts for the peak shaving strategy with varying EG limits and for IMG operation mode. The onset of observable variations in the solution occurs when the LCE for the IMG and GCMG operation modes are less than or equal to 0.5 $kgCO_2eq/kWh$. The results indicate that increasing the EG limits results in a reduction in both LCE and LCOE, as observed by the upward trend of the Pareto fronts.

The average variation between each Pareto curve is assessed by observing changes in the EG limits. A decrease in the EG limit from 140 kVA to 120 kVA results in an approximate 11% increase in LCOE and 21% in LCE. Further lowering the limit to 100 kVA increases the variation to 22% for LCOE and 18% for LCE. When the limit is reduced to 80 kVA, the increases in LCOE and LCE are 21% and 17%, respectively. The transition from 80 kVA to 60 kVA shows a significant jump, with LCOE surging by 70% and LCE by 40%. The subsequent reduction to 40 kVA results in a 74% rise in LCOE and an 70% increase in LCE. The final shift from a 40 kVA EG limit to an isolated microgrid leads to increases of 80% in LCOE and 82% in LCE. From these variations, it is evident that the average variation of LCOE and LCE between different Pareto curves is non-linear, and reductions in the EG limit significantly impact these metrics. These results underscore that the French EG provides cost-efficient and CO_2-efficient electricity services to end-users. This efficiency is largely due to the dominance of nuclear power plants within the French energy mix.

The optimization algorithm tends to decrease the required BESS capacity as the EG limit increases. These findings suggest that it is both economically and environmentally (in terms of CO_2 emissions) more favorable to rely on the EG rather than integrating a local BESS. As the EG limit is raised, the Pareto fronts become lower and steeper. This steeper Pareto front indicates that by depending more on the EG, it is possible to reduce the LCE without significantly increasing the LCOE However, reducing LCOE often requires accepting higher levels of LCE.

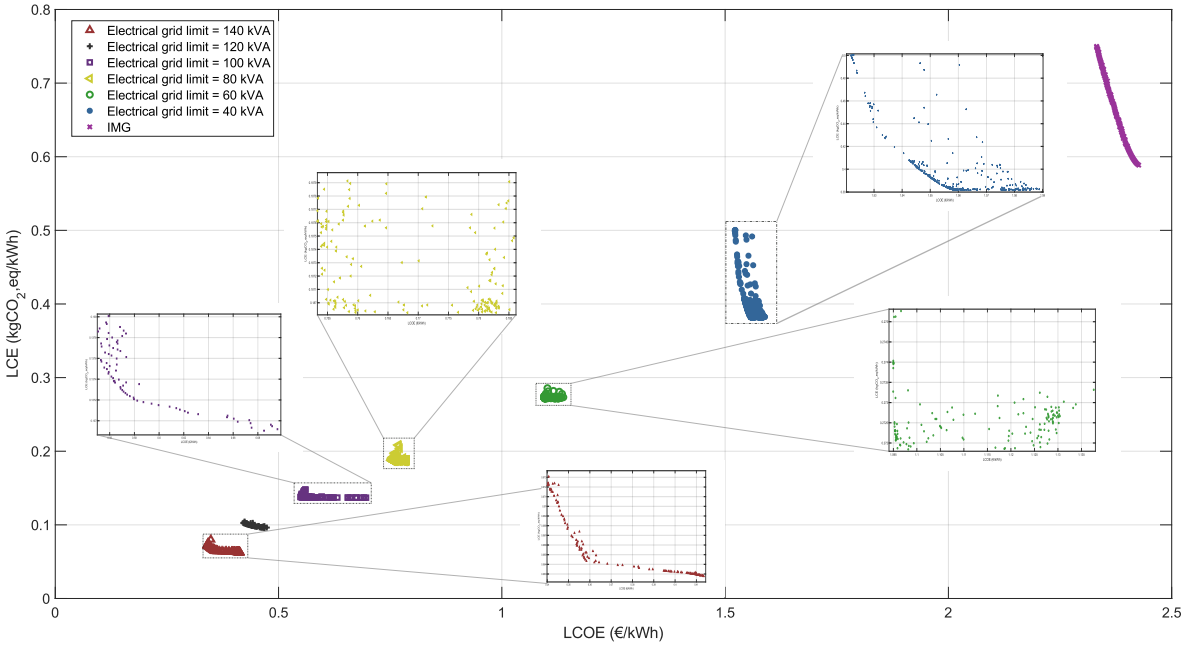

Figure 21: The trend of Pareto fronts for peak shaving strategy based on various EG limit.

III.3.4 Scalability Analysis

A scalability analysis is conducted for both IMG and GCMG operation modes for the 120 kVA EG limit. The load is increased from 0% to 30% in 5% increments. Results for both operation modes are presented in Fig. 22. For the IMG operation mode (Fig. 22a), the Pareto curves are so close that there are no significant differences between the solutions. However, as shown in the zoomed figure in Fig. 22a, increasing the load leads to a slight decrease in LCE and LCOE. This occurs because the percentage increase in load is higher than the percentage increase in the capacities of the microgrid components. The average difference between the two extreme solutions (from a 0% to a 30% load increase) is less than 1%. Shifting to the GCMG operation mode (Fig. 22b), an increase in load leads to an increase in both LCOE and LCE, as indicated by the upward trend of the Pareto curves. The primary reason for this increase is the EG limit set at 120 kVA. As the load exceeds this limit, the optimization tends to increase the capacities of microgrid components to satisfy the increased load. This increase in microgrid component capacities surpasses the load increase, which results having higher LCOE and LCE. The average difference between each Pareto curve is about 8% with the average difference between the two extreme solutions being approximately 46%.

III.3.5 Analysis of Utilized Energy Sources in French Electricity Grid

The French energy mix has undergone significant decarbonization, primarily attributed to the extensive integration of nuclear power in energy mix, which emits low levels of CO_2 [178]. This investigation illustrates the proportionate contribution of various energy sources to the EG of France, as demonstrated in Fig. 23 for several EG limits for scenarios where $LCE \leq 0.75\,\mathrm{kgCO_2eq/kWh}$. It can be observed that increasing the EG limit leads to a decrease

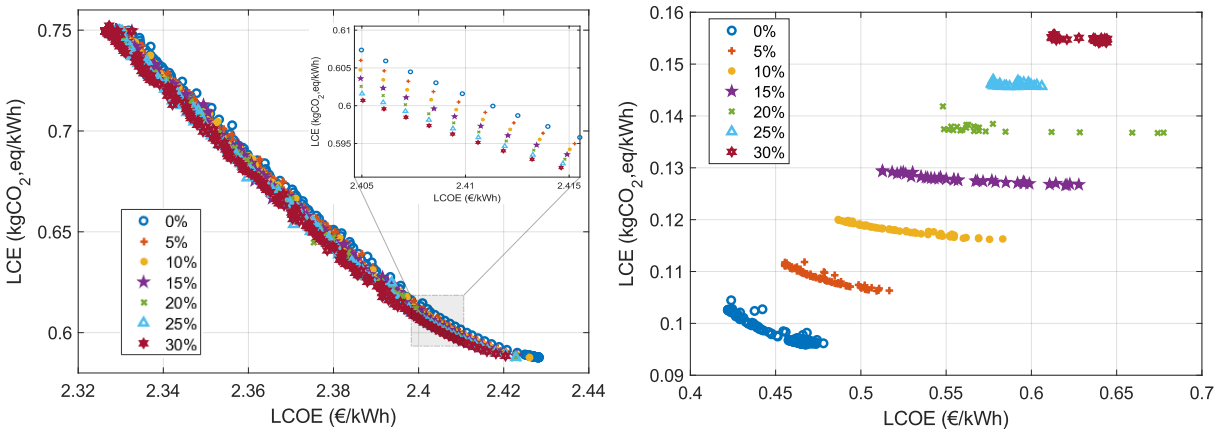

Figure 22: Scalability analysis results for the (a) IMG (b) GCMG operation modes.

in local renewable energy consumption within the microgrid, and an increase in the portion of the EG supply, primarily the nuclear consumption. Increasing the EG limit from 40 kVA to 140 kVA results in a reduction of local renewable consumption by about 62%, and an increase in nuclear consumption by about 44%, the EG renewable consumption by about 12%, and the EG non-renewable consumption by about 4%. These results emphasize the country's substantial dependence on local renewable energy consumption, accounting for at least 35% of the local renewable and 13% of the EG renewable consumption in the worst-case scenario. These findings align with the French government's ambitious goals to boost the use of renewable energy sources in electricity generation. Moreover, the electricity consumption derived from the nuclear EG remains the highest, highlighting the high reliance on nuclear power for electricity production in France. Additionally, connecting an IMG or maintaining a low EG limit remains costly in terms of LCOE and LCE. An ultimate solution could be by integrating more renewable production into the French energy mix, because although the case of 40 kVA has 97% local renewable consumption, the LCE of this case is higher than that of all other cases as seen in Fig. 21.

Fig. 24 presents the distribution of energy sources used over the year with a temporal resolution of one day for the scenario where $LCE \leq 0.75$ and for several EG limits. The results indicate a high reliance on local renewable consumption, specifically PV and BESS, followed by nuclear power production. The proportion of nuclear power increases in the winter season due to lower solar irradiation. As the EG limit increases, the EG supply in the winter season also increases, which increases the proportion of nuclear power consumption in the total energy consumption.

III.3.6 Maximisation of the Renewable Energy Consumption in the Microgrid

The case study reveals increasing the EG limit results in higher EG nuclear and non-renewable energy consumption, as illustrated in Fig. 23. However, when the main objective is considered to be enhancing renewable energy share consumed from the EG, the objective function modification should be required to minimize EG supply during periods of low renewable

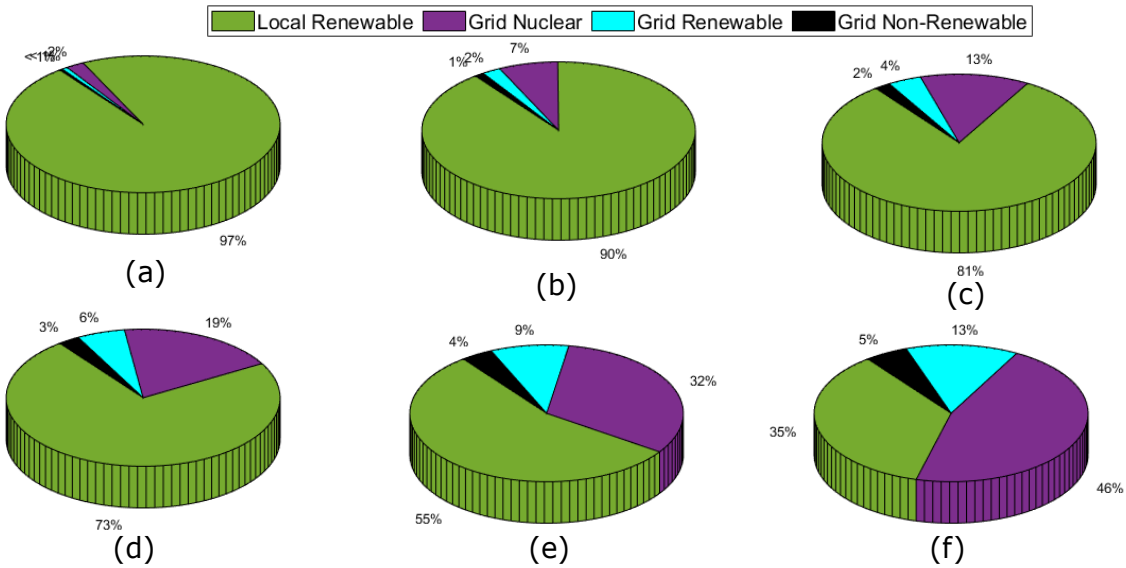

Figure 23: The percentage of energy sources utilized over the year for the case of lowest LCOE for the EG limit of (a) 40 kVA, (b) 60 kVA, (c) 80 kVA, (d) 100 kVA, (e) 120 kVA, (f) 140 kVA.

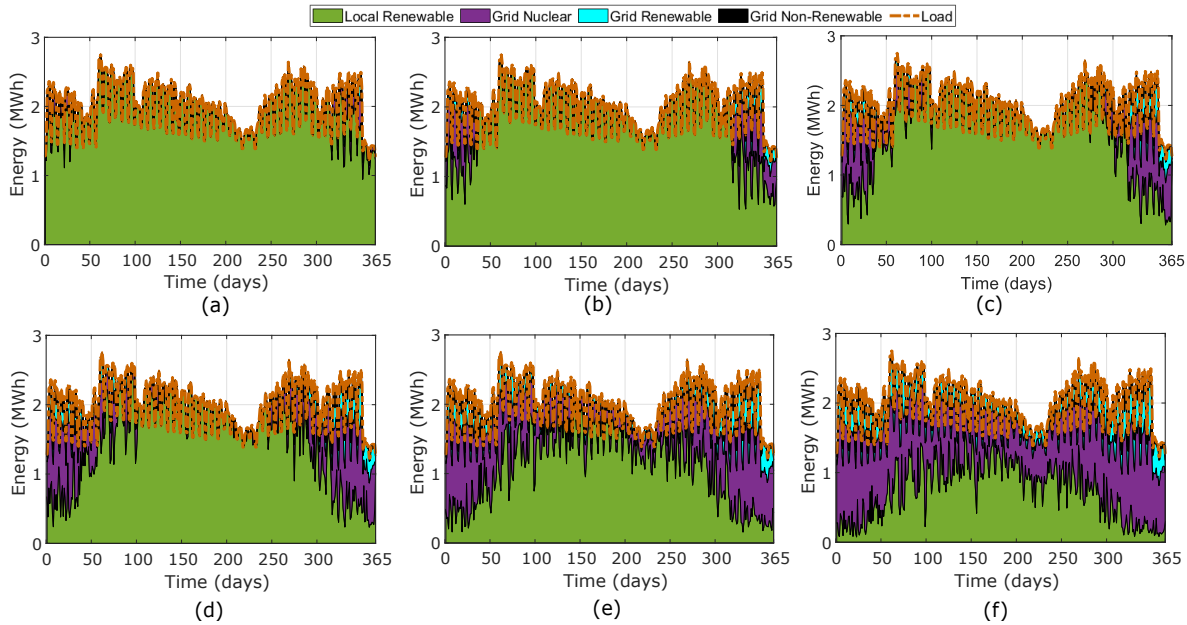

Figure 24: The distribution of energy sources utilized over the year for the case of lowest LCOE for the EG limit of (a) 40 kVA, (b) 60 kVA, (c) 80 kVA, (d) 100 kVA, (e) 120 kVA, (f) 140 kVA.

energy production. The new optimization problem is formulated as follows:

$$\min \left\{ p_{EG}^{s}(t) \cdot \kappa(t) \right\}, \tag{33}$$

$$LCOE \leq \tau \tag{34}$$

Here, $\kappa(t)$ represents the percentage share of EG nuclear and non-renewable energy at each time step t, while τ denotes the upper bound of the LCOE. The new optimization problem with

the objective function in Eq. (33) is solved by determining the following decision variables under the constraints in Eq. (4) to Eq. (18), along with Eq. (32) and Eq. (34): the BESS capacity (E_b), the number of PV panels (N_{PV}), the BESS charge/discharge powers ($p_b^c(t)/p_b^d(t)$), the EG supply/inject powers ($p_{EG}^s(t)/p_{EG}^{in}(t)$), and the auxiliary variables ($x_{aux}(t)$). Additionally, the capacities of the associated converters for PV, BESS, and EG ($M_{PV}^{DC/DC}$, $M_b^{DC/DC}$, $M_{EG}^{AC/DC}$) are determined.

This optimization is tested for EG limits of 100 kVA, 120 kVA, and 140 kVA. The results are presented as Pareto fronts between LCOE/LCE, EG nuclear and non-renewable energy consumption (MWh) in Fig. 25. The analysis indicates that decreasing LCOE/LCE leads to increased EG non-renewable and nuclear energy consumption. This occurs because the EG's intervention is lower when LCOE/LCE is high, resulting in reduced non-renewable and nuclear energy consumption.

In all three scenarios, nuclear and non-renewable consumption is non-zero when LCOE is below 2 €/kWh and carbon emissions are below 0.6 $kgCO_2$,eq/kWh. The primary difference among the 100 kVA, 120 kVA, and 140 kVA limits is that increasing the EG limit correlates with higher nuclear and non-renewable consumption rates. This analysis demonstrates that in the French EG context, increasing renewable energy consumption while decreasing LCOE and LCE is contradictory. Therefore, additional efforts are necessary to boost renewable energy production in the French energy mix.

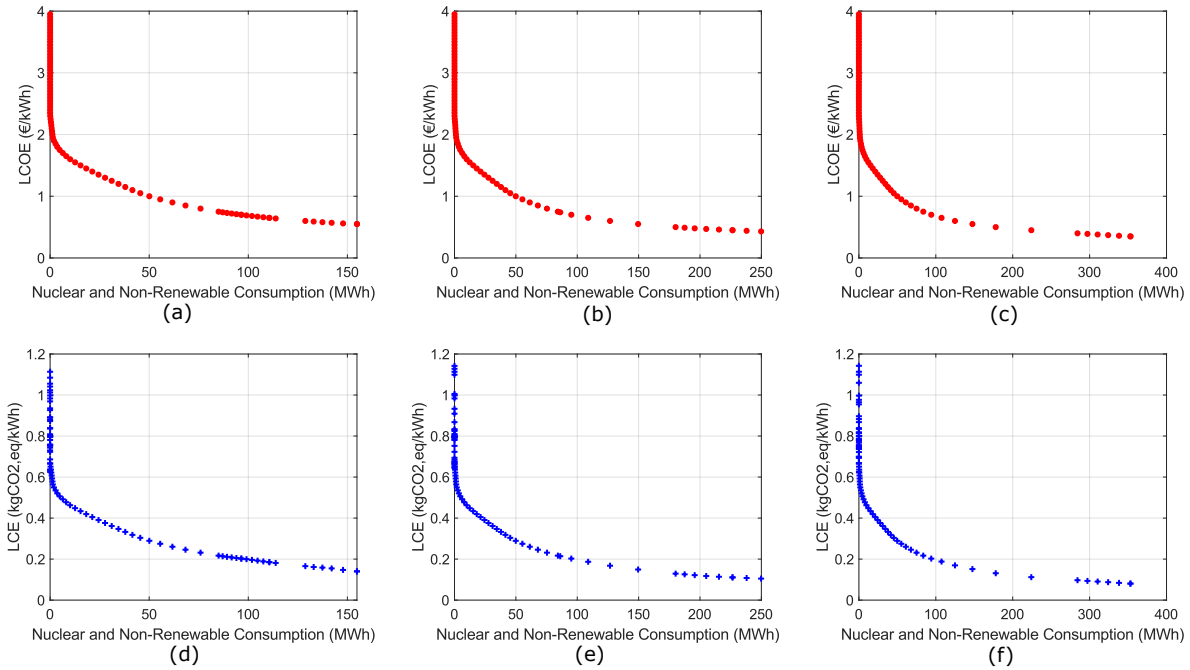

Figure 25: LCOE and LCE results of the EG limit of (a)(d) 100 kVA, (b)(e) 120 kVA, and (c)(f) 140 kVA.

III.4 Discussion

In this chapter, the battery degradation is not formulated in the optimization problem since the battery complete cycles are determined low in both operation modes. The energy capacity of the battery is obtained significantly higher compared to required charge and discharge powers in BESS converter, hence battery cycle is not performing high number of complete cycles.

The proposed methodology can be adjusted to accommodate a wide range of data types including costs, emissions, solar irradiation, and other variables. This flexibility makes it a useful tool for helping with decision-making in the field of microgrid planning. Moreover, it should be noted that the presented results are not generic which can vary based on the chosen PV and BESS models, and according to EG characteristics. Therefore, the proposed methodology can be used for testing the impact of the various equipment models in different EG which has different emission and price profiles.

For instance, when one of the main components, either PV or BESS, has lower costs and emissions in a microgrid with PV systems, BESS, load, and their converters, the solutions and the Pareto front show no variations. In the presented results the PV emissions are comparatively higher due to specific technology characteristics, but its cost remains lower.

III.5 Conclusions

In this chapter, an MILP optimization algorithm is presented to co-optimize equipment sizing and EM problems of a DC microgrid with the objectives of cost and emissions reduction. The analysis and results lead to several conclusions. In the IMG operation mode, the microgrid exhibits larger component capacities compared to GCMG. This difference is due to the necessity of coping with more challenging conditions, such as the absence of the EG during periods of low solar irradiation. The study reveals that BESS capacity increases as the LCE decreases, and the number of PV systems is higher when the LCOE is lower for both operation modes. This occurs because the BESS has a slightly lower LCE compared to the PV, and the LCOE of PV is also lower than that of BESS. Economically, the solution with a lower LCOE incurs the highest investment cost, whereas the solution with the lower LCE incurs the highest replacement cost, mainly due to BESS, which is the only component replaced over the project's lifetime. As the limit of the EG increases, the Pareto fronts for both peak shaving strategy become lower and steeper. In the IMG operation mode, increasing the load does not lead to higher LCOE and LCE; rather, it results in a reduction of both metrics. Conversely, in the GCMG operation mode, an increase in load corresponds to higher Pareto curves, which in turn leads to increased LCOE and LCE. From an environmental perspective, the findings indicate that in worst case 35% of the total production comes from local sources, with the remainder primarily reliant on the EG, which predominantly utilizes nuclear power in the French energy mix. It is also proven in the French case study that decreasing LCOE/LCE leads to increased non-renewable and nuclear energy consumption. Furthermore, it is shown that minimizing nuclear and non-renewable energy consumption will result in an increase in LCOE and LCE.

Chapter IV

Cost and Emission Minimization in University Building: A Multi-Objective MILP Study with Renewable Energy and EV Integration including Geographic and Technology Analysis

This chapter builds upon the work presented in Chapter III, which introduced a MILP algorithm to achieve global optimal solutions for optimizing both the sizing and EM of a microgrid. The optimization considered annual solar irradiation and the yearly load demand of a tertiary building on a university campus. This study extends the previous work by integrating a WT into the microgrid and incorporating the modeling and consideration of EV loads. The microgrid is evaluated in various cities across France, utilizing different technologies for PV systems, BESS, and WT. Consequently, this chapter presents a comprehensive geographical and technological analysis. The primary contributions of this chapter are as follows:

- a comparative analysis of three scenarios (PV/BESS, WT/BESS, and PV/WT/BESS) across the different studied cities;
- evaluation of the impact of seasonal fluctuations on the LCOE and LCE; and
- assessment of the influence of the choice of microgrid component technologies on the LCOE and LCE outcomes.

This chapter is organized as follows: Section IV.1 presents the system modeling, Section IV.2 details the modifications in the formulation of the joint multi-objective optimization problem, Section IV.3 provides the results and analysis, and finally, Section IV.4 concludes the chapter.

IV.1 System Modeling

In this chapter, two main microgrid components have been added: the WT and the EV load. The modeling of these two components is presented in this chapter, while the models of other components are detailed in Section III.1. The structure of the studied microgrid in this chapter is illustrated in Fig. 26.

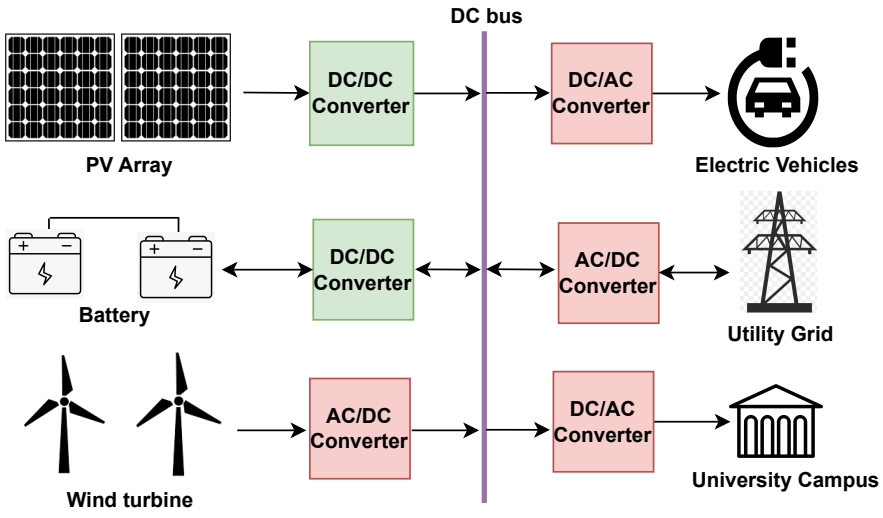

Figure 26: Architecture of the studied microgrid.

IV.1.1 Wind Turbine

The wind speed data, initially recorded at an altitude of H_{ref}, undergoes adjustment to match the wind conditions at the hub height h considering the difference in elevation. The adjusted wind speed (v_h) is calculated as follows [161]:

$$v_h(t) = V_{\text{ref}} \cdot \left(\frac{h}{H_{\text{ref}}} \right)^r \tag{1}$$

where V_{ref} is the wind speed measured at the altitude of H_{ref}, and the value of the roughness coefficient (r) is selected as 0.3 urban environment. The power output of the WT is determined as outlined in [161]:

$$p_{WT}(t) = N_{WT} \cdot \begin{cases} 0 & \text{if } v_h(t) < v_{cin} \text{ or } v_h(t) > v_{cout} \\ P_r \cdot \left(\frac{v_h(t)^3 - v_{cin}^3}{v_r^3 - v_{cin}^3} \right) & \text{if } v_{cin} \leq v_h(t) < v_r \\ P_r & \text{if } v_r \leq v_h(t) < v_{cout} \end{cases} \tag{2}$$

where N_{WT} is the number of WTs, $p_{WT}(t)$ denotes the power output of the WT (kW), P_r represents the turbine's rated power (kW). v_{cin} corresponds to the cut-in wind speed (m/s), v_{cout} corresponds to the cut-out wind speed (m/s), and v_r is the rated wind speed (m/s). The output power of a chosen WT (Schachner05 - SW05[179]) is shown in Fig. 27.

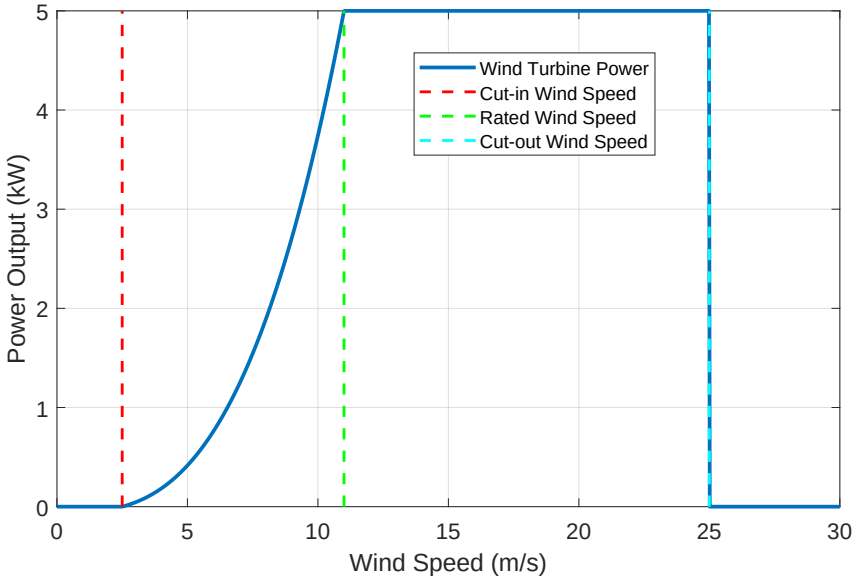

Figure 27: WT (Schachner05 - SW05[179]) output power.

IV.1.2 Electric Vehicle Load

It is imperative to develop advanced models that consider critical factors such as the plug-in time (t_{pin}) of EVs and the initial SOC (SOC_{EVinit}). In [159], data from a university campus is gathered to illustrate the PDFs of t_{pin} and SOC_{EVinit} for private EVs. The analysis reveals that the GEV closely matches the collected data. The equation for the GEV is derived as follows:

$$f(x;\mu,\sigma,\xi) = \begin{cases} \frac{1}{\sigma}\left[1+\xi\left(\frac{x-\mu}{\sigma}\right)\right]^{-\frac{1}{\xi}-1} \cdot \exp\left\{-\left[1+\xi\left(\frac{x-\mu}{\sigma}\right)\right]^{-\frac{1}{\xi}}\right\}, & \text{if } \xi \neq 0 \\ \frac{1}{\sigma}\exp\left\{-\frac{x-\mu}{\sigma}\right\}, & \text{if } \xi = 0 \end{cases} \tag{3}$$

where $f(x;\mu,\sigma,\xi)$ represents the GEV, where x is the random variable, μ is the location parameter, σ is the scale parameter, and ξ is the shape parameter, respectively. SOC_{EVinit}, the parameters of GEV are taken as $\xi = 0.0629$, $\sigma = 0.5493$, $\mu = 8.9068$. For t_p, the GEV parameters are: $\xi = 0.0474$, $\sigma = 7.9015$, $\mu = 12.8820$. The duration required for charging the EV varies based on the connection time, and the period needed to attain the maximum SOC for the EV SOC_{EVmax}, is computed as follows:

$$T_{char,a} = \frac{(SOC_{EVmax,a} - SOC_{EVinit,a}) \cdot EV_{cap,a}}{P_{cs}} \tag{4}$$

where $T_{char,a}$, $SOC_{EVmax,a}$, and $EV_{cap,a}$ are the charging duration, maximum SOC, and battery capacity of the EV a, respectively; and P_{cs} is the EVCS power rating. The plug-out time for EV is determined using a uniform distribution that ranges from zero to three hours after the EV charging time needed to reach the maximum SOC. This consideration is incorporated into the optimization problem to introduce a margin of flexibility, enabling the scheduling of EV charging. Without this margin, if the unplugging time coincides exactly with the EV charging duration, scheduling EV charging sessions would be unfeasible. The EV charging power demand is calculated as follows:

$$p_{EV,a}(t) = \begin{cases} \frac{(SOC_{EVmax,a} - SOC_{EVinit,a}) \cdot EV_{cap,a}}{\lfloor T_{char,a} \rceil}, & \text{if } t \geq t_{pin} \\ 0, & \text{otherwise} \end{cases} \tag{5}$$

Equation (10) calculates the EV a charging demand, denoted as $p_{EV,a}$, after the plug-in time t_p. In this equation, the energy needed to charge the EV is divided by the rounded-up charging duration $\lfloor T_{char,a} \rceil$ to calculate the actual EV power. This method is chosen, because the study operates on an hourly time scale, and charging the EV at a steady power rate might risk pushing the battery's SOC in the simulation beyond its permitted maximum level which physically not possible.

IV.2 Formulation of the Joint Multi-Objective Optimization Problem

In this chapter, the formulated optimization problem is similar from the one presented in Chapter III, Section III.2. However, the algorithm introduced in this chapter takes into account the WT and EV demand additionally compared to previous one. For that, this chapter introduces the equations that are modified, and the rest can be seen in Chapter III, Section III.2.

As other converters in the microgrid, the nominal power value of the associated converters of the WT and the EV load is considered to be equal or greater than electric power that flows

through them as stated below:

$$p_{WT}(t) \leq M_{WT}^{AC/DC} \tag{6}$$

$$p_{EV}(t)/\gamma_{EV}^{DC/AC} \leq M_{EV}^{DC/AC} \tag{7}$$

where $p_{EV}(t)$ corresponds to the EV load demand. The big M method is used by adding WT and EV powers as follows:

$$M \cdot x_{aux}(t) - \left(p_{buil}(t)/\gamma_{buil}^{DC/AC} + p_{EV}(t)/\gamma_{EV}^{DC/AC} - \gamma_{PV}^{DC/DC} \cdot p_{PV}^{MPPT}(t) - \gamma_{WT}^{AC/DC} \cdot p_{WT}(t)\right) \geq 0 \tag{8}$$

$$M \cdot (1 - x_{aux}(t)) - \left(\gamma_{PV}^{DC/DC} \cdot p_{PV}^{MPPT}(t) + \gamma_{WT}^{AC/DC} \cdot p_{WT}(t) - p_{buil}(t)/\gamma_{buil}^{DC/AC} - p_{EV}(t)/\gamma_{EV}^{DC/AC}\right) \geq 0 \tag{9}$$

The management of BESS discharge and EG supply to prevent the system load power from being exceeded is formulated as:

$$\begin{aligned} p_{EG}^{s}(t) \cdot \gamma_{EG}^{AC/DC} + p_b^d(t) \cdot \gamma_b^{DC/DC} \cdot \mu_d + M \cdot (1 - x_{aux}(t)) \geq \\ - \left(p_{buil}(t)/\gamma_{buil}^{DC/AC} + p_{EV}(t)/\gamma_{EV}^{DC/AC} - \gamma_{PV}^{DC/DC} \cdot p_{PV}^{MPPT}(t) - \gamma_{WT}^{AC/DC} \cdot p_{WT}(t)\right) \end{aligned} \tag{10}$$

The net power at the bus, $p_{\text{bus}}(t)$, of the microgrid system is calculated by summing the powers entering and leaving the bus, as expressed in Equation (11).

$$\begin{aligned} p_{bus}(t) = p_{buil}(t)/\gamma_{buil}^{DC/AC} + p_{EV}(t)/\gamma_{EV}^{DC/AC} - \\ \gamma_{PV}^{DC/DC} \cdot p_{PV}^{MPPT}(t) - \gamma_{WT}^{AC/DC} \cdot p_{WT}(t) + p_b^c(t)/\mu_c/\gamma_b^{DC/DC} + p_b^d(t) \cdot \gamma_b^{DC/DC} \cdot \mu_d + \\ p_{EG}^{s}(t) \cdot \gamma_{EG}^{AC/DC} + p_{EG}^{in}(t)/\gamma_{EG}^{DC/AC} \end{aligned} \tag{11}$$

The objective function aims to minimize the LCOE and the LCE calculated as follows:

$$LCOE = \frac{TC \cdot CRF}{\sum_{t_0}^{t_f} \left((p_{buil}(t)/\gamma_{buil}^{DC/AC}) + (p_{EV}(t)/\gamma_{EV}^{DC/AC})\right) \cdot \Delta t} \tag{12}$$

$$LCE = \frac{LCE_{PV} + LCE_{WT} + LCE_{BESS} + LCE_{EG} + LCE_{cables}}{\sum_{t_0}^{t_f} \left((p_{buil}(t)/\gamma_{buil}^{DC/AC}) + (p_{EV}(t)/\gamma_{EV}^{DC/AC})\right) \cdot \Delta t} \tag{13}$$

$$LCE_{WT} = \frac{\alpha_{WT} \cdot N_{WT} \cdot P_r}{Q} \tag{14}$$

The detailed calculation of the LCOE and LCE are presented in Section III.2.2. It should be noted that the WT costs and CO_2 emissions (Eq. (14)) are added in the LCOE and LCE calculations. The optimization problem is addressed by determining the following decision variables: BESS capacity (E_b), the number of PV panels (N_{PV}), the number of WTs (N_{WT}), BESS charge/discharge powers ($p_b^c(t)/p_b^d(t)$), EG supply/inject powers ($p_{EG}^{s}(t)/p_{EG}^{in}(t)$), and auxiliary variables ($x_{aux}(t)$). Additionally, the capacities of PV, WT, BESS, EG, EV, and building-associated CVs ($M_{PV}^{DC/DC}$, $M_{WT}^{AC/DC}$, $M_b^{DC/DC}$, $M_{EG}^{AC/DC}$, $M_{EV}^{DC/AC}$, $M_{buil}^{DC/AC}$) are also determined.

Parameter	Value	Unit	Parameter	Value	Unit
DualSun PV			**DC/DC & AC/DC & DC/AC CVs**		
NOCT	40	°C	Efficiency	95	%
PV module-rated power	400	Wp	Lifetime	10	years
Power temperature coefficient	-0.27	%/°C	Investment cost	80	€/kW
Lifetime	25	years	Maintenance cost	2	% of conv inv cost/year
Investment cost	612	€	Replacement cost	80	€/kW
Maintenance cost	1	% of PV inv cost/year	**System**		
CO_2 emissions	507.5	$kgCO_2$,eq/kWp	Cable CO_2 emissions	17680	$kgCO_2$,eq
Li-ion BESS			Project Lifetime	20	years
Charging efficiency	90	%	Discount rate	7	%
Discharging efficiency	90	%	Escalation rate	3	%
Max lifetime	10	years	Installation cost	40	% of PV inv cost
Unit capacity	2.55	kWh			
SOC initial	0.5	pu			
SOC min	0.2	pu	**EG**		
SOC max	1	pu	Grid power limit	140	kVA
Investment cost	1084	€	Inject tariff	0.07878	€/kWh
Maintenance cost	3	% of BESS inv cost/year	Fixed subscription cost	1000	€/year
Replacement cost	1084	€	Peak hour supply tariff	0.2460	€/kWh
CO_2 emissions	102	$kgCO_2$,eq/kWh	Off-Peak hour supply tariff	0.1824	€/kWh
Schachner05 WT			**EV**		
Rated power	5	kW	EV battery capacity	50	kWh
Investment cost	7250	€	EV max SOC	100	%
Maintenance cost	3	% of wind inv cost/year	EV min SOC	20	%
Cut in speed	2.5	m/s	**EV charging station**		
Rated wind speed	11	m/s	Charging station power	7	kW
Lifetime	20	years			
CO_2 emissions	1715	$kgCO_2$,eq/kW			

Table 6: Input parameters data of the microgrid system [174, 179, 102, 175, 173, 176, 171].

IV.3 Results and Analysis

In the studied microgrid, the load distribution encompasses the EVs and the university building. The infrastructure for EVs comprises five charging stations, each outfitted with dual 7 kW chargers that enables concurrent charging for up to 10 EVs. The arrival pattern of EVs follows a uniform distribution. On weekdays, the influx ranges from seven to 10 EVs, while weekends typically see one to two arrivals. During the vacation period on August, EVs arrivals may vary between one to four EVs due to summer vacation. The reduced range of one to four EV arrivals during the vacation period in August reflects the decrease in regular commuting and the shift towards more varied and less predictable travel patterns associated with the summer vacation season. The load profile of the university building is sourced from empirical data collected at a specific building within Université de Technologie de Compiègne in 2023. Both the EVs and university building's load characteristics are visually represented in Fig. 28 and Fig. 16b, respectively. The EG CO_2 emissions are considered dynamic as it is provided by the French transmission system operator (see Fig. 16c). In this study, a load growth of 1% is considered to anticipate potential future increases in demand and to ensure the resilience of the microgrid, while the EG tariffs remain the same as those used in III for all cities. The technical, economic, and environmental data utilized for this analysis are presented in Table 6.

The optimization problem is formulated using Python 3.8 and CPLEX optimization solver. The computations are carried out on a supercomputer equipped with an AMD EPYC 7763 64-Core Processor, 256 cores, and 1510GB of RAM, all running on the "Rocky Linux 9.1" operating system.

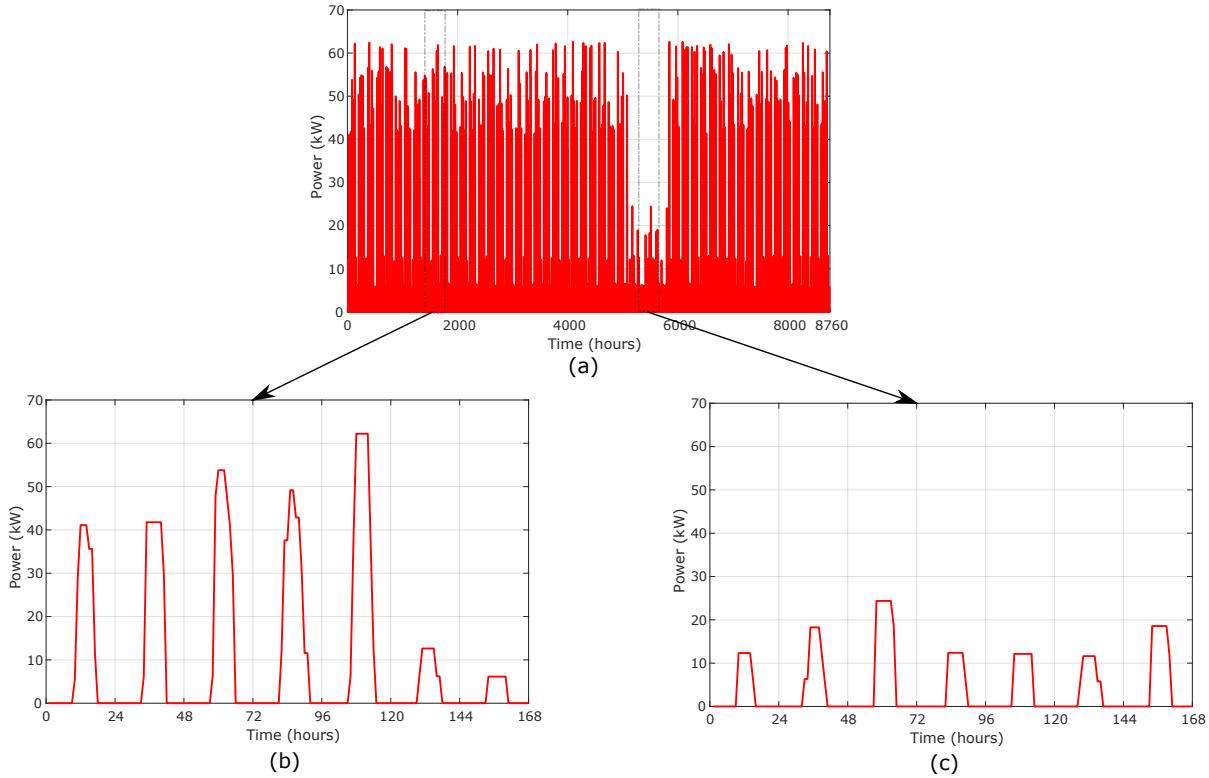

Figure 28: the (a) EV load with a detailed views for specific periods: (b) winter and (c) summer vacation

IV.3.1 Geographical Analysis

Several cities in France, representative of the entire country, were included in this study. These cities exhibit fluctuations between high wind speed and high solar irradiation. Additionally, cities from various regions including Europe, Africa, East Asia, America, the Middle East, and Australia were considered. Table 7 presents the solar irradiation, ambient temperature, and wind speed data for the considered regions over the course of one year, as retrieved from [180]. Descriptive statistics for this data are provided and detailed in Table 7. These statistics offer a summary of the dataset using several key measures. The mean, or average, signifies the typical value within the dataset. It is calculated as:

$$\text{Mean} = \frac{1}{n}\sum_{i=1}^{n} x_i \tag{15}$$

where n is the number of observations and x_i represents each individual value. The median, the middle value when data is ordered, offers a robust measure of central tendency. Standard deviation indicates the extent of variation in the dataset and is calculated as:

$$\text{Standard Deviation} = \sqrt{\frac{1}{n-1}\sum_{i=1}^{n}(x_i - \bar{x})^2} \tag{16}$$

where $\bar{x}$ is the mean of the dataset. Variance, the square of the standard deviation, quantifies the overall spread of data points around the mean and is given by:

$$\text{Variance} = \frac{1}{n-1}\sum_{i=1}^{n}(x_i - \bar{x})^2 \tag{17}$$

The range, the difference between maximum and minimum values, gives a quick sense of the total spread and is calculated as:

$$\text{Range} = \text{Max} - \text{Min} \tag{18}$$

The interquartile range (IQR) measures the spread of the middle 50% of the data, emphasizing the central portion's concentration without the influence of outliers, and is calculated as:

$$\text{IQR} = Q3 - Q1 \tag{19}$$

where $Q1$ is the 25th percentile and $Q3$ is the 75th percentile. The minimum and maximum values represent the dataset's lowest and highest points, respectively, which set its bounds. The 25th percentile (Q1) is the value below which 25% of data points fall, and the 75th percentile (Q3) is the value below which 75% of data points fall, that provides insight into the distribution's lower and upper ends.

A boxplot, also known as a box-and-whisker plot, provides a graphical summary of a dataset's distribution, emphasizing its central tendency, variability, and outliers. The plot fea-

City	**Solar irradiation (kWh/m^2)**	**Ambient temperature (°C)**	**Wind speed (km/h)**
Adelaide, AU	1758	14.98	11.8
Ajaccio, FR	1769	12.36	4.6
Bamako, ML	2300	27.89	9
Bern, CH	1658	9.12	4.8
Brest, FR	810	12.81	21.68
Cairo, EG	2624	22.18	13
Compiègne, FR	838	12.74	13.2
Dijon, FR	987	12.5	10.5
Doha, QA	2323	27.7	15.6
Le Havre, FR	873	12.17	17.02
Lille, FR	820	12.16	13.03
Lisboa, PT	1983	16.9	15.5
Lyon, FR	1124	13.31	8.44
Madrid, ES	1991	14.94	7.4
Marseille, FR	1375	16.59	19
Nagoya, JP	1775	15.57	9.4
New Delhi, IN	2027	27.17	9
Poitiers, FR	968	13.81	11.3
Rabat, MA	2259	18.72	8.06
Strasbourg, FR	964	12.44	8.12
Toronto, CA	1634	8	16.22
Toulouse, FR	1697	14.86	11.11
Tripoli, LB	2165	19.37	8.4
Twente, NL	1313	11.58	12.3
Washington, US	1868	11.5	7.7
Descriptive statistics			
Mean	1596.12	15.65	11.45
Median	1697.00	13.81	11.11
Standard Deviation	553.29	5.45	4.27
Variance	306132.03	29.72	18.24
Q1 (25th percentile)	987.00	12.36	8.40
Q3 (75th percentile)	1991.00	16.90	13.20
IQR	1004.00	4.54	4.80
Max	2624.00	27.89	21.68
Min	810.00	8.00	4.60
Range	1814.00	19.89	17.08

Table 7: Average solar irradiation, ambient temperature, and wind speed over one year in different cities

tures a box that represents the IQR, encapsulating the middle 50% of the data. Within this box, a line signifies the median (or midpoint) of the dataset, while a dashed line typically denotes the mean. The whiskers extend to the smallest and largest values within 1.5 times the IQR from the lower and upper quartiles, respectively. Values beyond this range are identified as outliers and are often marked with dots or asterisks. Boxplots are valuable for quickly discerning the dataset's skewness, spread, and anomalies, making them essential for exploratory data analysis. The boxplots for solar irradiation, ambient temperature, and wind speed are depicted in Fig. 29. The solar irradiation data exhibits a broad range with a mean of 1596.12 kWh/m^2 and considerable variability, evidenced by a standard deviation of 553.29 kWh/m^2. This indicates substantial differences in solar energy potential across the cities. The ambient temperature data shows a mean of 15.65 ℃, with most values falling between 12.36 ℃ and 16.90 ℃, and a few higher temperature outliers. Wind speed data reveals moderate variability, with a mean of 11.45 km/h, and most cities experiencing speeds between 8.40 km/h and 13.20 km/h. The outliers in both temperature and wind speed data suggest that some cities encounter more extreme climatic conditions. Overall, the data underscores significant geographical and climatic diversity, which is critical for renewable energy planning and environmental assessments.

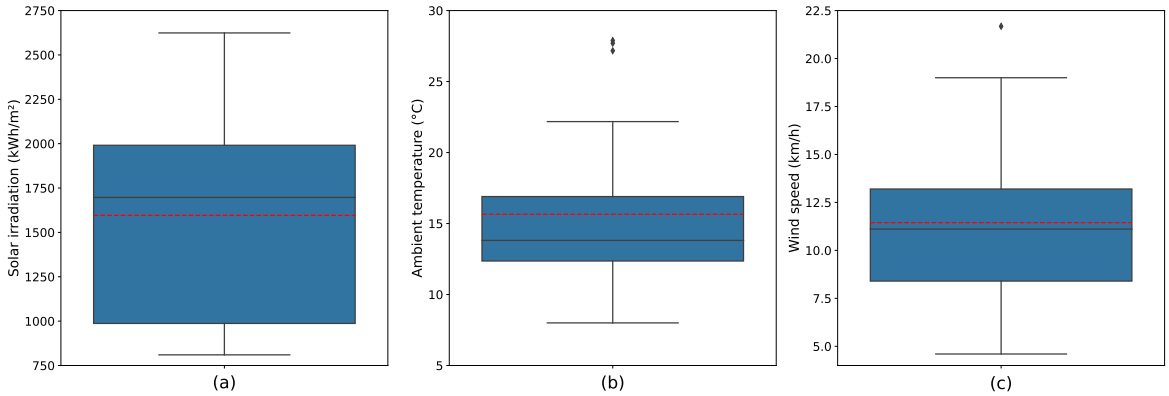

Figure 29: Box plot for the (a) solar irradiation, (b) ambient temperature, and (c) wind speed.

The optimization encompasses all cities specified in Table 7 for three different scenarios with the optimization includes results for scenarios where the LCE is less than or equal to 1.7 kgCO_2,eq/kWh, where the same load (EV and building) is used for each city:

1. Scenario 1 (S1): PV panels, BESS.
2. Scenario 2 (S2): WTs, BESS.
3. Scenario 3 (S3): PV panels, WTs, BESS.

The capacity analysis of the microgrid components and the detailed energy dispatch for some cities with high solar irradiation and those with high wind speed are presented in Tables 8 and 9, respectively. Additionally, the power profiles of these cities for one week in July are depicted in Fig. 30 and Fig. 31. Rabat, Tripoli, and Lisboa are identified as the cities with a high solar irradiation among the selected cities, whereas Brest, Marseille, and Le Havre are recognized as the cities with a high rate wind speed (see Table 7).

Parameter/City	Rabat			Tripoli			Lisboa		
	S1	S2	S3	S1	S2	S3	S1	S2	S3
Microgrid components capacities									
PV capacity (kWp)	381	-	381	303	-	303	389	-	295
WT capacity (kW)	-	3887	0	-	5812	0	-	1271	145
BESS capacity (kWh)	226	6327	226	461	7994	461	270	4688	169
PV CV capacity (kW)	410	-	410	302	-	302	413	-	310
WT CV capacity (kW)	-	1641	0	-	2937	0	-	1271	145
BESS CV capacity (kW)	57	205	57	94	344	94	67	206	49
EG CV capacity (kW)	147	140	147	140	147	140	147	147	147
EV CV capacity (kW)	66	66	66	66	66	66	66	66	66
Building CV capacity (kW)	164	164	164	164	164	164	164	164	164
Energy dispatch									
PV output energy (MWh/year)	824	-	824	623	-	623	602	-	562
WT output energy (MWh/year)	-	374	0	-	835	0	-	1105	126
Curtailed energy (MWh/year)	18.5	32.5	18.5	0.4	189	0.4	0	130	3
BESS energy (MWh/year)	63	80	63	101	193	101	116	157	43
EG supplied energy (MWh/year)	362	577	362	375	425	375	368	235	357
EG injected energy (MWh/year)	257	27	257	94	122	94	63	261	151
System losses energy (MWh/year)	93	74	93	87	130	87	88	130	74

Table 8: The microgrid components capacities and energy of Rabat, Tripoli, and Lisboa cities

IV.3.1.1 Cities with High Solar Irradiation Levels

Rabat and Tripoli are characterized by high solar irradiation levels but low wind speed. Consequently, the S1 and S3 for these cities yield the same results in terms of component capacities and energy dispatch. This occurs because integrating WT in S3 does not reduce the LCOE and LCE of the system. However, this is not the case for Lisboa, where relatively higher wind speed average is present. This means that integrating WT would decrease the LCOE and LCE. As shown in Table 8, the WT and BESS capacities are much higher in S2 compared to S1 and S3. This is primarily because when the EG reaches its limit, the load must be satisfied by WT and BESS. If the wind speed does not exceed the cut-in speed of the chosen WT, the optimization problem increases the BESS capacity to discharge and fully satisfy the load during these times of the year. The CVs reflect the components' capacities, showing high WT and BESS CV capacities in S2, which corresponds to their high capacities in this scenario. Since the load (EV and building) is fixed, the EV and building capacities remain constant.

Regarding energy dispatch, in all scenarios, the curtailed energy from the WT and PV is relatively small compared to the PV and wind output energy. This observation indicates that the BESS capacity and EG power limits are sufficient to absorb most of the surplus PV and wind energy. Additionally, the EG supply is always higher than the EG injection rate, highlighting the reliance on the EG. This suggests that the EG in France offers a more cost-effective solution compared to BESS, primarily due to the high investment cost of batteries. Furthermore, the EG limit is close to the maximum load peak, which explains the increased EG contribution in the microgrid. It should be noted that system losses include converters for PV, WT, BESS, electrical grid, EV load, and building load.

Fig. 30 represents one week (the first week of July) of the one-year simulation for S1, S2, and S3 for Rabat, Tripoli, and Lisboa. For S1 and S3 in Rabat and Tripoli (Fig. 30(a),

Fig. 30(b), Fig. 30(h), Fig.30(i)), it can be seen that the load is primarily covered by PV during the daytime and by BESS and EG supply during nighttime. In S2 for Rabat and Tripoli (Fig. 30(d), Fig. 30(e)), the load is mainly met by EG supply during this period with minor contributions from WT and BESS. For Lisboa, the S1 (Fig. 30(c)) is similar to those of Rabat and Tripoli. However, the S2 (Fig. 30(f)) shows a significant difference, where the load is mainly provided by WT. In the S3 (Fig. 30(j)), during periods without solar irradiation, WT energy contributes to load satisfaction along with EG and/or BESS.

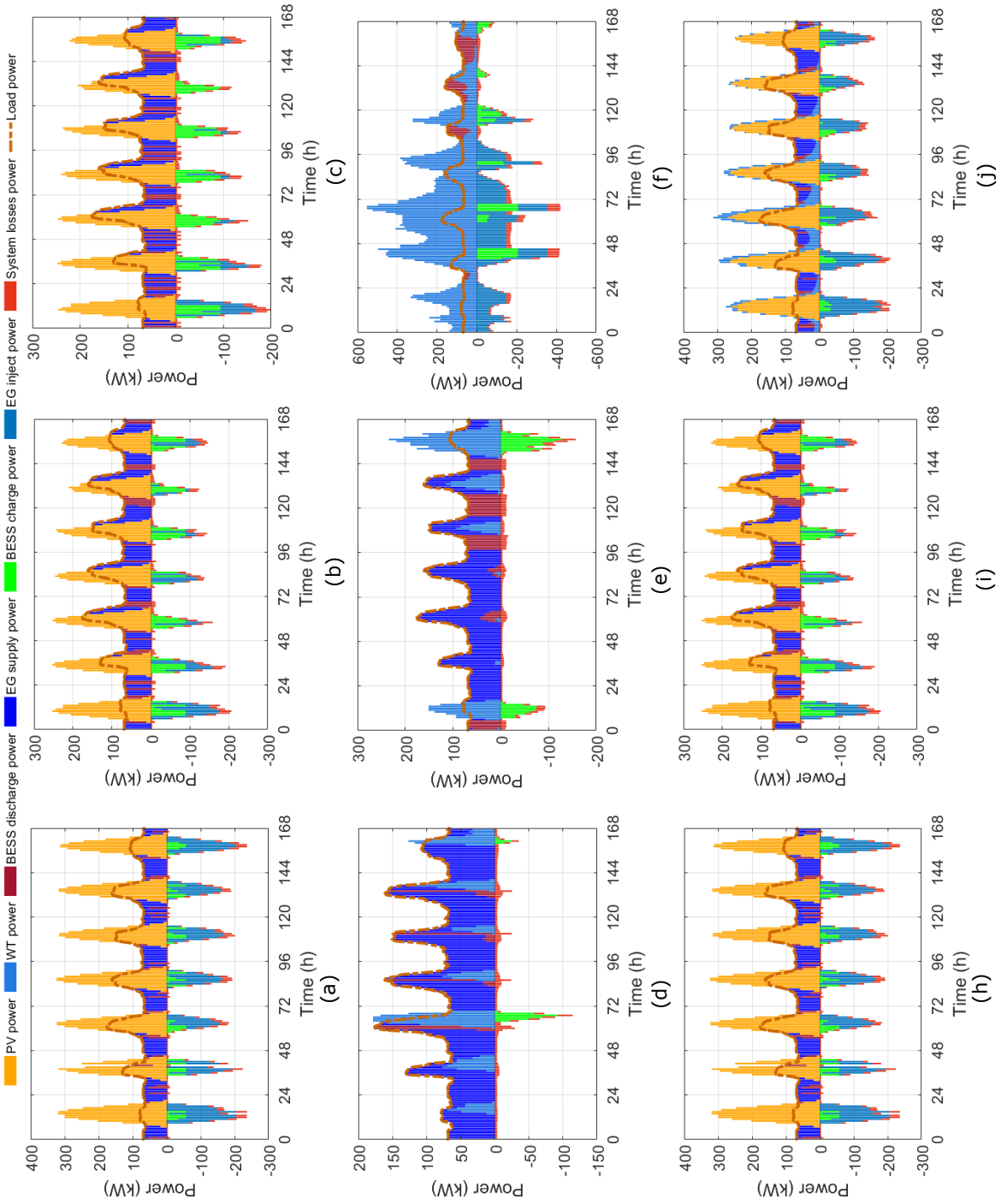

Figure 30: One week (1st of July's week) of the one-year simulation for S1 (a) Rabat (b) Tripoli (c) Lisboa, S2 (d) Rabat (e) Tripoli (f) Lisboa, S3 (h) Rabat (i) Tripoli (j) Lisboa.

IV.3.1.2 Cities with High Wind Speed Levels

Shifting to cities with relatively high wind speed rates, it is evident from Table 9 that the WT capacity has been reduced compared to cities with relatively low wind speed data as presented in Table 8. The BESS capacities have been reduced in S2, while they increase in S1. This is because in S2, the WT power is more abundant than in cities with low wind speed levels, and in S1, the solar irradiation levels are insufficient to fully cover the load. In this case, the BESS serves as a backup supply when the EG reaches its limit and there is an absence of EG supply. Unlike the results for high solar irradiation data, S1 and S3 of the same city do not have the same outcome. This is because PV has a lower cost compared to the chosen urban WT and BESS. Therefore, the optimization will choose to integrate PV if conditions permit, resulting in a reduced BESS capacity. However, in S3, the capacity of WT is higher than that of PV. As mentioned earlier, the CV capacities reflect their component capacities. Therefore, the PV capacity in S1 is higher than in S3, whereas the BESS CV is higher in S1 and S2 than in S3, because the reliance on BESS in these two scenarios is greater.

The energy dispatch analysis in Brest, Marseille, and Le Havre shows that the curtailed energy is generally higher than that in Rabat, Tripoli, and Lisboa. This leads to the conclusion that a city with high wind speed and low solar irradiation will result in higher curtailed energy rates due to the greater WT capacity for producing energy per unit in comparison with that of the PV panel. For the same reason, it can be seen that the EG injected energy is also higher in these cities compared to cities with low wind speed and high solar irradiation rates. A higher WT capacity will result in higher curtailed energy and greater system energy losses, as shown in Table 9. Considering S2 and S3 for Brest and Marseille, the EG supply energy is lower than that for Rabat and Tripoli, leading to the conclusion that Brest and Marseille have higher autonomy than Rabat and Tripoli. For example, the autonomy of Brest for S2 and S3 is 65% and 70%, respectively, while the autonomy of Rabat for S2 and S3 is 42% and 51%, respectively.

Fig. 31 represents one week (the first week of July) of the one-year simulation for S1, S2, and S3 for Brest, Marseille, and Le Havre. In the S1 case, it can be seen that the load is met by PV, EG, and BESS. However, in S2 and S3, the load is mainly covered by WT with minor contributions from EG, BESS, and PV (in the S3 case). This visual representation explains why the S2 and S3 in these cities have high autonomy.

IV.3.1.3 LCOE and LCE results

The heat maps depicted in Fig. 32 and Fig. 33 represent the LCOE and LCE values, respectively, for various cities under three distinct scenarios (S1, S2, and S3). These visual aids demonstrate considerable variability in both energy costs and carbon emissions across different locations and scenarios. In the case of LCOE, S2 consistently exhibits higher values, particularly for cities such as Bern, CH (5.5 €/kWh), Ajaccio, FR (4.5 €/kWh), and Washington, US (4.5 €/kWh). These increased costs in S2 suggest higher expenses due to specific local environmental factors that influence the costs of energy production. Conversely, most cities under S1 and S3 show lower and more stable LCOE values, indicating more predictable and affordable energy costs under these conditions. For instance, cities like Cairo, EG (0.22

Parameter/City	Brest			Marseille			Le Havre		
	S1	S2	S3	S1	S2	S3	S1	S2	S3
Microgrid components capacities									
PV capacity (kWp)	1146	-	43	457	-	217	1060	-	308
WT capacity (kW)	-	630	686	-	543	395	-	1131	693
BESS capacity (kWh)	2732	1892	1102	1160	1457	630	1611	1462	656
PV CV capacity (kW)	1130	-	42	460	-	217	1052	-	303
WT CV capacity (kW)	-	630	686	-	543	195	-	1131	693
BESS CV capacity (kW)	425	117	90	181	108	98	351	99	100
EG CV capacity (kW)	147	147	147	140	147	147	147	147	147
EV CV capacity (kW)	66	66	66	66	66	66	66	66	66
Building CV capacity (kW)	164	164	164	164	164	164	164	164	164
Energy dispatch									
PV output energy (MWh/year)	920	-	34	614	-	289	915	-	265
WT output energy (MWh/year)	-	1512	1648	-	1137	809	-	1425	873
Curtailed energy (MWh/year)	133	400	513	0.07	222	135	138	425	200
BESS energy (MWh/year)	280	78	57	189	88	62	247	70	65
EG supplied energy (MWh/year)	327	243	226	350	353	257	352	290	238
EG injected energy (MWh/year)	139	403	440	37	308	300	160	345	256
System losses energy (MWh/year)	158	134	136	110	118	103	150	126	102

Table 9: The microgrid components capacities and energy of Brest, Marseille, and Le Havre cities.

€/kWh), Doha, QA (0.28 €/kWh), and Lisboa, PT (0.27 €/kWh) maintain relatively low LCOE values across all scenarios, suggesting more efficient energy production. Similarly, S2 generally presents higher LCE values compared to S1 and S3. This trend is particularly evident in cities such as Bern, CH (1.62 $kgCO_2$,eq/kWh), Ajaccio, FR (1.37 $kgCO_2$,eq/kWh), and Bamako, ML (0.66 $kgCO_2$,eq/kWh), indicating a higher carbon footprint associated with energy production in these locations. In contrast, most cities exhibit lower and relatively consistent LCE values under S1 and S3. Cities like Cairo, EG (0.03 $kgCO_2$,eq/kWh), Lisboa, PT (0.035 $kgCO_2$,eq/kWh), and Toulouse, FR (0.038 $kgCO_2$,eq/kWh) demonstrate low emissions across all scenarios, suggesting more sustainable and environmentally friendly energy production practices. The heat maps effectively highlight cities and scenarios that may pose significant cost and environmental challenges. S2 stands out as particularly problematic for both LCOE and LCE, indicating potential uncertainties or higher risk factors associated with this scenario. The color gradients facilitate quick visual assessments, identifying areas where strategic interventions might be necessary to mitigate costs and reduce carbon emissions. This information is crucial for informed decision-making in energy investments and policy-making aimed at carbon reduction initiatives.

These results are consistent with the data presented in Table 7, which indicates that Cairo has the highest average solar irradiation. However, the ranking based on average solar irradiation does not consistently match the order of cities based on LCOE and LCE. This discrepancy is primarily due to the variations in solar irradiation across different months and seasons, rather than solely depending on the annual average solar irradiation. For example, although Dijon has a higher average solar irradiation than Poitiers, Poitiers achieves a lower LCOE and LCE. Fig. 34 illustrates this phenomenon by presenting the monthly solar irradiation data for both Dijon and Poitiers. It is noteworthy that during the summer and spring seasons, Dijon experiences higher levels of solar irradiation compared to Poitiers. However, during the autumn

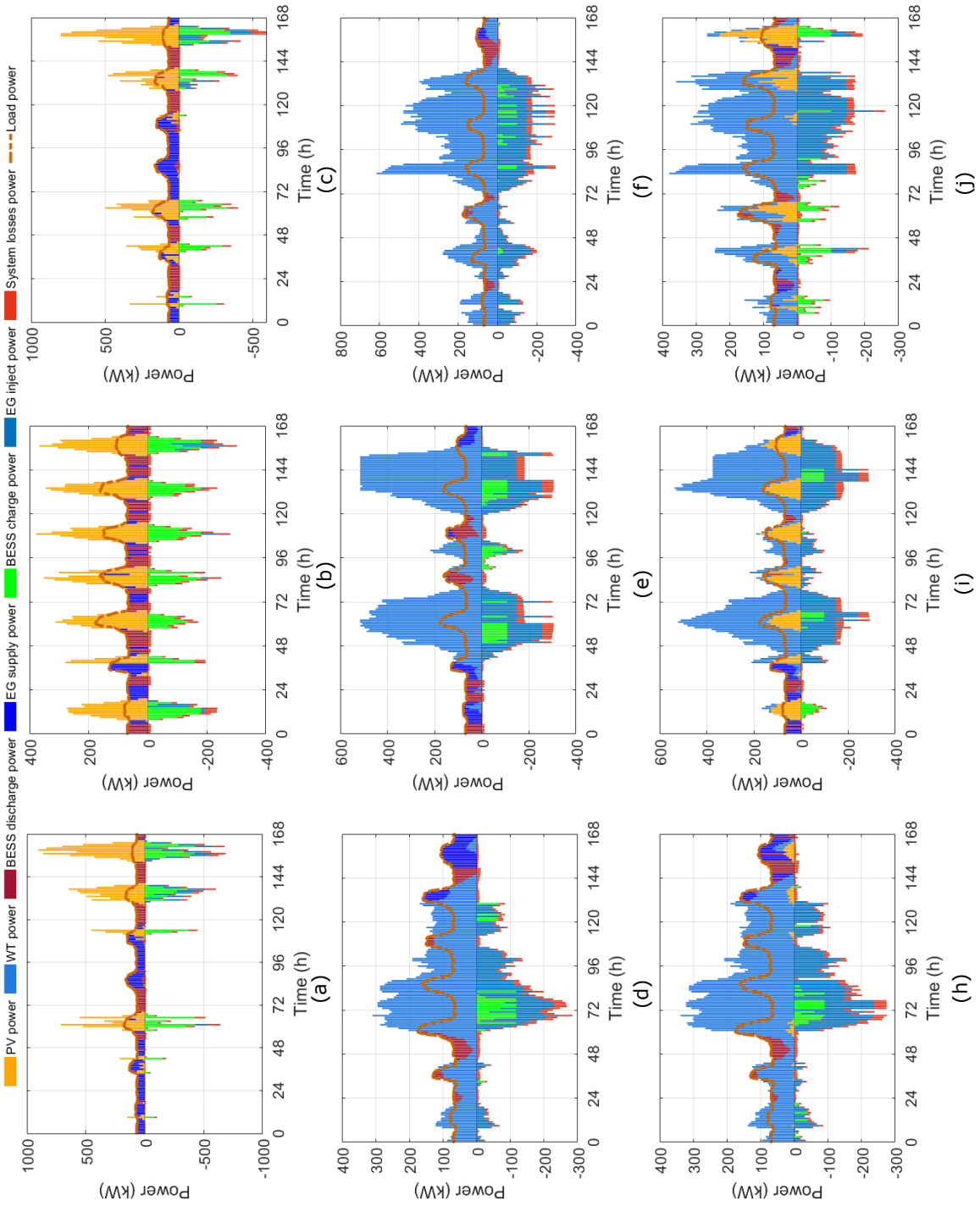

Figure 31: One week (1st of July's week) of the one-year simulation for S1 (a) Brest (b) Marseille (c) Le Havre, S2 (d) Brest (e) Marseille (f) Le Havre, S3 (h) Brest (i) Marseille (j) Le Havre.

and winter seasons, Dijon's solar irradiation is lower than that of Poitiers. As a result, to meet the load demand during the autumn and winter months in Dijon, the optimization algorithm increases the PV capacity. In contrast, while Poitiers' solar irradiation in summer and spring is not as high as that of Dijon, it is still sufficient to cover the load requirements. Moreover, the significantly higher solar irradiation in Poitiers during the autumn and winter seasons allows

for a lower PV capacity compared to Dijon. Thus, the LCOE and LCE can vary significantly between different cities even when the load remains the same, highlighting the importance of seasonal and monthly variations in solar irradiation in determining the optimal energy strategy.

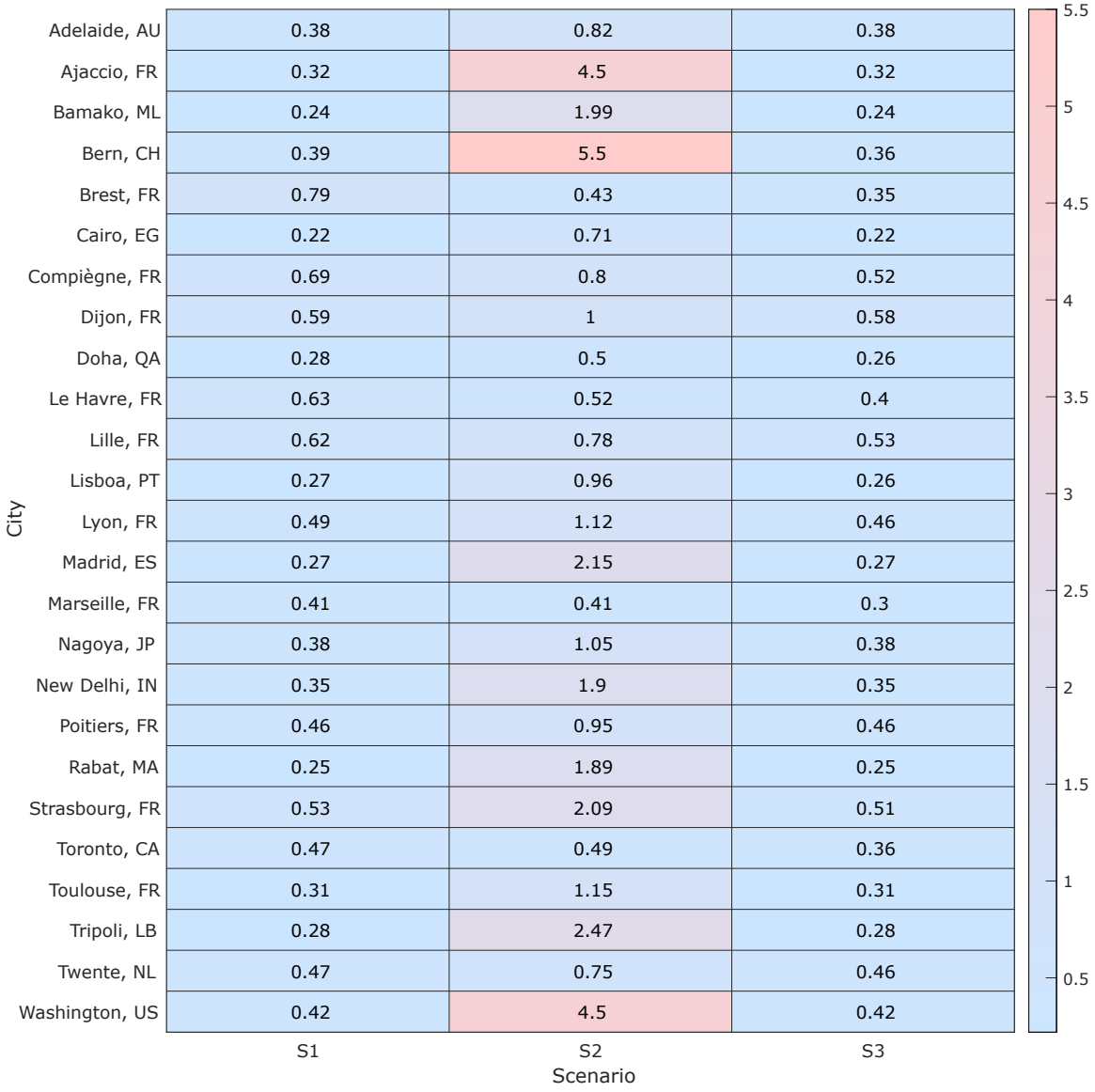

Figure 32: Heat map for the LCOE values of different studied cities.

The descriptive statistics are presented in Table 10, and the box plots for the LCOE and LCE results across the three scenarios are illustrated in Fig. 35. The LCOE and LCE reveal notable variability across the three analyzed scenarios (S1, S2, and S3), with S2 exhibiting the highest mean LCOE at 1.57 €/kWh and significant variability, as demonstrated by its standard deviation and variance. This suggests a wide range of cost outcomes for S2, further substantiated by a broad range and a high IQR. In contrast, S1 and S3 present lower mean values and considerably less variability, indicating more consistent cost outcomes. The median values for S1 and S3 closely approximate their means by pointing to symmetric distributions. However, the median for S2 is significantly lower than its mean, indicating a right-skewed distribution.

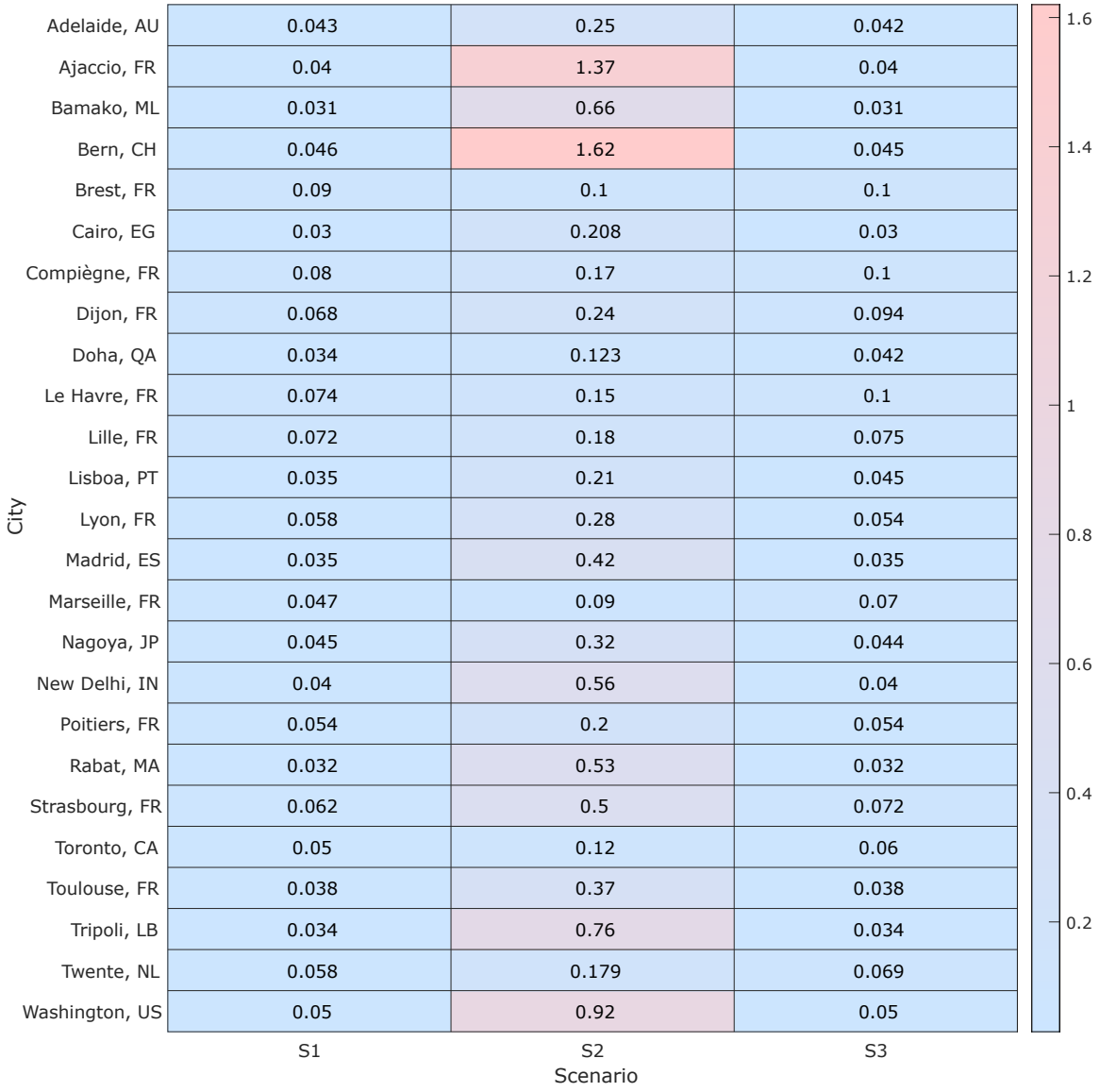

Figure 33: Heat map for the LCE values of different studied cities.

Similarly, S2 shows the highest mean LCE and the highest variability. The high range and IQR further underscore the substantial dispersion in carbon emissions for S2. Conversely, S1 and S3 exhibit lower mean values and minimal variability, as evidenced by their low standard deviations and variances. The median values for S1 and S3 closely match their means, suggesting symmetric distributions. In contrast, the median for S2 is markedly lower than its mean, indicating a right-skewed distribution. These analyses highlight S2 as the most variable and costly in terms of both LCOE and LCE, indicating higher uncertainty or risk factors associated with this scenario. Conversely, S1 and S3 appear to be more stable and cost-effective, suggesting they might be more reliable for cost and emission projections.

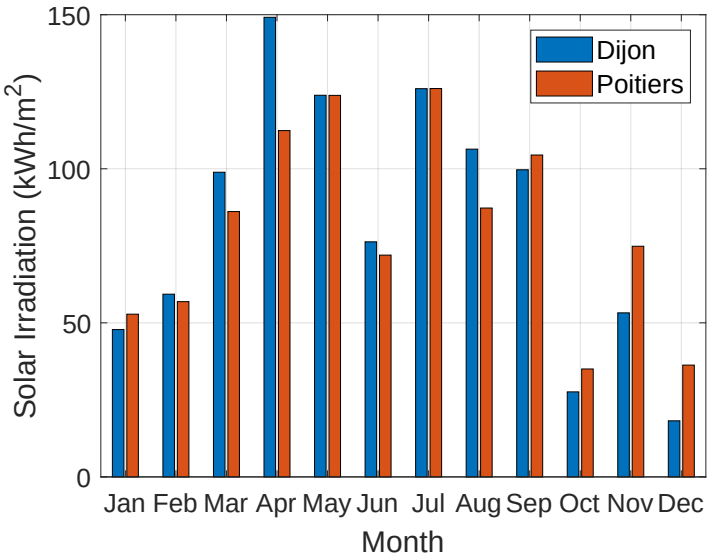

Figure 34: The monthly solar irradiation data for both Dijon and Poitiers.

Parameter/Variable	LCOE (€/kWh)			LCE (kgCO_2,eq/kWh)		
	S1	S2	S3	S1	S2	S3
Mean	0.42	1.57	0.36	0.05	0.42	0.05
Median	0.39	1	0.36	0.046	0.25	0.045
Standard Deviation	0.15	1.37	0.10	0.01	0.39	0.02
Variance	0.02	1.89	0.01	0.0003	0.15	0.0005
Q1 (25th Percentile)	0.28	0.75	0.28	0.035	0.179	0.04
Q3 (75th Percentile)	0.49	1.99	0.46	0.058	0.53	0.07
IQR	0.21	1.24	0.18	0.023	0.351	0.03
Max	0.79	5.5	0.58	0.09	1.62	0.1
Min	0.22	0.41	0.22	0.03	0.09	0.03
Range	0.57	5.09	0.36	0.06	1.53	0.07

Table 10: Descriptive statistics for LCOE and LCE values

IV.3.2 Analysis of Different PV, BESS and WT typologies

The technology analysis involves testing the optimization algorithm across various PV, BESS, and WT technologies. These technologies differ in cost and emissions profiles, encompassing five PV panels, two BESSs, and two WTs. The PV panels evaluated in this study include JinkoSolar, DualSun, JASolar, Systovi, and a PCM PV [181]. The WT models investigated are Schachner05 and Piggott2F16P [179]. Two types of BESSs, namely Li-ion and Lead acid, are analyzed. The parameters for the JinkoSolar PV have been previously detailed in Table 3, while the parameters for the DualSun PV and the Schachner05 WT are presented in Table 6. The technical, economic, and environmental parameters for the remaining technologies are compiled in Table 11. In the Compiègne case study, various configurations of PV panels, BESSs, and WTs were analyzed. These configurations, as detailed in Table 7, were evaluated using a specific load profile. The LCOE and LCE for each configuration are summarized in Fig. 36. The LCOE optimization was conducted under the constraint that the LCE should be less than or equal to 0.3 kgCO_2,eq/kWh. Among the configurations, the highest LCOE was observed in the Systovi/Li-ion/Piggott2F16P combination, while the highest LCE was recorded for the PCM/Li-ion/Schachner05 combination. Conversely, the lowest LCOE was

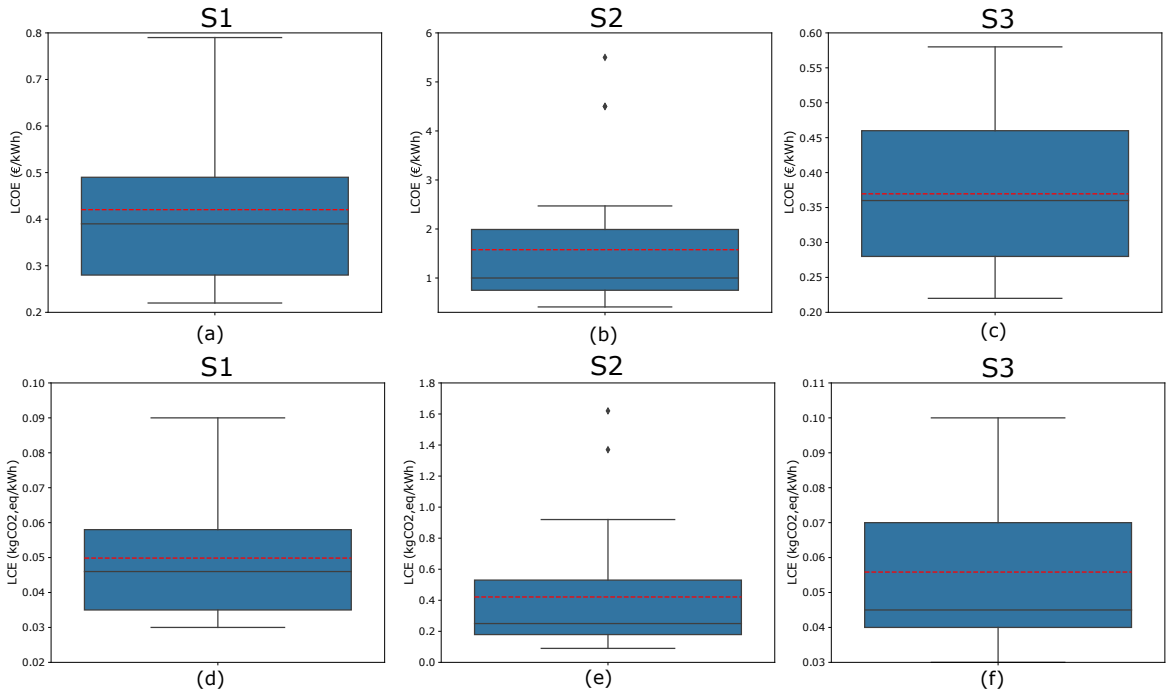

Figure 35: Box plot for the LCOE (a) S1, (b) S2, (c) S3, and for the LCE (d) S1, (e) S2, (f) S3.

found in the PCM/Lead acid/Schachner05 combination, and the lowest LCE was achieved with the Systovi/Li-ion/Piggott2F16P combination. Analyzing the mean LCOE values, the Systovi configuration had the highest mean LCOE at 0.67 €/kWh, whereas the PCM configuration had the lowest mean LCOE at 0.39 €/kWh. This discrepancy highlights the Systovi and PCM configurations as representing the extremes in terms of LCOE. In terms of LCE, the Systovi combination exhibited the lowest mean value of 0.11 $kgCO_2$,eq/kWh, while the PCM configuration showed the highest mean LCE at 0.27 $kgCO_2$,eq/kWh. This indicates that the Systovi and PCM configurations also represent the extremes in terms of LCE. The high LCE of the PCM PV panels can be attributed to the material used in them [181], whereas the low LCE of the Systovi PV panels is due to their local production in France, reducing transportation-related emissions [174]. When examining the BESS and WT combinations, the highest mean LCOE was found in the Li-ion/Piggott2F16P combination at 0.61 €/kWh, while the lowest mean LCOE was associated with the Lead acid/Schachner05 combination at 0.42 €/kWh. Regarding LCE, the Lead acid/Piggott2F16P combination had the highest mean value of 0.17 $kgCO_2$,eq/kWh, and the Li-ion/Piggott2F16P combination had the lowest mean value of 0.13 $kgCO_2$,eq/kWh.These results indicate that the impact of the BESS on LCE is more significant than that of the WT. Configurations with lower BESS LCE consistently correspond to lower overall LCE means, and vice versa. Thus, the BESS LCE plays a dominant role in determining the total LCE of the configurations.

Parameter	Value	Unit	Parameter	Value	Unit
JASolar PV			**Lead acid BESS**		
NOCT	45	°C	Charging efficiency	90	%
PV module-rated power	310	Wp	Discharging efficiency	90	%
Power temperature coefficient	-0.37	%/°C	Max lifetime	5	years
Lifetime	25	years	Unit capacity	1.8	kWh
Investment cost	450	€	SOC initial	0.5	pu
Maintenance cost	1	% of PV inv cost/year	SOC min	0.2	pu
CO_2 emissions	1349	$kgCO_2$,eq/kWp	SOC max	1	pu
PCM PV			Investment cost	200	€
NOCT	45	°C	Maintenance cost	3	% of BESS inv cost/year
PV module-rated power	200	Wp	Replacement cost	200	€
Power temperature coefficient	-45	%/°C	CO_2 emissions	146	$kgCO_2$,eq/kWh
Lifetime	25	years	**Piggott2F16P WT**		
Investment cost	90	€	Rated power	0.4	kW
Maintenance cost	1	% of PV inv cost/year	Investment cost	2000	€
CO_2 emissions	2625	$kgCO_2$,eq/kWp	Maintenance cost	3	% of wind inv cost/year
Systovi PV			Cut in speed	2.5	m/s
NOCT	42	°C	Rated wind speed	11	m/s
PV module-rated power	300	Wp	Lifetime	20	years
Power temperature coefficient	-0.26	%/°C	CO_2 emissions	1235	$kgCO_2$,eq/kW
Lifetime	25	years			
Investment cost	1000	€			
Maintenance cost	1	% of PV inv cost/year			
CO_2 emissions	227	$kgCO_2$,eq/kWp			

Table 11: Different PV, WT and BESS parameters data [174, 179, 102]

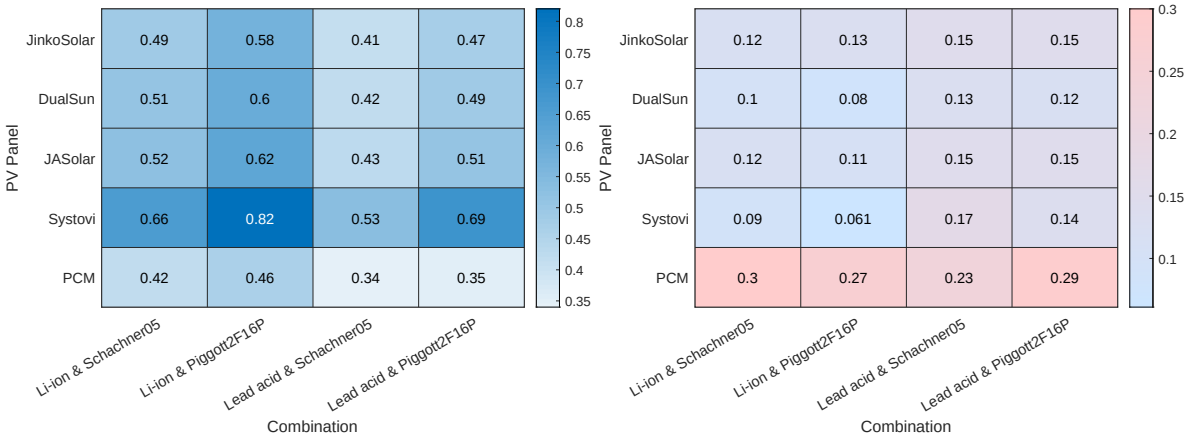

Figure 36: The heat map values of (a) LCOE and (b) LCE for different combinations of PV panels, BESS, and WT models.

IV.4 Conclusions

In this study, a MILP algorithm is developed for optimizing the size and EM of microgrids across various cities and technologies. The test case is based on the energy load of a university building including the consumption by EVs. The optimization problem considers the economic horizon over the project's lifetime with the objective of minimizing both the LCOE and LCE. Three scenarios were defined based on the inclusion of renewable energy sources: S1 excludes WTs, S2 excludes PV panels, and S3 includes both PV panels and WTs. The results indicate that cities with high solar irradiation exhibit the same LCOE and LCE in scenarios involving PV/BESS and PV/WT/BESS. This outcome is due to the optimization algorithm favoring PV integration over WT, as incorporating WTs does not reduce LCOE and LCE in these cities. Furthermore, scenarios including PV/WT/BESS yield the lowest LCOE and LCE values, while

the WT/BESS scenario results in the highest LCOE and LCE. It is also observed that the order of cities based on average solar irradiation or wind speed does not necessarily correspond to the order of LCOE and LCE. Monthly and daily fluctuations in solar irradiation and wind speed significantly impact these results. The study emphasizes the importance of a well-sized combination of renewable resources to optimize the economic and environmental performance of energy systems in different cities. There is no universal solution; hence, a thorough assessment of local conditions and available resources is crucial for making decisions tailored to each specific city. Regarding the technologies, locally produced PV panels contribute positively to the overall LCE of the microgrid, with PV panels incorporating PCM showing higher LCE. Additionally, the LCE associated with BESS plays a dominant role in determining the total LCE of the configurations.

Chapter V

Comparative Analysis of Cascaded MILP and Embedded APSO-MILP Algorithms for Multi-objective Microgrid Sizing with EV Demand Flexibility

This chapter encompasses an analysis of the project's lifetime from technical, economic, and environmental perspectives. It also takes into account battery degradation and allows for load shedding according to the VoLL except for critical loads in the university building. Additionally, a significant focus of the study is the flexibility of EV loads within the microgrid's EM system. This builds upon the foundation set by the previous chapter III, which focused on a MILP approach for minimizing energy costs and carbon emissions. The current chapter introduces two algorithms: Algorithm 1 employs a cascaded MILP approach, where the initial phase optimizes microgrid sizing and EM without EV flexibility over an 8760-hour horizon considering the project's lifetime. The subsequent phase focuses on daily EV flexibility alongside microgrid EM. Algorithm 2 integrates APSO with MILP for determining the sizes of microgrid components (PV panels, WTs, and BESS) through APSO, and for performing daily EM including EV flexibility with MILP. Notably, both algorithms incorporate a kWh throughput model for the BESS, addressing the degradation model not present in chapter III due to its non-linearity in a unified MILP approach. A significant improvement compared to the previous work is the inclusion of EV flexibility and urban WTs in the microgrid system. The optimization problems within both algorithms are implemented in Python and solved using CPLEX in order to minimize both the LCOE and the LCE. Loads are segregated between the EV and a university building with the latter's data derived from a research and teaching facility at the Université de Technologie de Compiègne. This data incorporates probabilistic modeling for EV load. The study utilizes real economic and environmental data while considering load growth and employing actual solar irradiation, ambient temperature, and wind speed data for realistic microgrid planning. The main contributions of this study are:

- addressing the challenges of sizing and EM of the microgrid taking into account the project lifetime. The emphasis is on attaining hourly energy optimization within the microgrid;
- incorporating technical, economic, and environmental aspects, the study develops an integrated multi-objective MILP algorithm for the microgrid domain. Two specific algorithms are designed to identify the optimal solution, aiming to reduce both the LCOE and the LCE of the microgrid;
- providing a comprehensive comparison between two different algorithms, with the first based on a mathematical approach and the second on an embedded approach (APSO & MILP);
- integrating EV flexibility in microgrid planning and EM within a MILP algorithm while maintaining a time horizon of 8760 hours with a one-hour time step;
- conducting a comparison between EV flexibility and non-EV flexibility scenarios considering both load shedding and non-load shedding conditions for each algorithm;
- consideration of the battery degradation and load shedding scenario for both EV and non critical loads of the university building.

The chapter is organized as follows: Section V.1 presents the battery degradation model.

The formulation of the optimization problem is discussed in Section V.2. Results are analyzed in Section V.3, and conclusions are drawn in Section V.4.

V.1 Battery Degradation Model

The microgrid studied in this chapter is the same one presented in Chapter IV, with the PV, BESS, and WT models being identical to those in Chapter III, Section III.1, and Chapter IV, Section IV.1. The battery degradation model is presented in this section.

The lifetime of BESS is influenced by various operating conditions, including charge factor, ampere-hour (Ah) throughput, highest discharge rate, time between full charges, time at low SOC, and partial cycling [182]. In this research, the Ah throughput method is transformed into the kWh throughput method as detailed in [183, 184]. This conversion involves multiplying the BESS terminal voltage by Ah with the assumption that the BESS terminal voltage is equivalent to the nominal voltage. The kWh throughput method involves quantifying the energy exchange of the BESS under the assumption that a fixed amount of energy can be cycled through the system before it is expected to degrade. This method does not take into account individual cycle depths or other specific parameters that consider the direction of power flow in or out of the BESS. The estimated kWh throughput is determined by factors (i.e. the DOD, cycles to failure, and BESS capacity in kWh) which are provided by the manufacturer. The calculation of the kWh lifetime throughput (L_n) for each DOD n can be carried out, as outlined in [185]:

$$L_n = E_b \cdot g_n \cdot f_n \tag{1}$$

In the equation provided, E_b represents the BESS capacity in kWh, g_n represents the n^{th} DOD in percentage, and f_n represents the number of cycles to failure for the n^{th} DOD. The BESS degradation cost per kWh delivered (€/kWh) (B_{deg}) is formulated as in [185]:

$$B_{deg} = \frac{C_b^{rep} \cdot N_b}{L_n \cdot E} \tag{2}$$

where C_b^{rep} is the BESS replacement cost, N_b is the BESS number, E is the square root of the round-trip efficiency of BESS.

V.2 Formulation of the Optimization Problem

The formulation of the optimization problem encompasses both an objective function and a set of constraints, laying the groundwork for achieving a balanced solution. In this context, the specific optimization problem formulations for Algorithm 1 and Algorithm 2 are detailed in this section. Algorithm 1 employs a cascaded MILP methodology, where each stage is defined by unique constraints and an objective function. On the other hand, Algorithm 2 distinguishes itself through a hybrid framework that integrates APSO and MILP by blending heuristic strategies with rigorous mathematical optimization. This combination allows Algorithm 2 to lever-

age the strengths of both approaches that facilitates a more dynamic and potentially efficient search for optimal solutions.

V.2.1 Algorithm 1: Cascaded MILP

The overall structure of the cascaded MILP algorithm is shown in Fig. 37. In the first stage, the sizing and EM are unified into a single optimization problem with an optimization horizon of 8760 while taking into account the 20-year project lifespan. However, the flexibility of EVs charging power is not considered within the first stage. This omission is driven by concerns regarding computational complexity. Explicitly incorporating detailed EV power flexibility within the MILP framework will significantly extend the computation time because of the high number of constraints and decision variables. The potential increase in computational complexity could strain the computer's capacity to handle a large number of linear equations. The first stage microgrid sizing output serves as an input for the second stage. Moreover, the daily EM of microgrid components is carried out, explicitly incorporating the flexibility of EVs. The computation of the LCOE and LCE is performed after the EM results for each microgrid component are obtained for all 365 days of the year. The LCOE and LCE calculations takes well into account the project lifespan. The detailed equations of each phase of the MILP cascade algorithm are presented in the following sections.

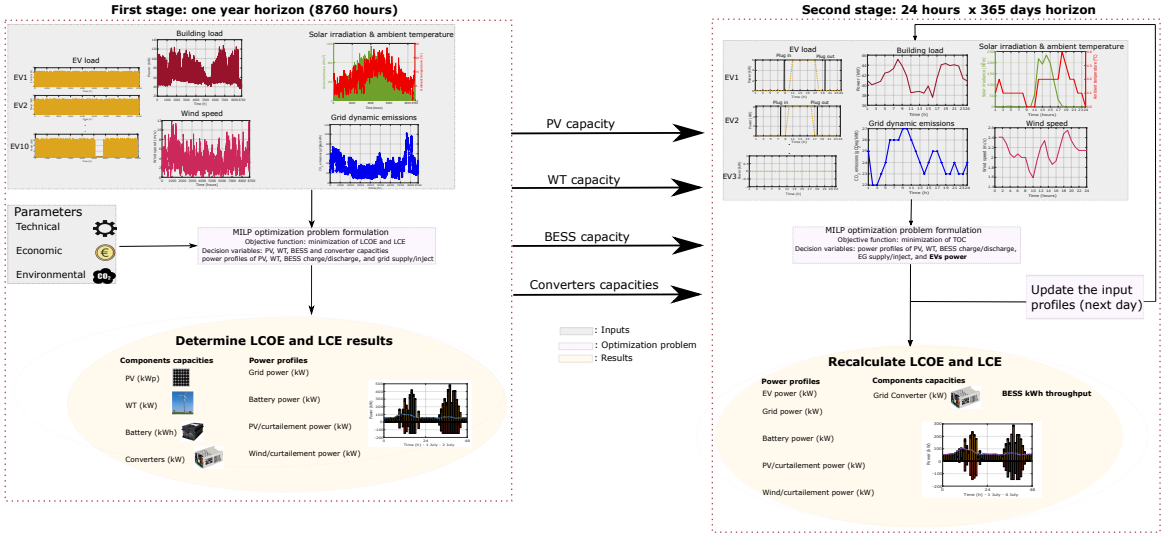

Figure 37: Cascaded MILP algorithm structure.

V.2.1.1 First Stage Constraints & Objective Functions

The first stage of the cascaded MILP algorithm is the combination of constraints presented in chapter III and chapter IV. However, the load shedding scenario is included in the analysis of the algorithm. Regulating bus power $p_{bus}(t)$ is crucial within the optimization algorithm's framework, directly influencing its strategic decisions. When $p_{bus}(t) \leq 0$, it indicates a restriction against load shedding with any excess energy from PV and WT resulting in negative

power. Conversely, enforcing $p_{bus}(t) = 0$ denotes a precise balance between energy production and consumption, which might not always align with economic efficiency. This scenario can prompt the algorithm to prefer scenarios that incorporate a larger capacity for the BESS to accommodate the surplus energy from PV and WT sources. Permitting $p_{bus}(t)$ to adopt positive values allows for the possibility of load shedding, although this should incur a cost to prevent the algorithm from opting to shed the entire load indiscriminately. It is essential to implement a constraint such as $p_{bus}(t) \leq p_{buil}^{shed}(t) + p_{EV}^{shed}(t)$, underscoring a critical limit where p_{buil}^{shed} and p_{EV}^{shed} serve as the decision variables for shedding loads related to buildings and EV, respectively, which are limited between as follows:

$$0 \leq p_{bui}^{shed}(t) \leq \text{LPSP} \cdot p_{buil}(t) \tag{3}$$

$$0 \leq p_{EV}^{shed}(t) \leq p_{EV}(t) \tag{4}$$

The optimization problem involves the minimization of LCOE and LCE. The LCOE is calculated as [68, 186] with the TC calculated by adding the building and EV shedding costs as follows:

$$TC = C^{inv} + C^{mtn} + C^{rep} + C^{EG} + C_{bui}^{pen} + C_{EV}^{pen} - C^{sv} \tag{5}$$

$$C_{bui}^{pen} = \sum_{t=t_0}^{t_f} p_{bui}^{shed}(t) \cdot \text{VoLL} \cdot \Delta t \tag{6}$$

$$C_{EV}^{pen} = \sum_{t=t_0}^{t_f} p_{EV}^{shed}(t) \cdot \text{VoLL} \cdot \Delta t \tag{7}$$

The EV and the building penalization costs (C_{bui}^{pen}, C_{EV}^{pen}) are considered as a VoLL, which represents the willingness to pay to avoid a kWh of a power outage (€/kWh) [187]. The weighted sum approach is employed to address the multi-objective optimization problem. To enable the optimization solver to find a suitable solution, it is necessary to normalize the two objectives. This normalization process [156], is achieved through min-max scaling, and it is expressed as follows:

$$LCOE_{norm} = \frac{LCOE - LCOE_{min}}{LCOE_{max} - LCOE_{min}} \tag{8}$$

$$LCE_{norm} = \frac{LCE - LCE_{min}}{LCE_{max} - LCE_{min}} \tag{9}$$

The normalized LCOE and LCE are denoted as $LCOE_{norm}$ and LCE_{norm}, respectively. Conducting optimization solely for LCE minimization yields $LCOE_{min}$ and LCE_{max} values. Conversely, optimizing without LCOE minimization results in LCE_{min} and $LCOE_{max}$ values. The weighted sum technique involves multiplying each objective function by a respective weight, denoted as w. This weight signify the priority assigned to each objective function, and the process is outlined as follows:

$$\min\{w \cdot LCOE_{norm} + (1-w) \cdot LCE_{norm}\} \tag{10}$$

In this study, the focus is on the two extreme strategies: LCOE and LCE minimizations. This is achieved by setting $w = 1$ for LCOE minimization and $w = 0$ for LCE minimization. The optimization problem expressed in Eq. (10) is addressed by determining the following decision variables: BESS capacity (E_b), the number of PV panels (N_{PV}), the number of WTs (N_{WT}), BESS charge/discharge powers ($p_b^c(t)/p_b^d(t)$), EG supply/inject powers ($p_{EG}^s(t)/p_{EG}^{in}(t)$), and

auxiliary variables ($x_{aux}(t)$). Additionally, the capacities of PV, WT, BESS, EG, EV, and building-associated CVs ($M_{PV}^{DC/DC}$, $M_{WT}^{AC/DC}$, $M_{b}^{DC/DC}$, $M_{EG}^{AC/DC}$, $M_{EV}^{DC/AC}$, $M_{buil}^{DC/AC}$) are also determined.

V.2.1.2 Second Stage Constraints & Objective Functions

In the second stage, constraints from Section V.2.1.1 are retained with some modifications and the incorporation of additional constraints. The optimization in this stage is performed day by day (24 hours), hence the optimization is repeated 365 time. The primary distinction between the first and second stage lies in the flexibility of EV power. Flexibility of EVs implies that the charging process does not necessarily start immediately upon plugging in the EV. Instead, the EV could charge at times when DERs production is high or when grid supply tariffs are at their lowest. The contrast between EV flexibility and non-flexibility is depicted in Fig. 38 [101]. EV flexibility in the context of optimization requires the addition of EV charging power

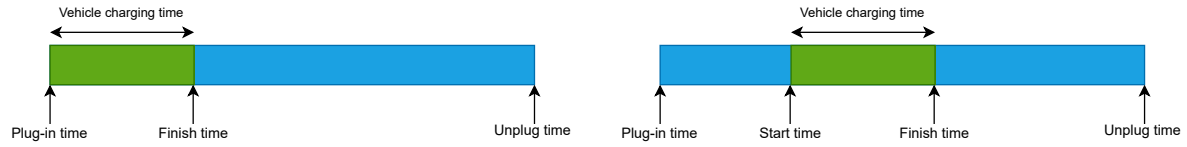

Figure 38: The difference between EV flexibility and non-flexibility [101]

as a decision variable. In this study, this decision variable is p_{EV}^{sche}. The constraints added to this stage are formulated as follows:

$$p_{EV,a}^{sche}(t,d) = \begin{cases} 0 \leq p_{EV,a}^{sche}(t,d) \leq P_{cs} & \text{if } t_{pin} \leq t \leq t_{pout} \\ 0, & \text{otherwise} \end{cases} \tag{11}$$

$$e_{EV,a}(t_{pout}) \leq SOC_{EV,a}^{des} \cdot EV_{cap,a} \tag{12}$$

$$e_{EV,a}(t) = e_{EV,a}(t-1) + p_{EV,a}^{sche}(t) \cdot \Delta t \tag{13}$$

$$p_{bus}(t) \leq p_{bui}^{shed}(t) \tag{14}$$

where d is the day index and t_{pout} is the unplug time. In Eq. (11), $p_{EV,a}^{sche}$ is equal to zero if the EV is not connected to the charging station. Otherwise, $p_{EV,a}^{sche}$ can go up to the maximum charger power limit (P_{cs}) to charge EV. In Eq. (12), EV battery state of energy ($e_{EV,a}$) could be less than or equal to the desired SOC ($SOC_{EV,a}^{des}$) at t_{pout} with the EV state of energy is calculated in Eq. (13). The permission of building load shedding is set by $p_{bus}(t)$ as in Eq. (14). It is noteworthy to mention that allowing building load and EV shedding is necessary in the second stage, because the optimization may not find a solution on days when PV/WT production, BESS discharge, and EG supply are not sufficient to meet the load. The objective function of the second stage, which is a single-objective of TOC minimization, is calculated as follows:

$$\min\{TOC = C_{EG}^{op} + C_{b}^{op} + C_{bui}^{pen} + C_{EV}^{pen}\} \tag{15}$$

$$C_{EG}^{op} = \sum_{t_0}^{t_f} \left(-p_{EG}^{s}(t) \cdot \lambda^{s}(t) - p_{EG}^{in}(t) \cdot \lambda^{in}\right) \cdot \Delta t \tag{16}$$

$$C_{b}^{op} = \sum_{t=t_0}^{t_f} -p_{b}^{d}(t) \cdot B_{deg} \cdot \Delta t \tag{17}$$

$$C_{EV,a}^{pen} = \left(SOC_{EV,a}^{des} \cdot EV_{cap,a} - e_{EV,a}(t_{pout})\right) \cdot \text{VoLL} \tag{18}$$

where C_{EG}^{op} and C_{b}^{op} are the total operation cost of the EG and BESS, respectively. C_{EV}^{pen} is the penalty cost of all connected EVs if the EV state of energy does not reach the desired state of energy. C_{bui}^{pen} is calculated as in Eq. (6). The objective function expressed in Eq. (15) is addressed by determining the following decision variables: BESS charge/discharge powers $p_b^c(t)/p_b^d(t)$, EG supply/inject powers $p_{EG}^{s}(t)/p_{EG}^{in}(t)$, and auxiliary variables $x_{aux}(t)$. Additionally, the EV scheduled power $p_{EV,a}^{sche}(t)$ and the building shedded power $p_{bui}^{shed}(t)$ are considered.

V.2.2 Algorithm 2: Embedded APSO & MILP

The structure of the embedded APSO & MILP algorithm is illustrated in Fig. 39. This microgrid sizing and EM are integrated into a single optimization platform by incorporating both APSO and MILP algorithms. Initially, the APSO algorithm generates a random population, which includes varied capacities of PV, WT, and BESS. This population is then evaluated through a day-by-day optimization process using MILP, which also incorporates EV flexibility. The optimization is carried out for each day of the year, totaling 365 days. After this annual cycle, the capacities of the converters are determined based on the peak powers that exceed their current capacities. Additionally, the energy delivered by the BESS is calculated to assess the need for any potential BESS replacements. The energy supplied or injected by the EG is also determined. These three sets of information, along with the capacities of the microgrid components, provide the necessary data to compute the LCOE and the LCE. This data is then fed back into the APSO to update the particles and evaluate their performance. This iterative process repeats until the difference between two consecutive iterations (LCOE and LCE results) is less than 10^{-6}. It should be noted that the MILP stage in this algorithm is the same as the second stage of the cascaded MILP algorithm presented in Section V.2.1.2 while the APSO algorithm is presented in the following section.

Heuristic optimization algorithms can find the near optimal solution of the non-convex, non-linear, and multi-modal problems by randomly exploring the search space of the objective function [188].The major advantage of the heuristic optimization over the deterministic algorithms is its ability to locate the near-global optimum without the dependence on the gradients. In this research, we propose the variant of the conventional Particle Swarm Optimization (PSO) method namely Accelerated PSO to solve the suggested platform [189]. This part of the section provides the brief introduction for PSO and APSO techniques.

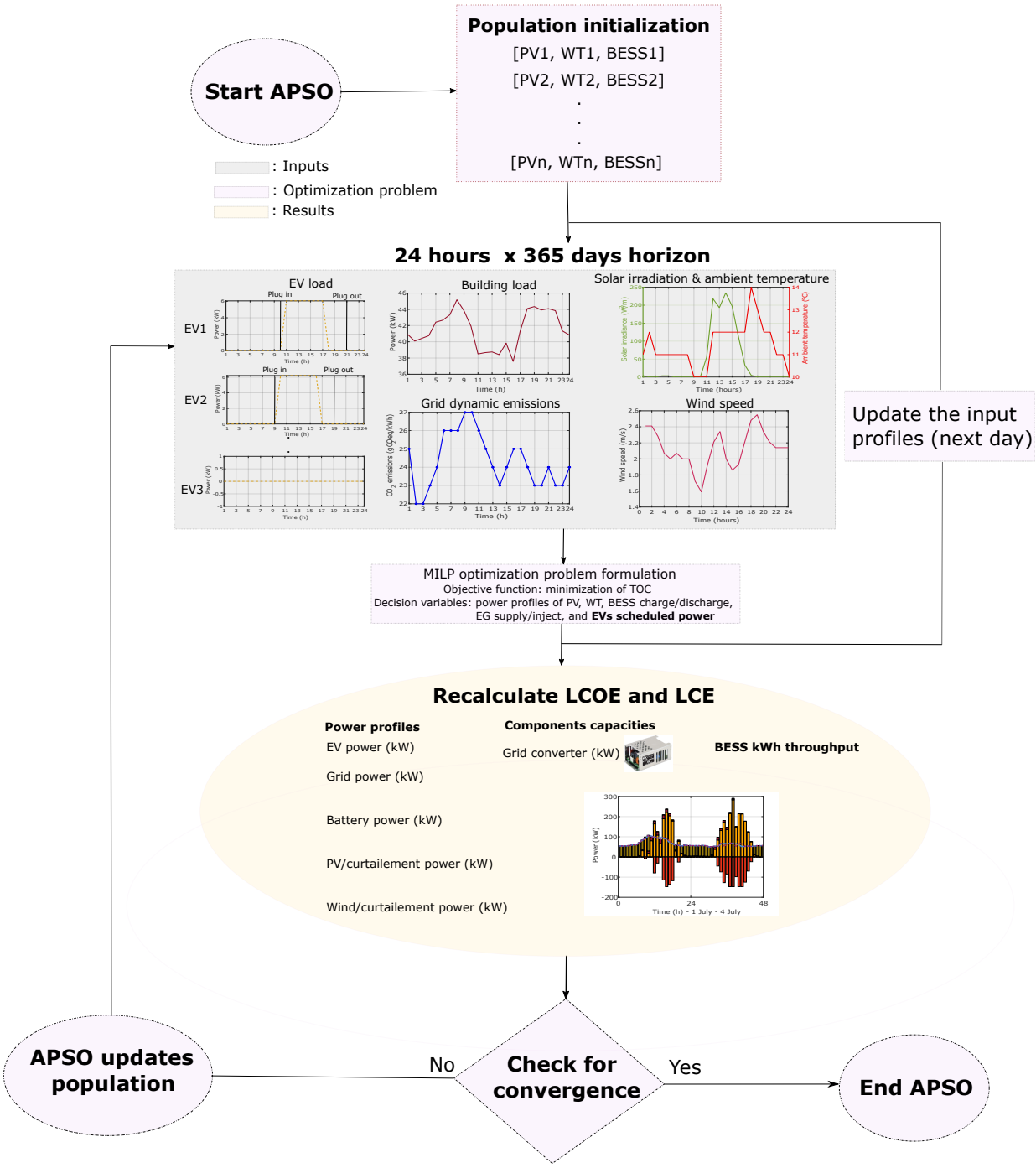

Figure 39: Embedded APSO & MILP algorithm structure.

V.2.2.1 Particle Swarm Optimization

The major components of the PSO are the exploitation and exploration of the objective function. Each particle which presents the possible solution of the objective function has a velocity V_P and position X_P components associated with it [190]. The particle's dimensions correspond to the decision variables of the objective function. The total number of particles constitute the population matrix of the optimization problem. At each iteration K, the X_P and V_P components are updated as follows:

$$V_P^{K+1} = V_P^K + \eta_1\beta_1 \odot (G_B - X_P^K) + \eta_2\beta_2 \odot (X_{best} - X_P^K) \tag{19}$$

where, η_1, η_2 represent the acceleration coefficients which control the movement of the velocity component V_P towards the global best G_B and local best X_{best} respectively. β_1, β_2 represent the uniform random numbers in the range [0,1]. The position component X_P can then be updated based on V_P as follows [191]:

$$X_P^{K+1} = X_P^K + V_P^{K+1} \tag{20}$$

At each iteration K, both the V_P and X_P components are updated using the criteria defined above till all the particles converge to the single point or the set termination criterion is achieved.

V.2.2.2 Accelerated Particle Swarm Optimization

APSO is the variant of the PSO which uses a single update equation using the global best position of the particles to update the position component. The advantage of using the APSO is its simple update criterion with minimal number of tuning parameters [192]. The update equation in the case of the APSO can be written as follows:

$$X_P^{K+1} = (1-\delta)X_P^K + \delta G_B + \alpha(C - \frac{1}{2}) \tag{21}$$

where, δ controls the movement of the component X_P towards the global best position G_B. α controls the random movement of the particles [193]. C represents the randomly generated vector in the range of [0,1]. Fig. 40 shows the vector diagrams for the PSO and APSO algorithms. This completes the brief introduction of the heuristic methods for solving the suggested platform.

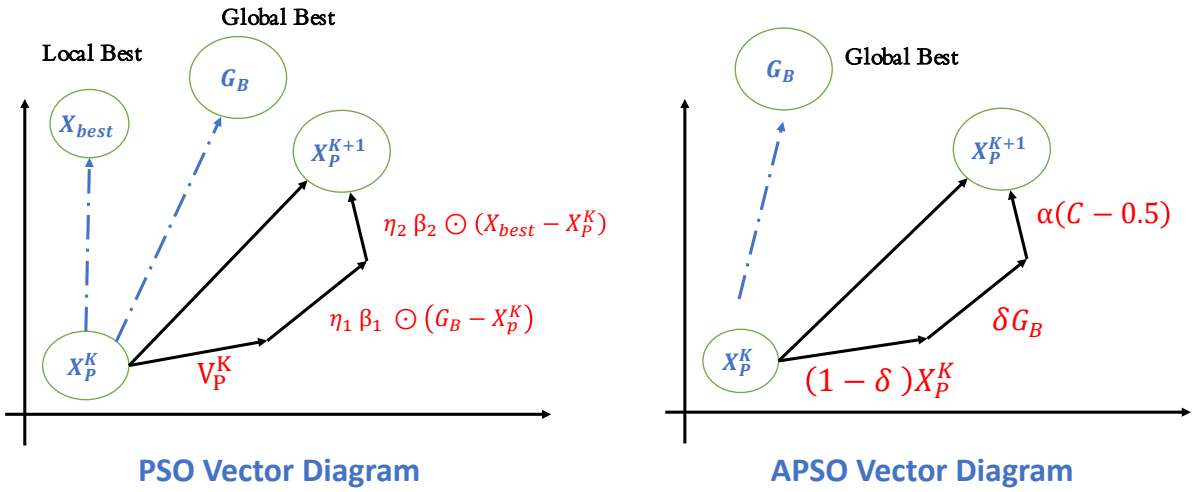

Figure 40: Vector diagrams for PSO and APSO methods.

V.3 Results and Analysis

In the studied microgrid, the demand power (includes EVs and the university building) is modeled as described in Chapter IV (see Fig.28). The solar irradiation and ambient temperature used in this chapter are the same used in Chapter III (see Fig. 16a) while the wind speed for Compiègne is presented in Fig. 41. Additionally, the EG's CO_2 emissions are modeled as in Chapter III (see Fig.16c). The technical, economic, and environmental data used in this study are the same as those presented in the previous chapter, in Table 6. The VoLL is 8.28 €/kWh for the case study in France [194], and the LPSP is 0.7.

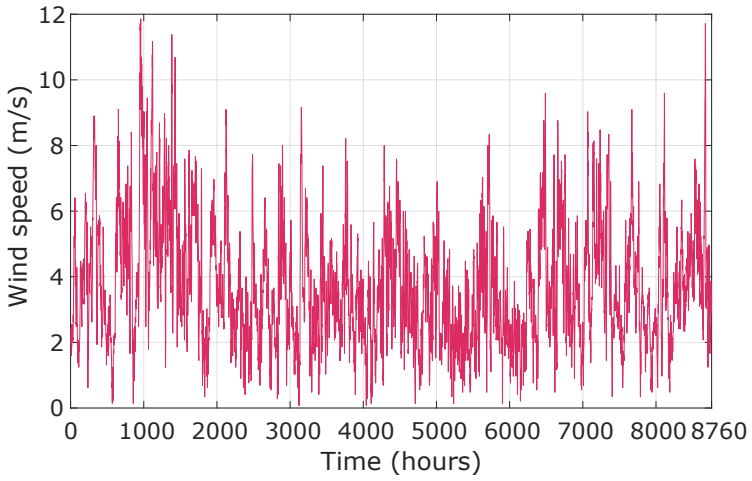

Figure 41: Wind speed data for Compiègne city [180].

The optimization covers a period of one year with hourly time steps, totaling 8760 hours, and takes into account the microgrid's 20-year lifespan. The optimization resolution significantly impacts computation time. This is evident from Algorithm 1, which relies exclusively on MILP and takes more than twice as long to compute as Algorithm 2 [171]. In contrast, Algorithm 2 utilizes parallel processing techniques, effectively reducing its computation time. By distributing the computational load across multiple processors, Algorithm 2 can perform simultaneous calculations, thereby enhancing efficiency and accelerating the overall optimization process. Comparisons are made by conducting simulations with the two algorithms presented across four different scenarios that vary based on the inclusion of EV flexibility and load shedding. The scenarios studied are listed as follows:

1. Scenario 1 (S1): No EV flexibility, without load shedding.
2. Scenario 2 (S2): No EV flexibility, with load shedding.
3. Scenario 3 (S3): EV flexibility, without load shedding.
4. Scenario 4 (S4): EV flexibility, with load shedding.

The optimization problem is structured and solved using Python 3.8 in conjunction with the CPLEX optimization solver. Computation tasks are executed on a high-performance supercomputer with operating system *"Rocky Linux 9.1"* and equipped with robust hardware specifications, including an AMD EPYC 7763 64-Core Processor, 256 cores, and 1510GB of RAM.

Additionally, Algorithm 2 employs parallelization techniques utilizing the `multiprocessing` library in Python. Each core is assigned to handle an independent particle, contributing to a total of 150 particles.

V.3.1 LCOE and LCE Analysis

In this section, LCOE and LCE results are presented under three weighting strategies: LCOE prioritization ($w = 1$), equality strategy ($w = 0.5$), and LCE prioritization ($w = 0$). Results for S1, S2, S3, and S4 using both algorithms are shown in Fig. 42. Analyses are conducted comparing outcomes between algorithms and among different scenarios.

Under the LCOE prioritization strategy ($w = 1$), it is observed that S1 exhibits the highest LCOE, while S4 shows the lowest. This discrepancy is attributed to the increased flexibility, such as load shedding and EV flexibility, which is provided in S4. The difference between the two cases is about 194% for LCOE and 520% for LCE. When S2 and S3 are compared, it is found that S2 has a lower LCOE than S3, indicating that load shedding has a more significant effect on minimizing the LCOE than EV flexibility. Shifting to the equality strategy (Fig. 42(b)), an increase in the LCOE for all scenarios in both algorithms is noted due to the decreased emphasis on LCOE. This trend is further accentuated under the LCE prioritization strategy (Fig. 42(c)), where the rise in LCOE for all scenarios is even more marked. Regarding LCE, as illustrated in Fig. 42(d)(e)(f), the outcomes generally mirror those of the LCOE, except for S2 in the Algorithm 1 for both the equality and LCE prioritization strategies. It is noted that S2 ranks lower in LCE outcomes compared to LCOE, a reflection of the higher load shedding levels in these strategies, which increase LCOE without impacting LCE. It is also noted that the strategy prioritizing LCE achieves the lowest LCE compared to the other strategies.

Comparing the performance across both algorithms, the S1 values in the Algorithm 2 are significantly higher than those of the Algorithm 1 for all prioritization strategies. This discrepancy can be attributed to two main reasons. Firstly, the minor load shedding observed in the second stage of the cascaded MILP algorithm plays a critical role. As demonstrated in Table 12, there is minor load shedding (involving EVs and buildings) for S1, despite load shedding being theoretically prohibited. This occurs due to separate stages of the cascaded MILP algorithm, which leads to potential insufficiency in the sizing of the microgrid components. The first stage, with an EM horizon of 8760 hours, may not fully satisfy the load requirements throughout the year in the second stage, which operates over 24 hours repeated 365 times. This discrepancy affects the SOC of the BESS throughout the year, especially under unpredictable weather conditions and occasionally results in a fully discharged BESS. Consequently, load shedding is implemented when the combined output of DERs and the EG fails to meet the demand. Secondly, the optimization problem horizon in the first stage of Algorithm 1 spans one year, whereas it is over 24 hours in Algorithm 2. To ascertain the accuracy of these approaches, Fig. 43 illustrates the results of the first and second stages of Algorithm 1. Since the first stage does not require load shedding, it offers a fair comparison with Algorithm 2. It is evident that the LCOE and LCE in S1 for all prioritization strategies are even lower than those in the second stage, that indicates that optimization over an 8760-hour horizon yields a more accurate solution than a 24-hour optimization horizon. This holds true for S2 and S3 but not for S4, as

Parameter/Algorithm	Algorithm 1				Algorithm 2			
	S1	S2	S3	S4	S1	S2	S3	S4
Microgrid components capacities								
PV (kWp)	516	329	516	329	1188	289	767	311
WT (kW)	190	160	190	160	1945	320	760	82
BESS (kWh)	405	55	405	55	414	57	219	17
PV DC/DC CV (kW)	553	352	553	553	553	434	370	332
WT AC/DC CV (kW)	190	165	190	165	361	321	336	82
BESS DC/DC CV (kW)	88.6	42	88.6	42	233	38	84	4
EG AC/DC CV (kW)	148	148	148	148	148	148	148	148
EV DC/AC CV (kW)	67	67	67	67	67	67	8	8
Building DC/AC CV (kW)	135	135	135	135	135	135	135	135
Energy dispatch								
PV energy (MWh)	561	358	561	358	1290	314	584	337
WT energy (MWh)	113	195	113	195	1157	190	346	48
BESS charge/discharge energy (MWh)	0.6	0.1	0.51	0.1	0.41	0.17	0.4	0.02
EG supply energy (MWh)	362	410	359	405	178	378	243	444
EG inject energy (MWh)	205	111	205	105	581	123	389	79
Curtailed energy (MWh)	63	1.5	63	3	1239	0	249	0.52
EV shedding energy (%)	0.07	0.23	0.22	0.21	0	1.13	0	0.46
Building shedding energy (%)	0.07	1	0	0	0	0.15	0	0

Table 12: LCOE, LCE, microgrid capacities, and energy results for the LCOE prioritization strategy

S4 in Algorithm 2 demonstrates better results in terms of LCOE and LCE for all prioritization strategies. So, allowing for the flexibility of load shedding and EV flexibility on the 24 hours optimization horizon prove to be more efficient than an 8760-hour horizon. Additionally, the comparison between both stages of Algorithm 1 reveals that S2 and S4 exhibit much higher LCOE in the first stage for cases where $w = 0.5$ and $w = 0$, a consequence of significant load shedding in the first stage, which is greatly reduced in the second stage by flexibility the EV. Regarding the comparison of LCE between the two stages of Algorithm 1, it is observed that the LCE mirrors the LCOE. S1, S2, and S3 in the first stage exhibit lower LCE values compared to their counterparts in the second stage. Conversely, scenario S4 in the first stage demonstrates a higher LCE value. This pattern holds across all three prioritization strategies employed.

V.3.2 Microgrid Components Capacities and Energy Analysis

The microgrid components capacities and energy production/consumption for both LCE and LCOE prioritization strategies are shown in Table 12 and Table 13, respectively. For both prioritization strategies, the predominant share of PV capacity compared to other microgrid components highlights its key role in energy supply, where it demonstrates the most substantial contribution to the microgrid's energy output. The selected PV panel exhibits lower cost and CO_2 emissions compared to other components of the microgrid, thereby that makes its implementation advantageous over the expansion of other component sizes.

Comparing S2 & S4 to S1 & S3 for both prioritization strategies, it can be seen that the adoption of load shedding has a notable impact on the sizing of the BESS by reducing its required capacity due to its higher LCE and LCOE in comparison to PV panels. This strategy is

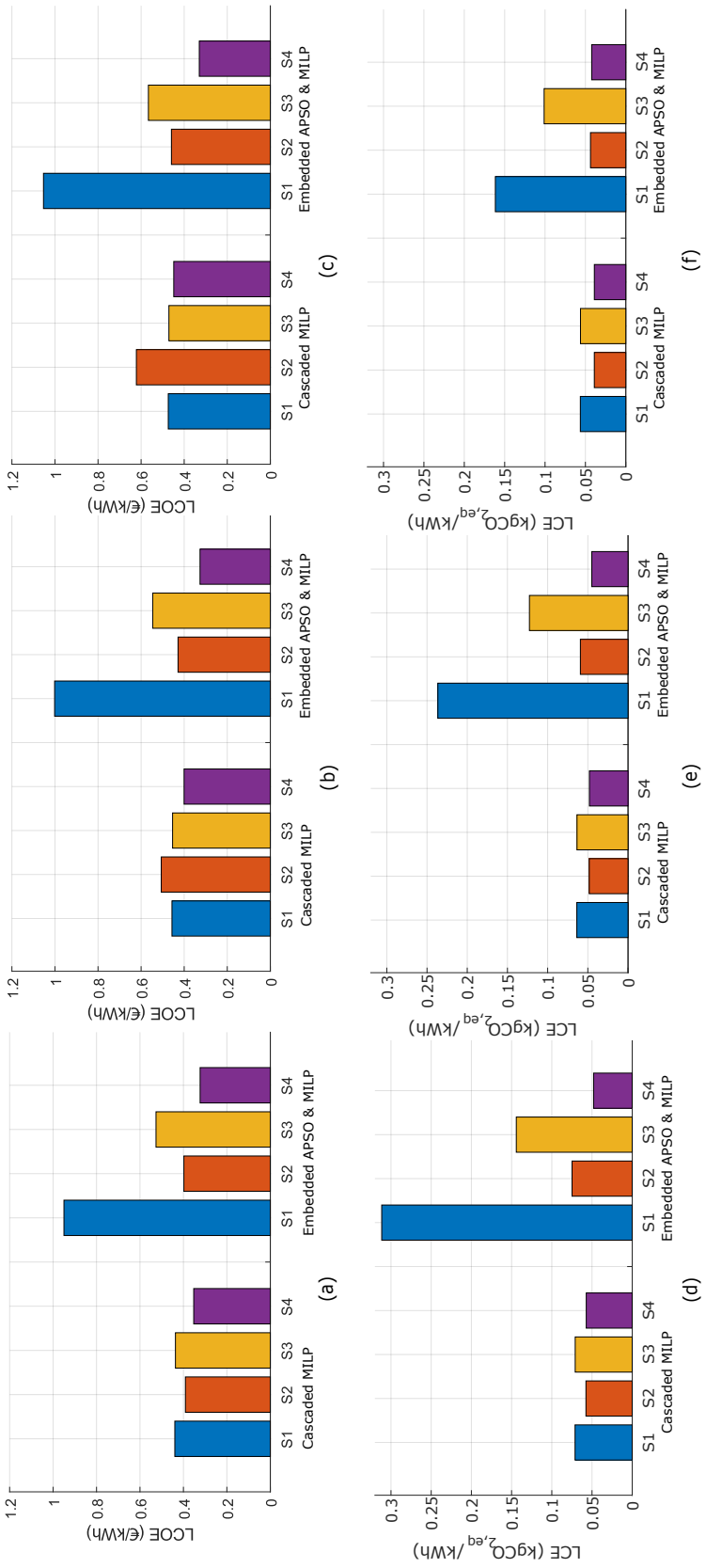

Figure 42: The LCOE and LCE results for both algorithms of: (a)(d)$w = 1$, (b)(e) $w = 0.5$, and (c)(f) $w = 0$.

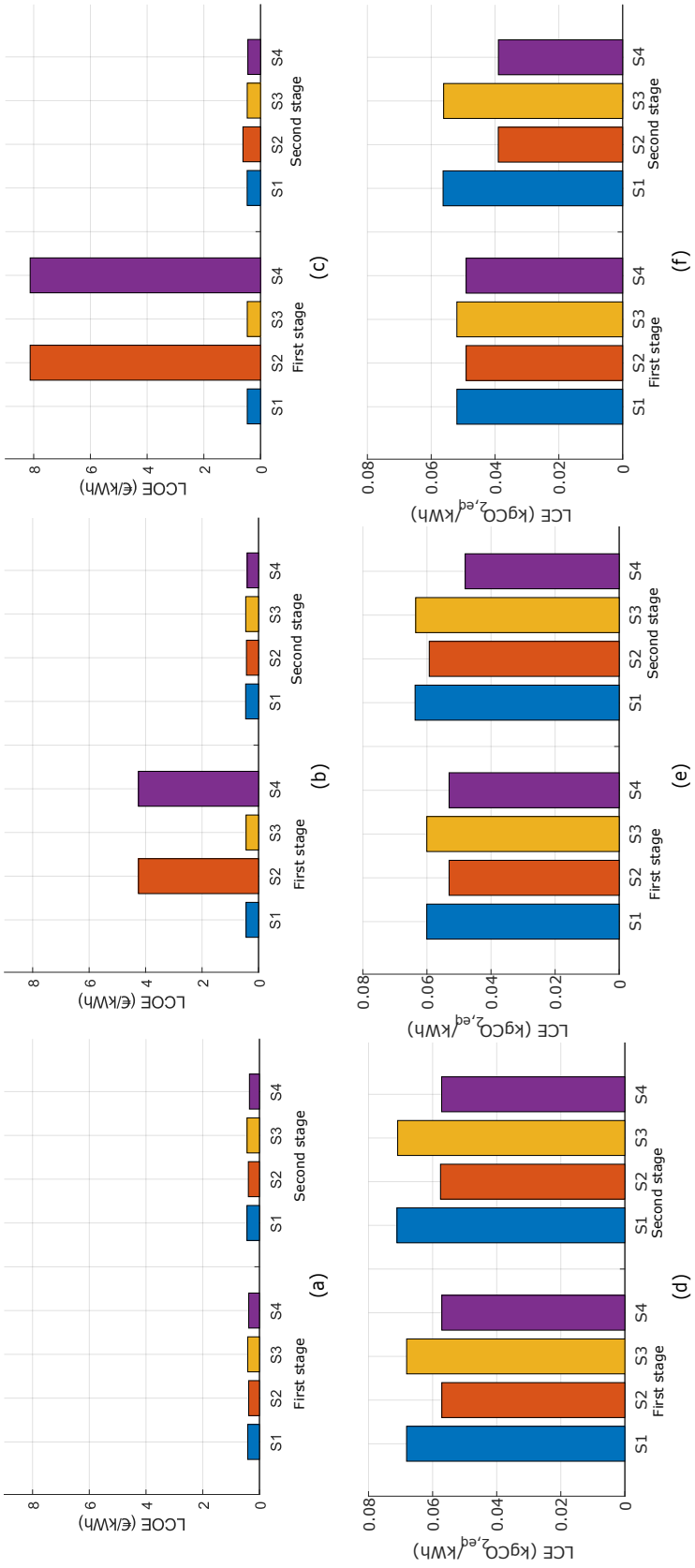

Figure 43: The LCOE and LCE results for both stages of the cascaded MILP algorithm of: (a)(d)$w = 1$, (b)(e) $w = 0.5$, and (c)(f) $w = 0$.

Parameter/Algorithm	Algorithm 1				Algorithm 2			
	S1	S2	S3	S4	S1	S2	S3	S4
Microgrid components capacities								
PV (kWp)	635	38	635	38	2789	156	1096	199
WT (kW)	5	6	5	6	295	39	285	44
BESS (kWh)	509	0	509	0	255	138	406	4
PV DC/DC CV (kW)	680	42	680	42	361	167	510	213
WT AC/DC CV (kW)	5	5	5	5	295	39	285	44
BESS DC/DC CV (kW)	477	0	477	0	235	38	148	1.17
EG AC/DC CV (kW)	148	49	148	49	148	148	148	148
EV DC/AC CV (kW)	67	67	67	67	67	67	8	8
Building DC/AC CV (kW)	135	135	135	135	135	135	135	135
Energy dispatch								
PV energy (MWh)	690	42	690	42	3028	170	1190	216
WT energy (MWh)	3	6	3	6	175	23	170	26
BESS charge/discharge energy (MWh)	0.35	0	0.56	0	0.20	0.20	0.28	0.01
EG supply energy (MWh)	470	680	406	680	238	552	285	519
EG inject energy (MWh)	219	0	220	0	473	9.5	353	20
Curtailed energy (MWh)	113	17	111	0	2175	0	510	0
EV shedding energy (%)	0.15	6.13	0.38	6.3	0	3.7	0	1.31
Building shedding energy (%)	0.10	1.86	0	0	0	0.47	0	0

Table 13: LCOE, LCE, microgrid capacities, and energy results for the LCE prioritization strategy

economically driven, as the high cost metrics of the BESS make it less favorable for scaling. In every scenario, the battery is consistently replaced following its predetermined lifetime, which is set at 10 years for this study. This practice stems primarily from the fact that the BESS is designed with excess capacity, eliminating the necessity for battery replacement prior to reaching its established lifetime. Nonetheless, including the battery's replacement cost within the objective function leads the optimization algorithm to minimize battery discharge. This approach, evident in both prioritization strategies, aims to avoid the need for battery replacement.

Further analysis shows that prioritizing the LCE strategy leads to a reduced capacity allocation for WT due to their higher LCE values compared to other microgrid components. The higher LCE associated with the small urban WT model used in this study needs careful interpretation. Although it may seem unusual compared to typical emissions numbers, it's essential to consider the unique characteristics of the WT in question. The urban WT model, as described in [179], has a higher emissions profile compared to larger WTs, like the 2 MW model in [195], which has emissions of about 832 kg CO2 equivalent per kW capacity. In S3 and S4 of Algorithm 2, the capacity of EV CVs decreases due to the implementation of EV flexibility, which successfully reduces peak demand from EV charging. This flexibility reduces stress on the microgrid infrastructure, lowering the need for CV capacities to meet demand. This phenomenon is not seen in Algorithm 1 because the sizing is done in the algorithm's first stage, where EV flexibility does not occur.

V.3.3 Economic & Environmental analysis

The economic and environmental aspects of the microgrid, considering both algorithms and prioritization strategies for the four scenarios, are illustrated in Fig. 44 and Fig. 45. In the economic analysis of Algorithm 1 (Fig.44(a) and Fig.44(b)), it is evident that in both prioritization strategy, the EG cost is a dominant cost in the planning of the microgrid. This observation suggests that the size of the components in the first stage of Algorithm 1 is insufficient to completely meet the load requirements. This insufficiency prompts the algorithm to increase the EG supply in the second stage to ensure load satisfaction, consequently raising the cost associated with EG. This scenario underscores the primary rationale for optimizing over a 24-hour horizon. Moreover, the load shedding cost displays higher rates with LCE prioritization, which reaches almost to 31% in S2. This phenomenon is linked to the explanations provided in the previous section V.3.1 by highlighting occurrences of load shedding during periods of inadequate local production and when the EG reaches its supply limit. While load shedding is not prevented in S4, its associated load shedding cost is not as elevated as in S2 due to the flexibility of the EV load. Additionally, in both prioritization strategies, the EG cost consistently surpasses in S2 and S4, while the PV cost is highest in S1 and S3. The costs related to PV, WT, BESS, converters, and deployment remain consistent in S1 & S3 and S2 & S4. This consistency arises from the identical conditions in S1 & S3 and S2 & S4 during the first stage, where the sizes of the components are determined. In the economic analysis of Algorithm 2 (Fig.44(c) and Fig.44(d)), it can be seen that scenarios of load shedding (S2 & S4) shows higher reliance on the EG and scenarios of load shedding prohibition (S1 & S3) shows higher reliance on DERs. Moreover, in S1 & S3 there is a reduction in the proportion of EG cost compared to Algorithm 1. In S1 of LCOE prioritization strategy it is even negative, that implies that the injection into the EG is higher than the EG supply. This suggests that Algorithm 2 favors local energy consumption as APSO with MILP operates concurrently to adjust the microgrid component sizes as explained in section V.3.2. Moreover, the WT participates more than 50% of the total amount in S1, indicating that the WT has a lower cost compared to the rest of the microgrid components. The PV cost in S1 for the LCE prioritization strategy contributes in more than 60 % of the total cost which shows that the PV has a lower CO_2 emissions compared to the rest of the microgrid components. In contrast to Algorithm 1, the costs for PV, WT, BESS, converters, and deployment are not identical between S1 & S3 and S2 & S4. This difference arises because EV flexibility is implemented in each scenario within an embedded optimization structure.

Focusing on the environmental analysis, in each of the four scenarios of the LCOE prioritization strategy of Algorithm 1 (Fig. 45(a)), it can be observed that PV, WT, and EG exhibit approximately equal emissions. However, the BESS emissions contribution in S1 & S3 is higher than that in S2 & S4. This is due to the necessity of avoiding load shedding in these scenarios, requiring BESS with higher discharge capacities. For Algorithm 1 LCE prioritization strategy (Fig. 45(b)), the emissions mainly come from EG and PV. This indicates that the LCE of the French EG is low, as concluded in [186]. In the Algorithm 2 LCOE prioritization strategy (Fig. 45(c)), the WT emissions constitute a large part of the overall emissions. While in the LCE prioritization strategy (Fig. 45(d)), the WT contribution decreases considerably, and the PV contribution doubles. This suggests that the WT LCE is much higher than that of PV. In

S2 & S4, emissions from the EG play the most significant role, whereas in scenarios S1 & S3, emissions from DERs are more influential. This reflects the findings presented in Fig. 44(d), where local production significantly impacts scenarios S2 & S4, while the cost associated with the EG is more critical in scenarios S1 & S3.

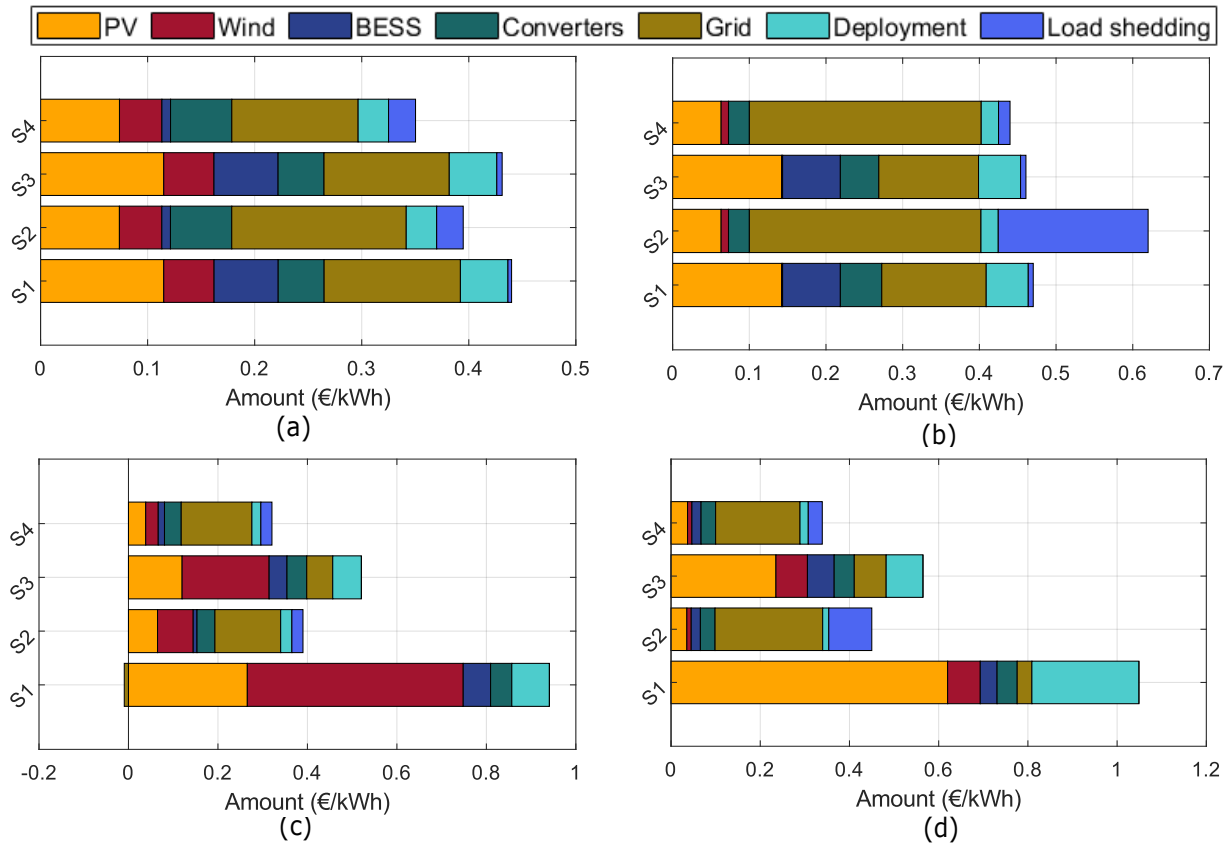

Figure 44: Economic analysis for the cascaded MILP algorithm for the (a) LCOE prioritization strategy and (b) LCE strategy, and for the Embedded APSO & MILP algorithm for the (c) LCOE prioritization strategy and (d) LCE strategy.

V.3.4 Power Profile Analysis

The power profiles corresponding to the LCOE minimization strategy for algorithms 1 and 2 are depicted in Fig. 46 and Fig. 47, respectively. Each figure displays situations across three days, which are chosen to highlight varied EM circumstances within the microgrid. Both algorithms demonstrate a significant rise in EG injection during the summer season (1-2 July) and a considerable EG supply during the autumn/winter season (2-3 January, 6-7 December). BESS intervention is predominantly observed during the autumn/winter season, notably when DERs output is at a low level.

Focusing on Fig. 46, S1 shows a substantial contribution from the WT capacity during the first 24 hours of the period from 2nd to 3rd January and satisfies most of the load. In the summer season (1st to 2nd July), increased injection into the EG is observed due to elevated solar irradiation and wind speeds levels. During the period from 6th to 7th December, the load is

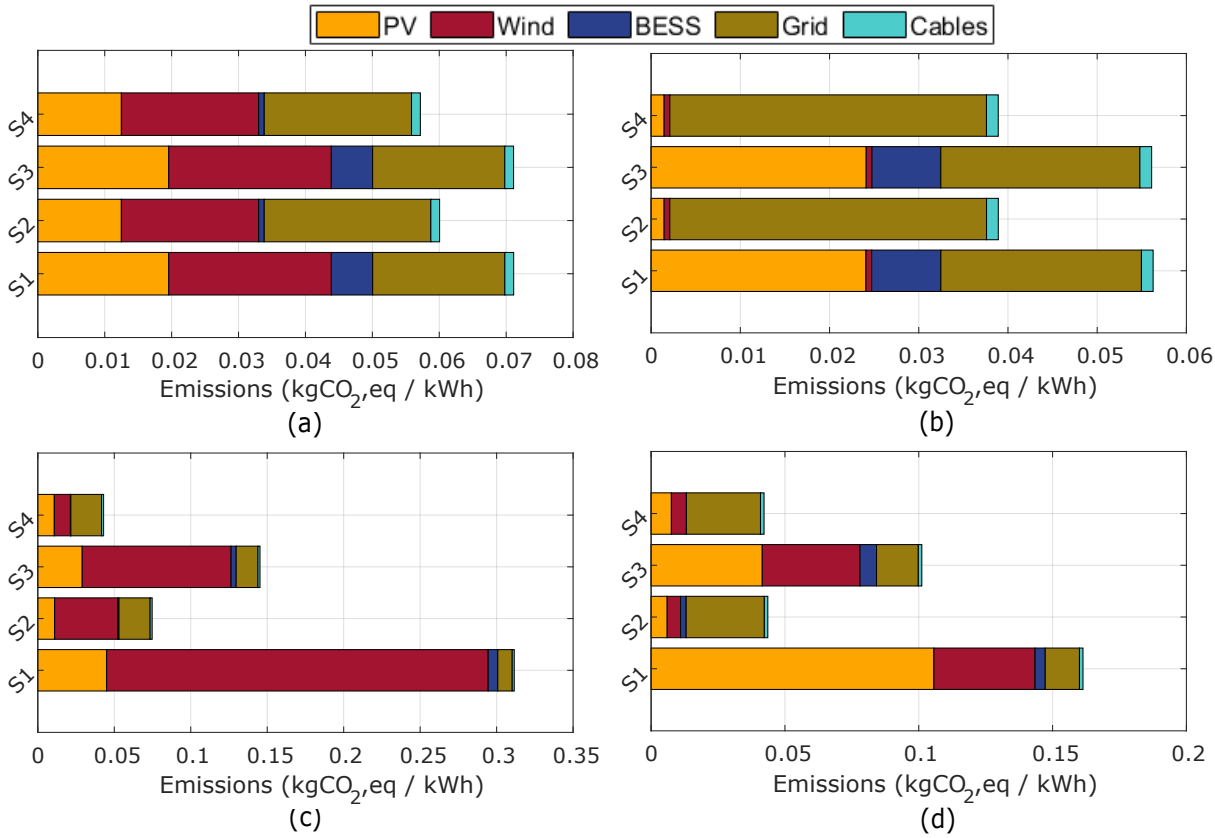

Figure 45: Environmental analysis for the cascaded MILP algorithm for the LCOE prioritization strategy (a) and LCE strategy (b), and for the Embedded APSO & MILP algorithm for the LCOE prioritization strategy (c) and LCE strategy (d).

primarily supplied by the EG and PV panels. S2 exhibits a higher contribution from the EG during the initial 24 hours of the period from 2nd to 3rd January compared to S1 due to the significantly lower shares of WT and PV in this scenario. Consequently, the EG injection is reduced from the 1st to 2nd July period. Moreover, S2 experiences minimal load shedding during periods of low solar irradiation and wind speeds, notably from 2nd to 3rd January and from 6th to 7th December. Rather than discharging the BESS when DERs generation is low, load shedding occurs during these times. In contrast, S3 maintains higher outputs from DERs and EG injections from 2nd to 3rd January than S2, and load shedding is avoided. This improvement is not achieved by increasing the size of the microgrid components but through implementing EV flexibility strategies. These strategies are particularly effective in January and December, aligning load demands with peak periods of solar irradiation and high wind speeds. In S4, load shedding is less frequent compared to S2; however, load shedding still occurs when load flexibility alone is insufficient to compensate during periods of exceptionally low solar DERs output.

In Fig. 47, the EM in Algorithm 2 shows no substantial differences from Algorithm 1, except for a few exceptions. First, the EG supply is predominant in all scenarios during January and December. Second, as previously discussed in Section V.3.1, load shedding occurs in all scenarios.

V.4 Conclusions

[h] This chapter offers an in-depth evaluation of two algorithms developed for optimizing microgrids with EV integration by focusing on reducing the LCOE and LCE over a long-term period. Algorithm 1 employs a cascaded MILP strategy, initially establishing the capacities of microgrid components and managing energy over an optimization period of 8760 hours without considering EV flexibility. The subsequent stage, applied daily over the course of a year, aims to manage energy with the inclusion of EV flexibility and BESS degradation modeling, where each optimization cycle lasts 24 hours. On the other hand, Algorithm 2 employs an embedded approach that merges APSO with MILP by incorporating both EV flexibility and BESS degradation into a single-stage optimization process that unfolds over 24-hour cycles throughout the 365 days of the year. This multi-objective optimization problem is addressed using the weighted sum method. Furthermore, the cost of load shedding is managed by employing the VoLL alongside the LPSP to establish the threshold for the level of load shedding.

The findings from this study lead to several conclusions. First, the Embedded APSO-MILP algorithm (Algorithm 2) ensures no load shedding under all scenarios, unlike the cascaded MILP approach (Algorithm 1), which exhibits marginal load shedding in scenarios where load shedding is explicitly prohibited. This discrepancy is attributed to the differing time horizons of the cascaded approach (8760 hours versus 365 days $\times$ 24 hours), which impacts the SOC of the BESS. Second, in terms of LCOE and LCE, no EV flexibility and no load shedding scenario of Algorithm 2 performs the worst, while scenario of incorporating EV control and load shedding of the same algorithm demonstrates the best outcomes for both metrics. This difference can be explained by the greater flexibility offered in scenario including options for load shedding and flexibility of electric vehicles, as compared to scenario where they are prohibited. Third, EV flexibility significantly reduces LCOE and LCE, thereby enhancing EM within the system by leveraging real-time solar irradiation. Fourth, prioritizing LCE leads to a reduction in the size of an urban WT, indicating a strategic compromise to meet environmental and cost objectives. Fifth, Algorithm 1 relies more on the EG for energy supply compared to Algorithm 2, which favors enhanced local energy production. This is because Algorithm 1 sets the sizes of components in its initial stage. If the sizes determined in advance turn out to be inadequate in the second stage, Algorithm 1 often addresses demand by relying on energy supplied from the EG. Conversely, due to its single-stage design, Algorithm 2 possesses the flexibility to adjust the sizes of DERs to match load requirements. Sixth, both algorithms exhibit a rise in EG injections during the summer months and a significant dependency on the EG during the autumn and winter seasons. The intervention of BESS becomes particularly crucial in these cooler months, primarily because the output from DERs tends to decrease due to shorter daylight hours and less favorable weather conditions, necessitating alternative sources to meet the demand. Across both prioritization strategies and algorithms, EG costs and emissions are notably higher in scenarios including load shedding (S2 & S4), while the costs associated with PV systems peak in scenarios prohibiting the load shedding (S1 & S3). This is because allowing for load shedding significantly reduces the capacity required from DERs, thus it increases the microgrid's reliance on the EG supply.

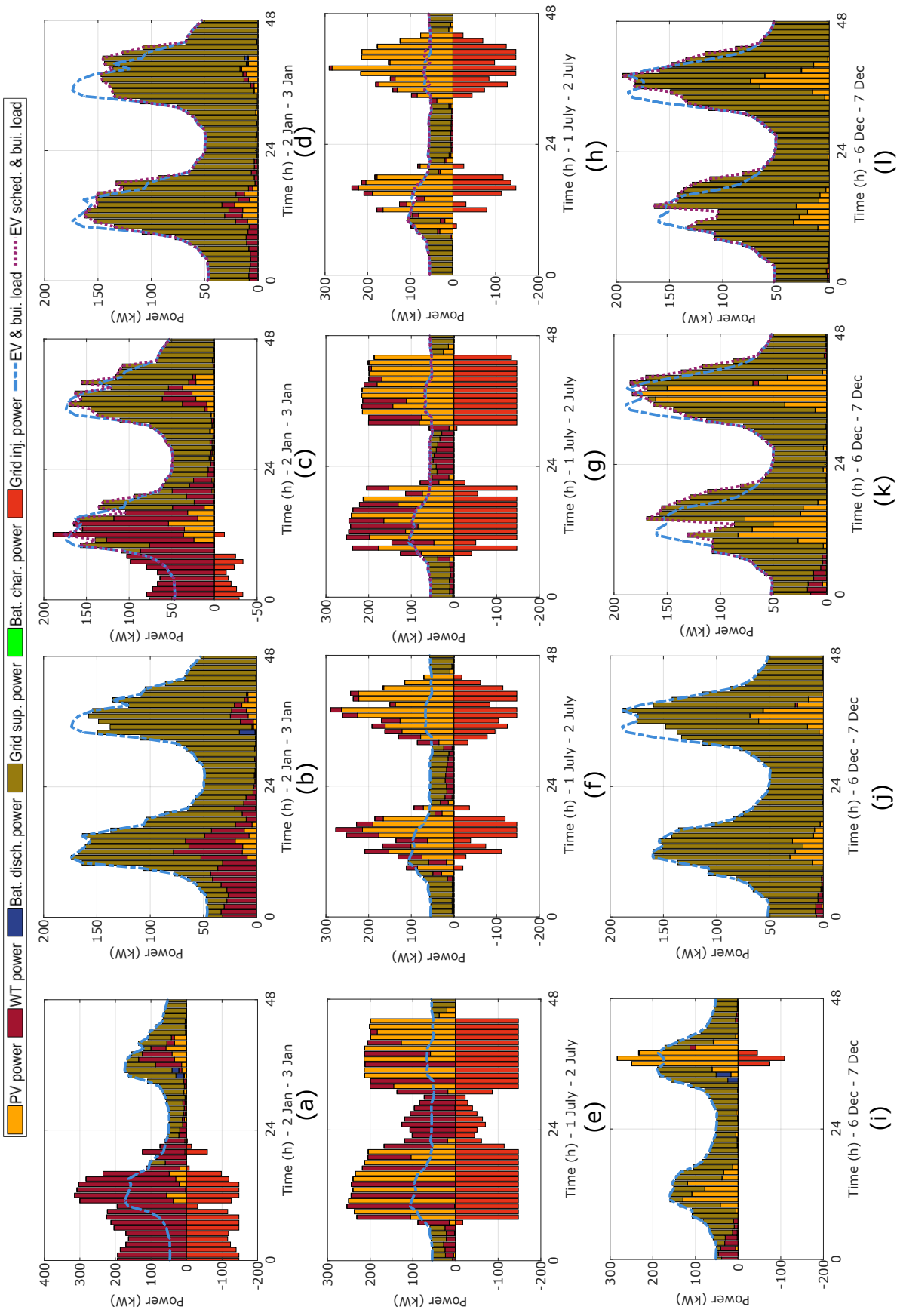

Figure 46: Power profiles for the Embedded APSO & MILP of the LCOE prioritization strategy for (a)(e)(i) S1, (b)(f)(j) S2, (c)(g)(k) S3 and (d)(h)(l) S4.

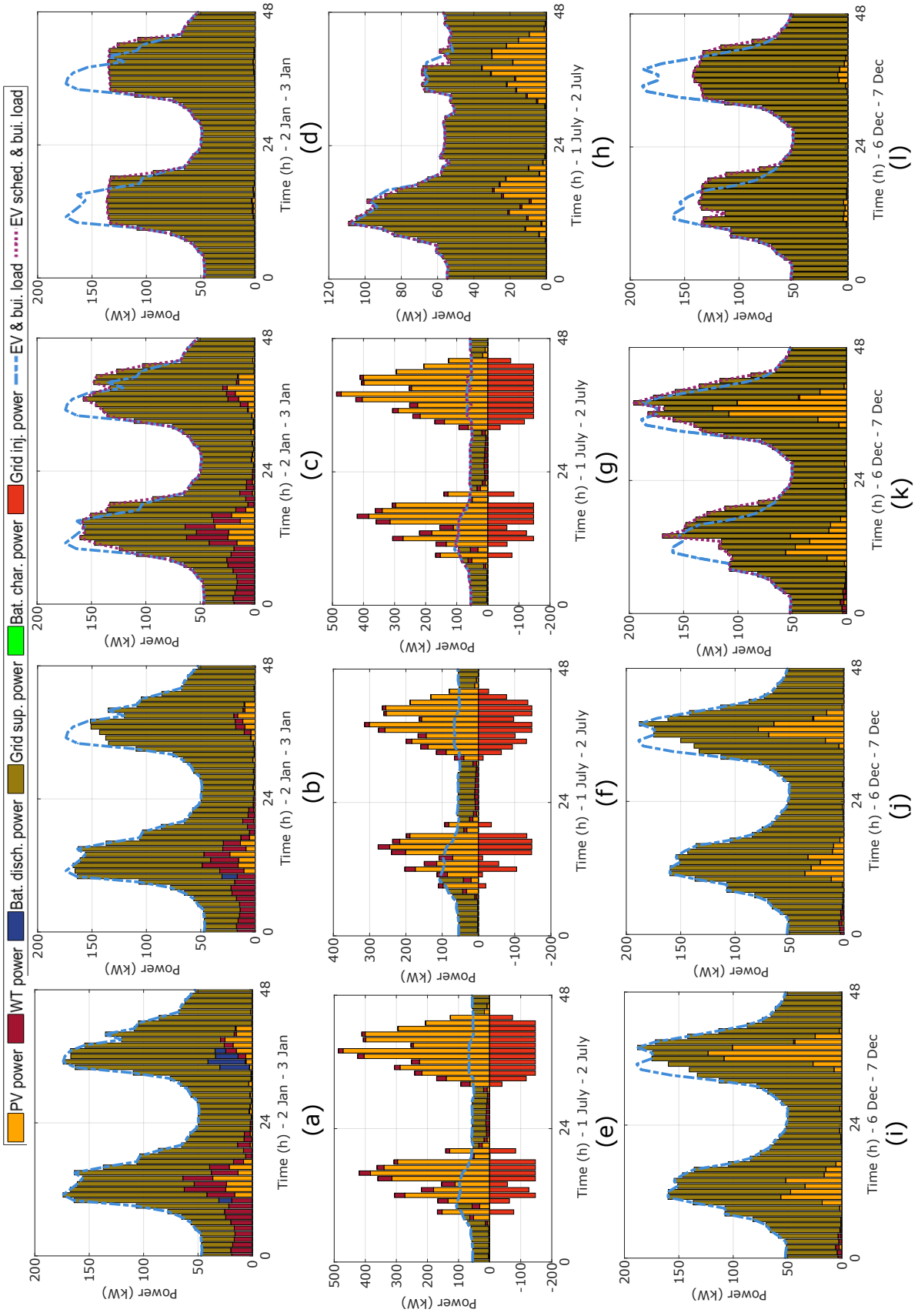

Figure 47: Power profiles for the cascaded MILP of the LCOE prioritization strategy for (a)(e)(i) S1, (b)(f)(j) S2, (c)(g)(k) S3 and (d)(h)(l) S4.

Chapter VI

Conclusions and Future Perspectives

As demonstrated in the previous chapters, optimization-based approaches —whether unified MILP, cascaded MILP, or embedded MILP combined with APSO— serve as effective decision-making tools for the planning (sizing and EM) of microgrids over the project lifetime. These methods ensure minimal costs and carbon emissions. This chapter reviews the contributions of this dissertation, discusses the results, and suggests several possible directions for future research.

VI.1 Contributions

This dissertation has focused on optimizing the sizing of microgrid components (RES, BESS, converters) and EM to minimize the LCOE and LCE over the project's lifetime. The main contributions are summarized as follows:

- A detailed review of recent research has been done, offering a clear analysis of the latest advancements in the field. The studies are organized based on their specific methods, including heuristic, mathematical, hybrid approaches, etc. Each method is carefully examined, pointing out both its strengths and weaknesses.
- The integration of sizing and EM challenges within the microgrid framework has been addressed, considering a project lifespan of 20 years and focusing on achieving optimal hourly EM. This includes incorporating technical, economic, and environmental aspects through the development of a unified multi-objective MILP algorithm. The primary goal of this algorithm is to find an optimal solution that minimizes both the LCOE and the LCE of the microgrid while optimizing computational efficiency.
- The LCE constraint value has been varied to analyze and compare the Pareto front and the variations in BESS and PV capacities for GCMG and IMG operation modes. Additionally, the influence of peak shaving on the LCOE and LCE of the microgrid has been evaluated by calculating the average variation for each EG limit. Furthermore, the impact of load increase on the LCOE and LCE for both IMG and GCMG operation modes has been assessed.
- An analysis of the energy sources utilized in the French electricity grid under different LCOE and LCE scenarios has been conducted. This assessment involves examining the proportional contribution of each energy source and exploring seasonal trends. Additionally, the maximization of renewable energy consumption within the microgrid has been pursued to enhance sustainability, reduce reliance on non-renewable sources, and improve overall energy efficiency.
- A comparative analysis of three scenarios (PV/BESS, WT/BESS, and PV/WT/BESS) across different cities has been performed with the impact of seasonal fluctuations on the LCOE and LCE has been evaluated. Moreover, the influence of the choice of microgrid component technologies on the LCOE and LCE outcomes has been assessed.

- A comprehensive comparison between two different algorithms has been provided. The first algorithm is based on a mathematical approach, while the second utilizes an embedded approach (APSO & MILP). Both algorithms aim for optimal sizing and EM over a project lifetime of 20 years, with a multi-objective function to minimize the LCOE and LCE. The optimization algorithm includes a battery degradation model that tracks the kWh delivered from the battery. Additionally, the integration of EV charging flexibility in microgrid planning and EM has been addressed within a MILP algorithm, using a time horizon of 8760 hours with a one-hour time step. For both algorithms, four scenarios were addressed: No EV flexibility, without load shedding; No EV flexibility, with load shedding; EV flexibility, without load shedding; and EV flexibility, with load shedding. An economic and environmental analysis, along with LCOE, LCE, and profile analysis, has been conducted for each scenario.

VI.2 Summary of Works

In this thesis, several outcomes can be derived. At first, a comprehensive review of the state-of-the-art methods in microgrid sizing and EM approaches is presented. Microgrid sizing approaches encompass commercial software, heuristic methods, mathematical models, and hybrid techniques. Commercial software solutions offer user-friendly interfaces and preconfigured models, making them accessible for practitioners. Heuristic methods, such as genetic algorithms and particle swarm optimization, provide flexible, near-optimal solutions, while mathematical models including linear and nonlinear programming, that ensure precision but can be computationally intensive. Hybrid approaches combine the strengths of both heuristic and mathematical methods to enhance accuracy and efficiency. In terms of EM, rule-based strategies offer simplicity and ease of implementation but may lack adaptability. Optimization-based approaches including metaheuristics, conventional optimization, and AI techniques, provide robust solutions for minimizing costs and maximizing performance. Metaheuristics excel in large, complex search spaces, while conventional methods offer exact solutions through well-defined formulations. AI approaches leverage machine learning to predict trends and adapt dynamically. Commercial software solutions also play a role in EM, providing tools for real-time monitoring and control. The review also highlights the distinction between multi-stage and single-stage optimization for microgrid sizing and EM, where multi-stage optimization integrates decisions for a cohesive system design, and single-stage optimization focuses on each aspect independently, potentially missing synergies. This state-of-the-art review offers a foundation for selecting appropriate methodologies and identifies areas for future research in microgrid sizing and EM.

In the second phase, the optimal sizing and EM of the microgrid are addressed using a MILP approach. This algorithm considers hourly EM along with the project's environmental and economic horizons throughout its lifetime. It specifically takes into account the dynamic emissions of the EG, the energy load of a university building, and meteorological data from Compiègne. The analysis yields several key conclusions. In IMG operation mode, the microgrid shows larger component capacities compared to GCMG mode due to the necessity of

managing more challenging conditions, such as the absence of EG during periods of low solar irradiation. The study reveals that as the LCE decreases, the capacity of the BESS increases. Additionally, the number of PV systems is higher when the LCOE is lower in both operation modes. This is because BESS has a slightly lower LCE compared to PV, and the LCOE of PV is also lower than that of BESS. Economically, the solution with the lowest LCOE incurs the highest initial investment cost, whereas the solution with the lowest LCE incurs the highest replacement cost, primarily due to BESS being the only component needing replacement over the project's lifetime. As the EG limit increases, the Pareto fronts for both peak shaving strategies become lower and steeper. In IMG operation mode, increasing the load does not lead to higher LCOE and LCE; instead, it results in a reduction of both metrics. Conversely, in GCMG operation mode, an increase in load results in higher Pareto curves, leading to increased LCOE and LCE. It is also demonstrated that in the French context, decreasing LCOE/LCE leads to increased non-renewable and nuclear energy consumption. Furthermore, minimizing nuclear and non-renewable energy consumption results in an increase in LCOE and LCE.

In the third phase, the same algorithm from the second step is applied to multiple cities worldwide, each varying in solar irradiation, wind speed, and ambient temperature. The study integrates EV demand into the university load using a probabilistic model. Additionally, WTs are included among the microgrid components. The optimization problem considers the economic horizon over the project's lifetime, aiming to minimize both the LCOE and LCE. Three scenarios were defined based on the inclusion of renewable energy sources: S1 excludes WTs, S2 excludes PV panels, and S3 includes both PV panels and WTs.The findings reveal that cities with high solar irradiation show similar LCOE and LCE in scenarios involving PV/BESS and PV/WT/BESS. This outcome occurs because the optimization algorithm favors PV integration over WTs, as incorporating WTs does not reduce LCOE and LCE in these cities. Moreover, scenarios including PV/WT/BESS achieve the lowest LCOE and LCE values, while the WT/BESS scenario results in the highest LCOE and LCE. It is also noted that the ranking of cities based on average solar irradiation or wind speed does not necessarily correspond to their ranking based on LCOE and LCE. Monthly and daily variations in solar irradiation and wind speed significantly influence these results. The study emphasizes the importance of a well-sized combination of renewable resources to optimize the economic and environmental performance of energy systems in different cities. There is no universal solution; thus, a thorough assessment of local conditions and available resources is essential for making tailored decisions for each specific city. Furthermore, the study highlights the role of technologies in these configurations. The results indicate that locally produced PV panels positively impact the overall LCE of the microgrid, with PV panels incorporating PCM showing higher LCE. Additionally, the LCE associated with BESS plays a dominant role in determining the total LCE of the configurations. Readers are referred to [186] for publication details concerning this chapter.

In the last phase, a comprehensive analysis of two algorithms designed to optimize microgrids with EV integration is presented, focusing on minimizing the LCOE and LCE over a long-term period. Algorithm 1 employs a two-step MILP approach: initially, it establishes the capacities of microgrid components and manages energy without considering EV flexibility, spanning an optimization period of 8760 hours. In the subsequent stage, applied daily over a year, it manages energy with the inclusion of EV flexibility and BESS degradation modeling,

each optimization cycle lasting 24 hours. In contrast, Algorithm 2 uses an integrated approach combining APSO with MILP, incorporating both EV flexibility and BESS degradation into a single-stage optimization process that runs in 24-hour cycles throughout the year. This multi-objective optimization problem is tackled using the weighted sum method. Additionally, the cost of load shedding is managed by employing the VoLL alongside the LPSP to establish the load shedding threshold. Several conclusions arise from this study. Firstly, the Embedded APSO-MILP algorithm (Algorithm 2) ensures no load shedding under all scenarios, unlike the cascaded MILP approach (Algorithm 1), which shows minor load shedding in scenarios where it is explicitly prohibited. This discrepancy is due to the different time horizons of the cascaded approach (8760 hours versus 365 days of 24 hours), affecting the SOC of the BESS. Secondly, in terms of LCOE and LCE, Algorithm 2 performs the worst in scenarios with no EV flexibility and no load shedding, while it achieves the best results when EV control and load shedding are incorporated. This difference is due to the greater flexibility offered by allowing load shedding and EV flexibility compared to prohibiting these options. Thirdly, EV flexibility significantly reduces LCOE and LCE, thereby improving EM within the system by leveraging real-time solar irradiation. Fourthly, prioritizing LCE leads to a reduction in the size of an urban WT, indicating a strategic compromise to meet environmental and cost objectives. Fifthly, Algorithm 1 relies more on the EG for energy supply compared to Algorithm 2, which favors enhanced local energy production. This is because Algorithm 1 sets the sizes of components in its initial stage, and if these sizes are inadequate in the second stage, it often relies on the EG to meet demand. Conversely, Algorithm 2, due to its single-stage design, can adjust the sizes of DERs to match load requirements. Lastly, both algorithms show an increase in EG injections during the summer months and significant reliance on the EG during the autumn and winter seasons. The intervention of BESS becomes crucial in these cooler months, primarily due to the decreased output from DERs because of shorter daylight hours and less favorable weather conditions, necessitating alternative sources to meet demand. Across both prioritization strategies and algorithms, EG costs and emissions are notably higher in scenarios including load shedding (S2 & S4), while the costs associated with PV systems peak in scenarios prohibiting load shedding (S1 & S3). This is because allowing load shedding significantly reduces the required capacity from DERs, increasing the microgrid's reliance on the EG supply. The work in this chapter is submitted to the Applied Energy journal, which is published by Elsevier.

VI.3 Future Perspectives

Despite the significant contributions of this thesis, there remain several areas for future research that could further enhance the outcomes and applicability of the targeted research perspective. The following suggestions outline potential directions for continued investigation and improvement:

- *Payback Time of Investments:* Conducting detailed analyses on the payback period of microgrid investments is crucial for providing a clearer financial perspective to stakeholders. Such studies would help in assessing the financial viability and long-term benefits of these investments, thereby facilitating more informed decision-making.

- *Incorporation of an Advanced Battery Degradation Model:* Integrating a more sophisticated model for battery degradation could significantly improve the accuracy of energy storage predictions. This advancement would enable better planning and management of battery life cycles, leading to more reliable and efficient energy systems.
- *Application of Artificial Intelligence for LCOE and LCE Prediction:* Employing artificial intelligence to predict the LCOE and LCE could greatly reduce computation time compared to traditional optimization algorithms. This approach could streamline the analysis process and enhance predictive accuracy.
- *Integration of Vehicle-to-Grid (V2G) Technology:* Investigating the integration of V2G technology could provide additional flexibility and efficiency in energy systems. V2G enables electric vehicles to supply energy back to the grid, assisting in balancing supply and demand and potentially lowering overall energy costs.
- *Exploration of Hydrogen Storage Solutions:* Examining the role of hydrogen as a storage medium for renewable energy could unveil new possibilities for long-term energy storage. Hydrogen storage can effectively address the intermittency issues associated with renewable energy sources, offering a clean and efficient solution for energy storage.
- *Comprehensive Uncertainty Analysis:* Performing thorough uncertainty analyses is essential for understanding the risks and variability inherent in renewable energy projects. This understanding can aid in developing robust strategies to mitigate potential risks, thereby improving decision-making processes and project outcomes.

Exploring these future research directions can significantly broaden the scope and impact of optimization-based approaches in microgrid planning. Focusing on these areas enhances the resilience, efficiency, and sustainability of microgrids, advancing toward a cleaner and more reliable energy future.

Chapter VII

Appendices

VII.1 Publications

Most of the works presented in this thesis have been published in various international journals and conferences. The details are listed as follows:

Journal Papers

- (*Submitted*) **F. Agha Kassab**, B. Celik, F. Locment, M. Sechilariu, S. Liaquat, and T. M. Hansen, "Comparative Analysis of Cascaded MILP and Embedded APSO-MILP Algorithms for Multi-objective Microgrid Sizing with EV Demand Flexibility," Applied Energy, 2024.
- (*Submitted*) S. Liaquat, T. Hussain, **F. Agha Kassab**, B. Celik, R. Fourney, and T. M. Hansen, "An Integrated Two-Stage P2P-DR Transactive Energy Trading Platform using MILP and ADMM," Applied Energy, 2024
- **F. Agha Kassab**, R. Rodriguez, B. Celik, F. Locment, and M. Sechilariu, "A Comprehensive Review of Sizing and Energy Management Strategies for Optimal Planning of Microgrids with PV and Other Renewable Integration," Applied Sciences, vol. 14, no. 22, article 10479, 2024.
- **F. Agha Kassab**, B. Celik, F. Locment, M. Sechilariu, S. Liaquat, and T. M. Hansen, "Optimal sizing and energy management of a microgrid: A joint MILP approach for minimization of energy cost and carbon emission," Renewable Energy, vol. 224, p. 120186, 2024.
- S. Liaquat, T. Hussain, **F. Agha Kassab**, B. Celik, R. Fourney, and T. M. Hansen, "Comparative Analysis of Peer-to-Peer PV Trading Strategies under the Influence of Network Constraints with Prosumer Sensitivity towards Network Coefficients," Applied Sciences, vol. 13, no. 18, Article 10044, 2023.

Conference Papers

- S. Liaquat, T. Hussain, **F. Agha Kassab**, B. Celik, A. Suvedi, R. Fourney, and T. M. Hansen, "Thermal and Energy Management of an HVAC System Using OCHRE in a Transactive Market Framework," 2024 56th North American Power Symposium (NAPS), IEEE, pp. 1-6, 2024.
- **F. Agha Kassab**, B. Celik, S.C. Mohamad, F. Locment, M. Sechilariu, S. Liaquat ,and T. M. Hansen, "Optimizing Microgrid Sizing, Energy Management, and Electric Vehicle Integration in Various French Cities," in Electrimacs 2024, Castello de la Plana, Spain, 2024, pp. 1-6.
- **F. Agha Kassab**, B. Celik, F. Locment, M. Sechilariu, and T. M. Hansen, "Combined Optimal Sizing and Energy Management of a DC Microgrid using MILP," in 2023 IEEE Belgrade PowerTech, Belgrade, Serbia, 2023, pp. 1-6.

- S. C. Mohamad, A. Alchami, **F. Agha Kassab**, N. Dougier, B. Celik, M. Sechilariu, and F. Locment, "Minimisation du coût énergétique dans un microréseau DC pilotant une station de recharge de véhicules électriques," in Symposium de Génie Electrique (SGE 2023), Lille, France, Jul. 2023.

- **F. Agha Kassab**, B. Celik, F. Locment, and M. Sechilariu, "Optimal sizing of an isolated DC microgrid using multiobjective optimization with linear programming," in Jeunes Chercheurs en Génie Électrique (JCGE22), Croisic, France, Jun. 2022.

Workshops and Seminars

- **F. Agha Kassab**, B. Celik, F. Locment, and M. Sechilariu: "Optimizing Microgrid Sizing, Energy Management, and Electric Vehicle Integration in Various Cities," 30-minute conference, Virtual Workshop IEA PVPS T17 meeting, 5 March 2024 (web conference). Audience: researchers, industrialists, institutions.

- **F. Agha Kassab**, B. Celik, F. Locment, and M. Sechilariu: "Optimizing Microgrid Sizing, Energy Management, and Integration of Various Technologies, Including Electric Vehicle Chargers," 30-minute conference, IEA PVPS T17 meeting, 24 October 2023 (web conference). Audience: researchers, industrialists, institutions.

- **F. Agha Kassab**, B. Celik, F. Locment, and M. Sechilariu: "Combined Optimal Sizing and Energy Management of a DC Microgrid using MILP," 15-minute conference, IEEE Belgrade PowerTech, 23 June 2023, Belgrade. Audience: researchers, industrialists, institutions, PhD students.

- **F. Agha Kassab**, B. Celik, F. Locment, and M. Sechilariu: "Optimal Sizing and Energy Management of a Microgrid: A Joint MILP Approach for Minimization of Energy Cost and Carbon Emission," 30-minute conference, IEA PVPS T17 meeting, 22 May 2023, Lisboa. Audience: researchers, industrialists, institutions.

- **F. Agha Kassab**, B. Celik, F. Locment, and M. Sechilariu: "Combined Optimal Sizing and Energy Management of a DC Microgrid using MILP," 20-minute presentation, Journée scientifique du GT Micro-réseaux (GDR SEEDS), 16 December 2022, web conference. Audience: researchers, PhD students.

- **F. Agha Kassab**, B. Celik, F. Locment, and M. Sechilariu: "Combined Optimal Sizing and Energy Management of a DC Microgrid using MILP," 15-minute presentation, Conference des Jeunes Chercheurs en Génie Electrique, June 2022, Le Croisic. Audience: researchers, PhD students.

Bibliography

[1] Izhar Us Salam, Muhammad Yousif, Muhammad Numan, and Moatasim Billah. Addressing the challenge of climate change: The role of microgrids in fostering a sustainable future - a comprehensive review. *Renewable Energy Focus*, 48:100538, 2024.

[2] Nicoletta Matera, Domenico Mazzeo, Cristina Baglivo, and Paolo Maria Congedo. Will climate change affect photovoltaic performances? a long-term analysis from 1971 to 2100 in italy. *Energies*, 15(24), 2022.

[3] Rebecca Lindsey. Climate change: Global sea level. *Available online: Climate. gov (accessed on 14 August 2022)*, 2021.

[4] Bojan Škerlak, Michael Sprenger, Stephan Pfahl, Evangelos Tyrlis, and Heini Wernli. Tropopause folds in era-interim: Global climatology and relation to extreme weather events. *Journal of Geophysical Research: Atmospheres*, 120(10):4860–4877, 2015.

[5] NASA. What is climate change?, 2024. Accessed: May 14, 2024.

[6] Nathanael Dougier. *Modélisation systémique pour l'optimisation multi-objectifs de systèmes énergétiques – Application aux micro-réseaux électriques isolés.* Theses, HESAM Université, January 2022.

[7] International Energy Agency. World total energy supply by source, 1971-2019, 2019. Accessed: May 14, 2024.

[8] Saheed Matemilola, Oluwaseun Fadeyi, and Timothy Sijuade. Paris agreement. *Encyclopedia of Sustainable Management; Springer: Cham, Switzerland*, pages 1–5, 2020.

[9] International Energy Agency. Renewables 2023, 2023. Accessed: May 14, 2024.

[10] Eco2mix - CO2 emissions per kwh of electricity generated in France, 2023. Available online at: https://www.rte-france.com/en/eco2mix/co2-emissions.

[11] Jae Woong Shim, Youngho Cho, Seog-Joo Kim, Sang Won Min, and Kyeon Hur. Synergistic control of smes and battery energy storage for enabling dispatchability of renewable energy sources. *IEEE Transactions on Applied Superconductivity*, 23(3):5701205–5701205, 2013.

[12] International Energy Agency. Grid-scale storage, 2024. Accessed: May 14, 2024.

[13] Tesla. Model s. https://www.tesla.com/models. Accessed: 2024-06-17.

[14] Nissan. Leaf. https://www.nissanusa.com/vehicles/electric-cars/leaf.html. Accessed: 2024-06-17.

[15] Chevrolet. Volt. https://www.chevrolet.com/electric/volt-plug-in-hybrid. Accessed: 2024-06-17.

[16] Toyota. Prius prime. https://www.toyota.com/priusprime/. Accessed: 2024-06-17.

[17] Toyota. Prius. https://www.toyota.com/prius/. Accessed: 2024-06-17.

[18] BMW. i3 with range extender. https://www.bmwusa.com/vehicles/bmwi/i3/2021/bmw-i3-range-extender.html. Accessed: 2024-06-17.

[19] Toyota. Mirai. https://www.toyota.com/mirai/. Accessed: 2024-06-17.

[20] Hyundai. Nexo. https://www.hyundaiusa.com/us/en/vehicles/nexo. Accessed: 2024-06-17.

[21] International Energy Agency. Electric vehicles, 2023. Accessed: May 14, 2024.

[22] Intergovernmental Panel on Climate Change. Climate change 2021: Synthesis report, 2021. Accessed: May 14, 2024.

[23] Muhammad Fahad Zia, Elhoussin Elbouchikhi, and Mohamed Benbouzid. Microgrids energy management systems: A critical review on methods, solutions, and prospects. *Applied Energy*, 222:1033–1055, 2018.

[24] Anne Sjoerd Brouwer, Machteld van den Broek, William Zappa, Wim C. Turkenburg, and André Faaij. Least-cost options for integrating intermittent renewables in low-carbon power systems. *Applied Energy*, 161:48–74, 2016.

[25] Ce Shang, Dipti Srinivasan, and Thomas Reindl. Generation-scheduling-coupled battery sizing of stand-alone hybrid power systems. *Energy*, 114:671–682, 2016.

[26] Shivashankar Sukumar, Hazlie Mokhlis, Saad Mekhilef, Kanendra Naidu, and Mazaher Karimi. Mix-mode energy management strategy and battery sizing for economic operation of grid-tied microgrid. *Energy*, 118:1322–1333, 2017.

[27] Manuela Sechilariu and Fabrice Locment. Chapter 1 - connecting and integrating variable renewable electricity in utility grid. In Manuela Sechilariu and Fabrice Locment, editors, *Urban DC Microgrid*, pages 1–33. Butterworth-Heinemann, 2016.

[28] Gokul Sidarth Thirunavukkarasu, Mehdi Seyedmahmoudian, Elmira Jamei, Ben Horan, Saad Mekhilef, and Alex Stojcevski. Role of optimization techniques in microgrid energy management systems—a review. *Energy Strategy Reviews*, 43:100899, 2022.

[29] International Energy Agency. Smart grids, 2024. Accessed: May 14, 2024.

[30] Md. Mustafa Kamal, Imtiaz Ashraf, and Eugen Fernandez. Optimal sizing of standalone rural microgrid for sustainable electrification with renewable energy resources. *Sustainable Cities and Society*, 88:104298, 2023.

[31] Saleh Cheikh-Mohamad, Manuela Sechilariu, and Fabrice Locment. Pv-powered charging station: Energy management and cost optimization. In *2021 IEEE 30th International Symposium on Industrial Electronics (ISIE)*, pages 1–6, 2021.

[32] P.N.D. Premadasa, C.M.M.R.S. Silva, D.P. Chandima, and J.P. Karunadasa. A multi-objective optimization model for sizing an off-grid hybrid energy microgrid with optimal dispatching of a diesel generator. *Journal of Energy Storage*, 68:107621, 2023.

[33] Daniele Groppi, Benedetto Nastasi, Matteo Giacomo Prina, and Davide Astiaso Garcia. The eplanopt model for favignana island's energy transition. *Energy Conversion and Management*, 241:114295, 2021.

[34] Samuel Sarpong Asamoah, Joseph Parbey, Isaac Kwasi Yankey, and Alfred Awuah. Techno-economic assessment of a central grid-connected wind farm in ghana using retscreen® expert. *Heliyon*, 9(1):e12902, 2023.

[35] Abdulhameed Babatunde Owolabi, Benyoh Emmanuel Kigha Nsafon, Jong Wook Roh, Dongjun Suh, and Jeung-Soo Huh. Measurement and verification analysis on the energy performance of a retrofit residential building after energy efficiency measures using retscreen expert. *Alexandria Engineering Journal*, 59(6):4643–4657, 2020.

[36] Abdulhameed Babatunde Owolabi, Benyoh Emmanuel Kigha Nsafon, Jong Wook Roh, Dongjun Suh, and Jeung-Soo Huh. Validating the techno-economic and environmental sustainability of solar pv technology in nigeria using retscreen experts to assess its viability. *Sustainable Energy Technologies and Assessments*, 36:100542, 2019.

[37] M. Zandi, M. Bahrami, S. Eslami, R. Gavagsaz-Ghoachani, A. Payman, M. Phattanasak, B. Nahid-Mobarakeh, and S. Pierfederici. Evaluation and comparison of economic policies to increase distributed generation capacity in the iranian household consumption sector using photovoltaic systems and retscreen software. *Renewable Energy*, 107:215–222, 2017.

[38] Mohammed Okoe Alhassan, Richard Opoku, Felix Uba, George Y. Obeng, Charles K.K. Sekyere, and Peter Nyanor. Techno-economic and environmental estimation assessment of floating solar pv power generation on akosombo dam reservoir in ghana. *Energy Reports*, 10:2740–2755, 2023.

[39] Ausnain Naveed, Sheeraz Iqbal, Saba Munir, Anis ur Rehman, Mahdiyeh Eslami, and Salah Kamel. Renewable energy integration in healthcare systems: A case study of a hospital in azad jammu and kashmir. *IET Renewable Power Generation*, n/a(n/a), 2024.

[40] Chin E. Lin, Bao Chau Phan, and Ying-Chih Lai. Optimal design of hybrid renewable energy system using homer: A case study in the philippines. In *2019 SoutheastCon*, pages 1–6, 2019.

[41] Marwa Mallek, Mohamed Ali Elleuch, Jalel Euchi, and Yacin Jerbi. Optimum design of on-grid pv/wind hybrid system for desalination plant: A case study in sfax, tunisia. *Desalination*, 576:117358, 2024.

[42] S. Conti, R. Nicolosi, S. A. Rizzo, and H. H. Zeineldin. Optimal dispatching of distributed generators and storage systems for mv islanded microgrids. *IEEE Transactions on Power Delivery*, 27(3):1243–1251, 2012.

[43] P. Li and M. Zheng. Multi-objective optimal operation of hybrid ac/dc microgrid considering source-network-load coordination. *J. Mod. Power Syst. Clean Energy*, 7:1229–1240, 2019.

[44] Ali Deihimi, Babak Keshavarz Zahed, and Reza Iravani. An interactive operation management of a micro-grid with multiple distributed generations using multi-objective uniform water cycle algorithm. *Energy*, 106:482–509, 2016.

[45] Amrutha Raju Battula, Sandeep Vuddanti, and Surender Reddy Salkuti. A day ahead demand schedule strategy for optimal operation of microgrid with uncertainty. *Smart Cities*, 6(1):491–509, 2023.

[46] Aliasghar Baziar and Abdollah Kavousi-Fard. Considering uncertainty in the optimal energy management of renewable micro-grids including storage devices. *Renewable Energy*, 59:158–166, 2013.

[47] Mousa Marzband, Ebrahim Yousefnejad, Andreas Sumper, and José Luis Domínguez-García. Real time experimental implementation of optimum energy management system in standalone microgrid by using multi-layer ant colony optimization. *International Journal of Electrical Power & Energy Systems*, 75:265–274, 2016.

[48] Sirus Mohammadi, Soodabeh Soleymani, and Babak Mozafari. Scenario-based stochastic operation management of microgrid including wind, photovoltaic, micro-turbine, fuel cell and energy storage devices. *International Journal of Electrical Power & Energy Systems*, 54:525–535, 2014.

[49] Mehdi Shamshirband, Javad Salehi, and Farhad Samadi Gazijahani. Decentralized trading of plug-in electric vehicle aggregation agents for optimal energy management of smart renewable penetrated microgrids with the aim of co2 emission reduction. *Journal of Cleaner Production*, 200:622–640, 2018.

[50] Kutaiba S. El-Bidairi, Hung Duc Nguyen, S.D.G. Jayasinghe, Thair S. Mahmoud, and Irene Penesis. A hybrid energy management and battery size optimization for standalone microgrids: A case study for flinders island, australia. *Energy Conversion and Management*, 175:192–212, 2018.

[51] Taher Niknam, Faranak Golestaneh, and Ahmadreza Malekpour. Probabilistic energy and operation management of a microgrid containing wind/photovoltaic/fuel cell generation and energy storage devices based on point estimate method and self-adaptive gravitational search algorithm. *Energy*, 43(1):427–437, 2012. 2nd International Meeting on Cleaner Combustion (CM0901-Detailed Chemical Models for Cleaner Combustion).

[52] Hossein Shahinzadeh, Alireza Gheiratmand, S. Hamid Fathi, and Jalal Moradi. Optimal design and management of isolated hybrid renewable energy system (wt/pv/ores). In *2016 21st Conference on Electrical Power Distribution Networks Conference (EPDC)*, pages 208–215, 2016.

[53] Mohamed El-Hendawi, Hossam A. Gabbar, Gaber El-Saady, and El-Nobi A. Ibrahim. Control and ems of a grid-connected microgrid with economical analysis. *Energies*, 11(1), 2018.

[54] Yibao Jiang, Can Wan, Chen Chen, Mohammad Shahidehpour, and Yonghua Song. A hybrid stochastic-interval operation strategy for multi-energy microgrids. *IEEE Transactions on Smart Grid*, 11(1):440–456, 2020.

[55] Ryosuke Hayashi, Hirotaka Takano, Welma Mogiti Nyabuto, Hiroshi Asano, and Tuyen Nguyen-Duc. Bilevel optimization model for sizing of battery energy storage systems in a microgrid considering their economical operation. *Energy Reports*, 9:728–737, 2023. 2022 9th International Conference on Power and Energy Systems Engineering.

[56] Katayoun Rahbar, Jie Xu, and Rui Zhang. Real-time energy storage management for renewable integration in microgrid: An off-line optimization approach. *IEEE Transactions on Smart Grid*, 6(1):124–134, 2015.

[57] Saleh Cheikh-Mohamad, Berk Celik, Manuela Sechilariu, and Fabrice Locment. Pv-powered charging station with energy cost optimization via v2g services. *Applied Sciences*, 13(9), 2023.

[58] Saleh Cheikh-Mohamad, Manuela Sechilariu, and Fabrice Locment. Real-time power management including an optimization problem for pv-powered electric vehicle charging stations. *Applied Sciences*, 12(9), 2022.

[59] Saleh Cheikh-Mohamad, Manuela Sechilariu, and Fabrice Locment. Pv-powered charging station: Energy management with v2g operation and energy cost analysis. In *2022 7th International Conference on Smart and Sustainable Technologies (SpliTech)*, pages 01–06, 2022.

[60] Javier Silvente, Georgios M. Kopanos, Efstratios N. Pistikopoulos, and Antonio Espuña. A rolling horizon optimization framework for the simultaneous energy supply and demand planning in microgrids. *Applied Energy*, 155:485–501, 2015.

[61] Zhou Wu, Henerica Tazvinga, and Xiaohua Xia. Demand side management of photovoltaic-battery hybrid system. *Applied Energy*, 148:294–304, 2015.

[62] Pawel Malysz, Shahin Sirouspour, and Ali Emadi. An optimal energy storage control strategy for grid-connected microgrids. *IEEE Transactions on Smart Grid*, 5(4):1785–1796, 2014.

[63] Wencong Su, Jianhui Wang, and Jaehyung Roh. Stochastic energy scheduling in microgrids with intermittent renewable energy resources. *IEEE Transactions on Smart Grid*, 5(4):1876–1883, 2014.

[64] Yaël Thiaux, Thu Thuy Dang, Louis Schmerber, Bernard Multon, Hamid Ben Ahmed, Seddik Bacha, and Quoc Tuan Tran. Demand-side management strategy in stand-alone hybrid photovoltaic systems with real-time simulation of stochastic electricity consumption behavior. *Applied Energy*, 253:113530, 2019.

[65] Bing Yan, Peter B. Luh, Guy Warner, and Peng Zhang. Operation and design optimization of microgrids with renewables. *IEEE Transactions on Automation Science and Engineering*, 14(2):573–585, 2017.

[66] Mehrdad Ghahramani, Morteza Nazari-Heris, Kazem Zare, and Behnam Mohammadi-Ivatloo. Energy and reserve management of a smart distribution system by incorporating responsive-loads /battery/wind turbines considering uncertain parameters. *Energy*, 183:205–219, 2019.

[67] Nathanael Dougier, Pierre Garambois, Julien Gomand, and Lionel Roucoules. Multi-objective non-weighted optimization to explore new efficient design of electrical microgrids. *Applied Energy*, 304:117758, 2021.

[68] Aakash Hassan, Yasir M. Al-Abdeli, Martin Masek, and Octavian Bass. Optimal sizing and energy scheduling of grid-supplemented solar pv systems with battery storage: Sensitivity of reliability and financial constraints. *Energy*, 238:121780, 2022.

[69] Badis Bacha, Hatem Ghodbane, Habiba Dahmani, Abir Betka, Abida Toumi, and Aissa Chouder. Optimal sizing of a hybrid microgrid system using solar, wind, diesel, and battery energy storage to alleviate energy poverty in a rural area of biskra, algeria. *Journal of Energy Storage*, 84:110651, 2024.

[70] Aymen Chaouachi, Rashad M. Kamel, Ridha Andoulsi, and Ken Nagasaka. Multiobjective intelligent energy management for a microgrid. *IEEE Transactions on Industrial Electronics*, 60(4):1688–1699, 2013.

[71] Yu-Kai Chen, Yung-Chun Wu, Chau-Chung Song, and Yu-Syun Chen. Design and implementation of energy management system with fuzzy control for dc microgrid systems. *IEEE Transactions on Power Electronics*, 28(4):1563–1570, 2013.

[72] Faisal A. Mohamed and Heikki N. Koivo. Multiobjective optimization using modified game theory for online management of microgrid. *European Transactions on Electrical Power*, 21(1):839–854, 2011.

[73] Mosaddek Hossain Kamal Tushar, Adel W. Zeineddine, and Chadi Assi. Demand-side management by regulating charging and discharging of the ev, ess, and utilizing renewable energy. *IEEE Transactions on Industrial Informatics*, 14(1):117–126, 2018.

[74] Chun-Xia Dou and Bin Liu. Multi-agent based hierarchical hybrid control for smart microgrid. *IEEE Transactions on Smart Grid*, 4(2):771–778, 2013.

[75] Jesus Aguila-Leon, Carlos Vargas-Salgado, Cristian Chiñas-Palacios, and Dácil Díaz-Bello. Energy management model for a standalone hybrid microgrid through a particle swarm optimization and artificial neural networks approach. *Energy Conversion and Management*, 267:115920, 2022.

[76] Manuel E. Gamez Urias, Edgar N. Sanchez, and Luis J. Ricalde. Electrical microgrid optimization via a new recurrent neural network. *IEEE Systems Journal*, 9(3):945–953, 2015.

[77] Elizaveta Kuznetsova, Yan-Fu Li, Carlos Ruiz, Enrico Zio, Graham Ault, and Keith Bell. Reinforcement learning for microgrid energy management. *Energy*, 59:133–146, 2013.

[78] Xin Qiu, Tu A. Nguyen, and Mariesa L. Crow. Heterogeneous energy storage optimization for microgrids. *IEEE Transactions on Smart Grid*, 7(3):1453–1461, 2016.

[79] Sunanda Sinha and S.S. Chandel. Review of software tools for hybrid renewable energy systems. *Renewable and Sustainable Energy Reviews*, 32:192–205, 2014.

[80] O. Erdinc and M. Uzunoglu. Optimum design of hybrid renewable energy systems: Overview of different approaches. *Renewable and Sustainable Energy Reviews*, 16(3):1412–1425, 2012.

[81] A. Jamalaiah, Ch. Padmanabha Raju, and R. Srinivasarao. Optimization and operation of a renewable energy based pv-fc-micro grid using homer. In *2017 International Conference on Inventive Communication and Computational Technologies (ICICCT)*, pages 450–455, 2017.

[82] Sayed Jamal al-Din Hosseini, Majid Moazzami, and Hossein Shahinzadeh. Optimal sizing of an isolated hybrid wind/pv/battery system with considering loss of power supply probability. *Majlesi Journal of Electrical Engineering*, 11(3):63–69, 2017.

[83] Hossein Shahinzadeh, Majid Moazzami, S. Hamid Fathi, and Gevork B. Gharehpetian. Optimal sizing and energy management of a grid-connected microgrid using homer software. In *2016 Smart Grids Conference (SGC)*, pages 1–6, 2016.

[84] Divine Khan Ngwashi, Arsene Kafatiya Arnold, Shu Godwill Ndeh, and Emmanuel Tanyi. Optimal design and sizing of a multi-microgrids system: Case study of goma in the democratic republic of the congo. *Scientific African*, 22:e01913, 2023.

[85] Barun K. Das, Mahmudul Hasan, and Fazlur Rashid. Optimal sizing of a grid-independent pv/diesel/pump-hydro hybrid system: A case study in bangladesh. *Sustainable Energy Technologies and Assessments*, 44:100997, 2021.

[86] Abdulla Al Wahedi and Yusuf Bicer. Techno-economic optimization of novel standalone renewables-based electric vehicle charging stations in qatar. *Energy*, 243:123008, 2022.

[87] Phap Vu Minh, Sang Le Quang, and Manh-Hai Pham. Technical economic analysis of photovoltaic-powered electric vehicle charging stations under different solar irradiation conditions in vietnam. *Sustainability*, 13(6), 2021.

[88] Vendoti Suresh, Muralidhar M., and R. Kiranmayi. Modelling and optimization of an off-grid hybrid renewable energy system for electrification in a rural areas. *Energy Reports*, 6:594–604, 2020.

[89] Mohammad Hossein Amrollahi and Seyyed Mohammad Taghi Bathaee. Techno-economic optimization of hybrid photovoltaic/wind generation together with energy storage system in a stand-alone micro-grid subjected to demand response. *Applied Energy*, 202:66–77, 2017.

[90] HOMER. HOMER software, 2024. [Online] Available: https://homerenergy.com/.

[91] Krishnil Ram, Shyamal S. Chand, Ravneel Prasad, Ali Mohammadi, and Maurizio Cirrincione. Microgrids for green hydrogen production for fuel cell buses – a techno-economic analysis for fiji. *Energy Conversion and Management*, 300:117928, 2024.

[92] Ayong Hiendro, Rudi Kurnianto, Managam Rajagukguk, Yohannes M. Simanjuntak, and Junaidi. Techno-economic analysis of photovoltaic/wind hybrid system for on-shore/remote area in indonesia. *Energy*, 59:652–657, 2013.

[93] Rohit Sen and Subhes C. Bhattacharyya. Off-grid electricity generation with renewable energy technologies in india: An application of homer. *Renewable Energy*, 62:388–398, 2014.

[94] Mohan L. Kolhe, K.M. Iromi Udumbara Ranaweera, and A.G.B. Sisara Gunawardana. Techno-economic sizing of off-grid hybrid renewable energy system for rural electrification in sri lanka. *Sustainable Energy Technologies and Assessments*, 11:53–64, 2015.

[95] Muhammad Mudasser, Emmanuel K. Yiridoe, and Kenneth Corscadden. Cost-benefit analysis of grid-connected wind–biogas hybrid energy production, by turbine capacity and site. *Renewable Energy*, 80:573–582, 2015.

[96] National Geographic. GIS (Geographic Information System). [Online] Available: https://education.nationalgeographic.org/resource/geographic-information-system-gis/.

[97] Fethi Khlifi, Habib Cherif, and Jamel Belhadj. Environmental and economic optimization and sizing of a micro-grid with battery storage for an industrial application. *Energies*, 14(18), 2021.

[98] İpek Çetinbaş, Bünyamin Tamyürek, and Mehmet Demirtaş. Sizing optimization and design of an autonomous ac microgrid for commercial loads using harris hawks optimization algorithm. *Energy Conversion and Management*, 245:114562, 2021.

[99] Mansour Alramlawi and Pu Li. Design optimization of a residential pv-battery microgrid with a detailed battery lifetime estimation model. *IEEE Transactions on Industry Applications*, 56(2):2020–2030, 2020.

[100] Iván Jiménez-Vargas, Juan M. Rey, and German Osma-Pinto. Sizing of hybrid microgrids considering life cycle assessment. *Renewable Energy*, 202:554–565, 2023.

[101] Soheil Mohseni, Roomana Khalid, and Alan C. Brent. Stochastic, resilience-oriented optimal sizing of off-grid microgrids considering EV-charging demand response: An efficiency comparison of state-of-the-art metaheuristics. *Applied Energy*, 341:121007, 2023.

[102] Jean-Laurent Duchaud, Gilles Notton, Christophe Darras, and Cyril Voyant. Multi-objective particle swarm optimal sizing of a renewable hybrid power plant with storage. *Renewable Energy*, 131:1156–1167, 2019.

[103] Nasser Yimen, Theodore Tchotang, Abraham Kanmogne, Idriss Abdelkhalikh Idriss, Bashir Musa, Aliyu Aliyu, Eric C. Okonkwo, Sani Isah Abba, Daniel Tata, Lucien Meva'a, Oumarou Hamandjoda, and Mustafa Dagbasi. Optimal sizing and techno-economic analysis of hybrid renewable energy systems—a case study of a photovoltaic/wind/battery/diesel system in fanisau, northern nigeria. *Processes*, 8(11), 2020.

[104] Yongli Wang, Xiaohai Wang, Haiyang Yu, Yujing Huang, Huanran Dong, ChengYuan Qi, and Niyigena Baptiste. Optimal design of integrated energy system considering economics, autonomy and carbon emissions. *Journal of Cleaner Production*, 225:563–578, 2019.

[105] Akbar Maleki, Morteza Gholipour Khajeh, and Mehran Ameri. Optimal sizing of a grid independent hybrid renewable energy system incorporating resource uncertainty, and load uncertainty. *International Journal of Electrical Power & Energy Systems*, 83:514–524, 2016.

[106] Kamal Anoune, Mohsine Bouya, Abdelali Astito, and Abdellatif Ben Abdellah. Sizing methods and optimization techniques for pv-wind based hybrid renewable energy system: A review. *Renewable and Sustainable Energy Reviews*, 93:652–673, 2018.

[107] Masoud Sharafi and Tarek Y. ELMekkawy. Multi-objective optimal design of hybrid renewable energy systems using pso-simulation based approach. *Renewable Energy*, 68:67–79, 2014.

[108] Abba Lawan Bukar, Chee Wei Tan, and Kwan Yiew Lau. Optimal sizing of an autonomous photovoltaic/wind/battery/diesel generator microgrid using grasshopper optimization algorithm. *Solar Energy*, 188:685–696, 2019.

[109] Bineeta Mukhopadhyay and Debapriya Das. Optimal multi-objective long-term sizing of distributed energy resources and hourly power scheduling in a grid-tied microgrid. *Sustainable Energy, Grids and Networks*, 30:100632, 2022.

[110] Afifa Akter, Ehsanul Islam Zafir, Nazia Hasan Dana, Rahul Joysoyal, Subrata K. Sarker, Li Li, S M Muyeen, Sajal K. Das, and Innocent Kamwa. A review on microgrid optimization with meta-heuristic techniques: Scopes, trends and recommendation. *Energy Strategy Reviews*, 51:101298, 2024.

[111] Ahmad Alzahrani, Muhammad Arsalan Hayat, Asif Khan, Ghulam Hafeez, Farrukh Aslam Khan, Muhammad Iftikhar Khan, and Sajjad Ali. Optimum sizing of standalone microgrids: Wind turbine, solar photovoltaic, and energy storage system. *Journal of Energy Storage*, 73:108611, 2023.

[112] Da Huo, Marcos Santos, Ilias Sarantakos, Markus Resch, Neal Wade, and David Greenwood. A reliability-aware chance-constrained battery sizing method for island microgrid. *Energy*, 251:123978, 2022.

[113] Mohammad Rasol Jannesar, Alireza Sedighi, Mehdi Savaghebi, and Josep M. Guerrero. Optimal placement, sizing, and daily charge/discharge of battery energy storage in low voltage distribution network with high photovoltaic penetration. *Applied Energy*, 226:957–966, 2018.

[114] Rodney Kizito, Zeyu Liu, Xueping Li, and Kai Sun. Stochastic optimization of distributed generator location and sizing in an islanded utility microgrid during a large-scale grid disturbance. *Sustainable Energy, Grids and Networks*, 27:100516, 2021.

[115] Agnès François, Robin Roche, Dominique Grondin, and Michel Benne. Assessment of medium and long term scenarios for the electrical autonomy in island territories: The reunion island case study. *Renewable Energy*, 216:119093, 2023.

[116] S. Brisset and M. Ogier. Collaborative and multilevel optimizations of a hybrid railway power substation. *Int. J. Numer. Model. Electron. Netw. Devices Fields*, 32(4), 2019.

[117] Zachary K. Pecenak, Michael Stadler, and Kelsey Fahy. Efficient multi-year economic energy planning in microgrids. *Applied Energy*, 255:113771, 2019.

[118] Zheng Guo, Rui Cheng, Zhaofeng Xu, Pei Liu, Zhe Wang, Zheng Li, Ian Jones, and Yong Sun. A multi-region load dispatch model for the long-term optimum planning of china's electricity sector. *Applied Energy*, 185:556–572, 2017.

[119] Qi Zhang, Benjamin C. Mclellan, Tetsuo Tezuka, and Keiichi N. Ishihara. An integrated model for long-term power generation planning toward future smart electricity systems. *Applied Energy*, 112:1424–1437, 2013.

[120] Alireza Rezvani, Majid Gandomkar, Maziar Izadbakhsh, and Abdollah Ahmadi. Environmental/economic scheduling of a micro-grid with renewable energy resources. *Journal of Cleaner Production*, 87:216–226, 2015.

[121] S. Ashok. Optimised model for community-based hybrid energy system. *Renewable Energy*, 32(7):1155–1164, 2007.

[122] Nima Nikmehr and Sajad Najafi Ravadanegh. Optimal power dispatch of multi-microgrids at future smart distribution grids. *IEEE Transactions on Smart Grid*, 6(4):1648–1657, 2015.

[123] Yiannis A. Katsigiannis, Pavlos S. Georgilakis, and Emmanuel S. Karapidakis. Hybrid simulated annealing–tabu search method for optimal sizing of autonomous power systems with renewables. *IEEE Transactions on Sustainable Energy*, 3(3):330–338, 2012.

[124] Nahar Alshammari and Johnson Asumadu. Optimum unit sizing of hybrid renewable energy system utilizing harmony search, jaya and particle swarm optimization algorithms. *Sustainable Cities and Society*, 60:102255, 2020.

[125] Hai Lan, Shuli Wen, Ying-Yi Hong, David C. Yu, and Lijun Zhang. Optimal sizing of hybrid pv/diesel/battery in ship power system. *Applied Energy*, 158:26–34, 2015.

[126] Abdolvahhab Fetanat and Ehsan Khorasaninejad. Size optimization for hybrid photovoltaic–wind energy system using ant colony optimization for continuous domains based integer programming. *Applied Soft Computing*, 31:196–209, 2015.

[127] André Malheiro, Pedro M. Castro, Ricardo M. Lima, and Ana Estanqueiro. Integrated sizing and scheduling of wind/pv/diesel/battery isolatedsystems. *Renewable Energy*, 83:646–657, 2015.

[128] Thomas Schütz, Xiaolin Hu, Marcus Fuchs, and Dirk Müller. Optimal design of decentralized energy conversion systems for smart microgrids using decomposition methods. *Energy*, 156:250–263, 2018.

[129] Yun Liu, Hoay Beng Gooi, and Huanhai Xin. Distributed energy management for the multi-microgrid system based on admm. In *2017 IEEE Power & Energy Society General Meeting*, pages 1–5, 2017.

[130] Ragheb Rahmaniani, Teodor Gabriel Crainic, Michel Gendreau, and Walter Rei. The benders decomposition algorithm: A literature review. *European Journal of Operational Research*, 259(3):801–817, 2017.

[131] JF Benders. Partitioning procedures for solving mixed-variables programming problems. *Numer. Math.*, 4:238–252, 1962.

[132] A.M. Geoffrion. Generalized benders decomposition. *J. Optim. Theory Appl.*, 10:237–260, 1972.

[133] Ahmed Ibrahim, Octavia A. Dobre, Telex M. N. Ngatched, and Ana Garcia Armada. Bender's decomposition for optimization design problems in communication networks. *IEEE Network*, 34(3):232–239, 2020.

[134] R. Rahmaniani, S. Ahmed, T.G. Crainic, M. Gendreau, and W. Rei. The benders dual decomposition method. *Oper. Res.*, 68(3):878–889, 2020.

[135] Bei Li, Robin Roche, and Abdellatif Miraoui. Microgrid sizing with combined evolutionary algorithm and milp unit commitment. *Applied Energy*, 188:547–562, 2017.

[136] Yang Zhang, Pietro Elia Campana, Anders Lundblad, and Jinyue Yan. Comparative study of hydrogen storage and battery storage in grid connected photovoltaic system: Storage sizing and rule-based operation. *Applied Energy*, 201:397–411, 2017.

[137] M. Bashir and J. Sadeh. Size optimization of new hybrid stand-alone renewable energy system considering a reliability index. In *2012 11th International Conference on Environment and Electrical Engineering*, pages 989–994, 2012.

[138] Gurkan Soykan, Gulfem Er, and Ethem Canakoglu. Optimal sizing of an isolated microgrid with electric vehicles using stochastic programming. *Sustainable Energy, Grids and Networks*, 32:100850, 2022.

[139] Fouad Boutros, Moustapha Doumiati, Jean-Christophe Olivier, Imad Mougharbel, and Hadi Kanaan. New modelling approach for the optimal sizing of an islanded microgrid considering economic and environmental challenges. *Energy Conversion and Management*, 277:116636, 2023.

[140] Apurva Narayan and Kumaraswamy Ponnambalam. Risk-averse stochastic programming approach for microgrid planning under uncertainty. *Renewable Energy*, 101:399–408, 2017.

[141] Sergio Balderrama, Francesco Lombardi, Fabio Riva, Walter Canedo, Emanuela Colombo, and Sylvain Quoilin. A two-stage linear programming optimization framework for isolated hybrid microgrids in a rural context: The case study of the "el espino" community. *Energy*, 188:116073, 2019.

[142] Nicolo' Stevanato, Francesco Lombardi, Emanuela Colmbo, Sergio Balderrama, and Sylvain Quoilin. Two-stage stochastic sizing of a rural micro-grid based on stochastic load generation. In *2019 IEEE Milan PowerTech*, pages 1–6, 2019.

[143] Célia Masternak, Simon Meunier, Stéphane Brisset, and Vincent Reinbold. Microgrid sizing and energy management using benders decomposition algorithm. *Sustainable Energy, Grids and Networks*, 38:101314, 2024.

[144] Yanhong Yang, Wei Pei, Qunhai Huo, Jianjun Sun, and Feng Xu. Coordinated planning method of multiple micro-grids and distribution network with flexible interconnection. *Applied Energy*, 228:2361–2374, 2018.

[145] Adarsh Nagarajan and Raja Ayyanar. Design and scheduling of microgrids using benders decomposition. In *2016 IEEE 43rd Photovoltaic Specialists Conference (PVSC)*, pages 1843–1847, 2016.

[146] Sergio Montoya-Bueno, Jose Ignacio Muñoz-Hernandez, Javier Contreras, and Luis Baringo. A benders' decomposition approach for renewable generation investment in distribution systems. *Energies*, 13(5), 2020.

[147] Tae Hyun Kim, Hansol Shin, Kyuhyeong Kwag, and Wook Kim. A parallel multi-period optimal scheduling algorithm in microgrids with energy storage systems using decomposed inter-temporal constraints. *Energy*, 202:117669, 2020.

[148] Raji Atia and Noboru Yamada. Sizing and analysis of renewable energy and battery systems in residential microgrids. *IEEE Transactions on Smart Grid*, 7(3):1204–1213, 2016.

[149] Minjian Cao, Qingshan Xu, Jilin Cai, and Bin Yand. Optimal sizing strategy for energy storage system considering correlated forecast uncertainties of dispatchable resources. *International Journal of Electrical Power & Energy Systems*, 108:336–346, 2019.

[150] Chiemeka Onyeka Okoye and Oğuz Solyalı. Optimal sizing of stand-alone photovoltaic systems in residential buildings. *Energy*, 126:573–584, 2017.

[151] Homeyra Akter, Harun Or Rashid Howlader, Ahmed Y. Saber, Paras Mandal, Hiroshi Takahashi, and Tomonobu Senjyu. Optimal sizing of hybrid microgrid in a remote island considering advanced direct load control for demand response and low carbon emission. *Energies*, 14(22), 2021.

[152] Hongbo Ren, Qiong Wu, Weijun Gao, and Weisheng Zhou. Optimal operation of a grid-connected hybrid pv/fuel cell/battery energy system for residential applications. *Energy*, 113:702–712, 2016.

[153] Jian Chen, Weitong Zhang, Jiaqi Li, Wen Zhang, Yutian Liu, Bo Zhao, and Yicheng Zhang. Optimal sizing for grid-tied microgrids with consideration of joint optimization of planning and operation. *IEEE Transactions on Sustainable Energy*, 9(1):237–248, 2018.

[154] Tao Ma, Hongxing Yang, Lin Lu, and Jinqing Peng. Pumped storage-based standalone photovoltaic power generation system: Modeling and techno-economic optimization. *Applied Energy*, 137:649–659, 2015.

[155] Ardjouna. Chebabhi, Ilyes. Tegani, Abdelouahab Djoubair. Benhamadouche, and Okba. Kraa. Optimal design and sizing of renewable energies in microgrids based on financial considerations a case study of biskra, algeria. *Energy Conversion and Management*, 291:117270, 2023.

[156] Lidiane Sartini de Oliveira and Sezimária F. P. Saramago. Multiobjective optimization techniques applied to engineering problems. *J. Braz. Soc. Mech. Sci. & Eng.*, 32(1):94–105, March 2010.

[157] Youssef Amry, Elhoussin Elbouchikhi, Franck Le Gall, Mounir Ghogho, and Soumia El Hani. Optimal sizing and energy management strategy for EV workplace charging station considering pv and flywheel energy storage system. *Journal of Energy Storage*, 62:106937, 2023.

[158] Oussama Ouramdane, Elhoussin Elbouchikhi, Yassine Amirat, Franck Le Gall, and Ehsan Sedgh Gooya. Home energy management considering renewable resources, energy storage, and an electric vehicle as a backup. *Energies*, 15(8), 2022.

[159] Shabieh Ul Hassan, Muhammad Yousif, Shahid Nawaz Khan, Syed Ali Abbas Kazmi, and Kashif Imran. A decision-centric approach for techno-economic optimization and environmental assessment of standalone and grid-integrated renewable-powered electric vehicle charging stations under multiple planning horizons. *Energy Conversion and Management*, 294:117571, 2023.

[160] Ying Yang, Weige Zhang, Shaoyuan Wei, and Zhenpo Wang. Optimal sizing of on-board energy storage systems and stationary charging infrastructures for a catenary-free tram. *Energies*, 13(23), 2020.

[161] Soheil Mohseni, Roomana Khalid, and Alan C. Brent. Metaheuristic-based isolated microgrid sizing and uncertainty quantification considering EVs as shiftable loads. *Energy Reports*, 8:11288–11308, 2022.

[162] Mahmoud M. Gamil, Tomonobu Senjyu, Hasan Masrur, Hiroshi Takahashi, and Mohammed Elsayed Lotfy. Controlled V2Gs and battery integration into residential microgrids: Economic and environmental impacts. *Energy Conversion and Management*, 253:115171, 2022.

[163] Seyed Amir Mansouri, Amir Ahmarinejad, Mohammad Sadegh Javadi, and João P.S. Catalão. Two-stage stochastic framework for energy hubs planning considering demand response programs. *Energy*, 206:118124, 2020.

[164] Mohammad Hasan Ghodusinejad, Younes Noorollahi, and Rahim Zahedi. Optimal site selection and sizing of solar EV charge stations. *Journal of Energy Storage*, 56:105904, 2022.

[165] Yongyi Huang, Hasan Masrur, Molla Shahadat Hossain Lipu, Harun Or Rashid Howlader, Mahmoud M. Gamil, Akito Nakadomari, Paras Mandal, and Tomonobu Senjyu. Multi-objective optimization of campus microgrid system considering electric vehicle charging load integrated to power grid. *Sustainable Cities and Society*, 98:104778, 2023.

[166] Manuela Sechilariu and Fabrice Locment. Chapter 6 - experimental evaluation of urban direct current microgrid. In Manuela Sechilariu and Fabrice Locment, editors, *Urban DC Microgrid*, pages 209–250. Butterworth-Heinemann, 2016.

[167] Manuela Sechilariu and Fabrice Locment. Chapter 2 - photovoltaic source modeling and control. In Manuela Sechilariu and Fabrice Locment, editors, *Urban DC Microgrid*, pages 35–91. Butterworth-Heinemann, 2016.

[168] Changjie Yin, Hongwei Wu, Fabrice Locment, and Manuela Sechilariu. Energy management of dc microgrid based on photovoltaic combined with diesel generator and supercapacitor. *Energy Conversion and Management*, 132:14–27, 2017.

[169] Bhanu Babaiahgari, Md Habib Ullah, and Jae-Do Park. Coordinated control and dynamic optimization in dc microgrid systems. *International Journal of Electrical Power & Energy Systems*, 113:832–841, 2019.

[170] Shuoqi Wang, Dongxu Guo, Xuebing Han, Languang Lu, Kai Sun, Weihan Li, Dirk Uwe Sauer, and Minggao Ouyang. Impact of battery degradation models on energy management of a grid-connected dc microgrid. *Energy*, 207:118228, 2020.

[171] Fadi Agha Kassab, Berk Celik, Fabrice Locment, Manuela Sechilariu, and Timothy M. Hansen. Combined optimal sizing and energy management of a dc microgrid using milp. In *2023 IEEE Belgrade PowerTech*, pages 1–6, 2023.

[172] Fatemeh Bagheri, Hanane Dagdougui, and Michel Gendreau. Stochastic optimization and scenario generation for peak load shaving in smart district microgrid: sizing and operation. *Energy and Buildings*, 275:112426, 2022.

[173] Comparateur Electricité / Comparateur Gaz, 2020. Available online at: https://selectra.info/energie.

[174] Les données environnementales et sanitaires de référence pour le bâtiment, 2024. https://www.base-inies.fr/iniesV4/dist/consultation.html.

[175] Batconnect, 2024. https://batconnect.fr/solutions/.

[176] Prix de l'électricité en France 2023 : tarifs, comparatif des offres, 2024. Available online at: https://www.fournisseurs-electricite.com/guides/prix/kwh-electricite/france.

[177] Ming Cheng, Xuan Zhang, Aihua Ran, Guodan Wei, and Hongbin Sun. Optimal dispatch approach for second-life batteries considering degradation with online soh estimation. *Renewable and Sustainable Energy Reviews*, 173:113053, 2023.

[178] Rapports d'activité 2021 de la CRE, 2021. Available online at: https://www.cre.fr/Documents/Publications/Rapports-d-activite/rapport-d-activite-2021.

[179] Larissa Zajicek, Markus Drapalik, Iris Kral, and Wolfgang Liebert. Energy efficiency and environmental impacts of horizontal small wind turbines in austria. *Sustainable Energy Technologies and Assessments*, 59:103411, 2023.

[180] Photovoltaic Geographical Information System - PVGIS, 2023. Available online at: https://re.jrc.ec.europa.eu/pvgtools/en/.

[181] Daniele Colarossi, Eleonora Tagliolini, Alessia Amato, and Paolo Principi. Life cycle assessment and circularity evaluation of a PV panel integrated with phase change material. *Renewable Energy*, 2022.

[182] Vojtech Svoboda, Heinz Wenzl, Rudi Kaiser, Andreas Jossen, Ian Baring-Gould, James Manwell, Per Lundsager, Henrik Bindner, Tom Cronin, Per Nørgård, Alan Ruddell, Adolfo Perujo, Kevin Douglas, Carlos Rodrigues, António Joyce, Stathis Tselepis, Nico van der Borg, Frans Nieuwenhout, Nigel Wilmot, Florence Mattera, and Dirk Uwe Sauer. Operating conditions of batteries in off-grid renewable energy systems. *Solar Energy*, 81(11):1409–1425, 2007.

[183] Atri Bera, Saleh Almasabi, Yuting Tian, Raymond H. Byrne, Babu Chalamala, Tu A. Nguyen, and Joydeep Mitra. Maximising the investment returns of a grid-connected battery considering degradation cost. *IET gener. transm. distrib.*, 14(21):4711–4718, November 2020.

[184] Ya Guo, Su Sheng, Norma Anglani, and Brad Lehman. Optimal Power Management for Grid-Connected Microgrid Considering Modelling of Different Electricity Cost and Battery Degradation Cost. In *2019 20th Workshop on Control and Modeling for Power Electronics (COMPEL)*, pages 1–7, Toronto, ON, Canada, June 2019. IEEE.

[185] Chiara Bordin, Harold Oghenetejiri Anuta, Andrew Crossland, Isabel Lascurain Gutierrez, Chris J. Dent, and Daniele Vigo. A linear programming approach for battery degradation analysis and optimization in offgrid power systems with solar energy integration. *Renewable Energy*, 101:417–430, 2017.

[186] Fadi Agha Kassab, Berk Celik, Fabrice Locment, Manuela Sechilariu, Sheroze Liaquat, and Timothy M. Hansen. Optimal sizing and energy management of a microgrid: A joint MILP approach for minimization of energy cost and carbon emission. *Renewable Energy*, page 120186, 2024.

[187] Will Gorman. The quest to quantify the value of lost load: A critical review of the economics of power outages. *The Electricity Journal*, 35(8):107187, October 2022.

[188] Baseem Khan and Pawan Singh. Selecting a meta-heuristic technique for smart micro-grid optimization problem: A comprehensive analysis. *IEEE Access*, 5:13951–13977, 2017.

[189] Y Xin-She. An introduction with metaheuristic applications. *Engineering Optimization*, 2010.

[190] Dongshu Wang, Dapei Tan, and Lei Liu. Particle swarm optimization algorithm: an overview. *Soft computing*, 22:387–408, 2018.

[191] Jingzhong Fang, Weibo Liu, Linwei Chen, Stanislao Lauria, Alina Miron, and Xiaohui Liu. A survey of algorithms, applications and trends for particle swarm optimization. *International Journal of Network Dynamics and Intelligence*, pages 24–50, 2023.

[192] Sheroze Liaquat, Robert Fourney, Timothy M Hansen, Tanveer Hussain, and Berk Celik. A leader-follower based parallel accelerated particle swarm optimization algorithm for smart grid resource allocation. In *2023 North American Power Symposium (NAPS)*, pages 1–6. IEEE, 2023.

[193] Muhammad Salman Fakhar, Syed Abdul Rahman Kashif, Sheroze Liaquat, Akhtar Rasool, Sanjeevikumar Padmanaban, Muhammad Ahmad Iqbal, Muhammad Anas Baig, and Baseem Khan. Implementation of apso and improved apso on non-cascaded and cascaded short term hydrothermal scheduling. *IEEE Access*, 9:77784–77797, 2021.

[194] Abhishek Shivakumar, Manuel Welsch, Constantinos Taliotis, Dražen Jakšić, Tomislav Baričević, Mark Howells, Sunay Gupta, and Holger Rogner. Valuing blackouts and lost leisure: Estimating electricity interruption costs for households across the european union. *Energy Research & Social Science*, 34:39–48, 2017.

[195] Shifeng Wang, Sicong Wang, and Jinxiang Liu. Life-cycle green-house gas emissions of onshore and offshore wind turbines. *Journal of Cleaner Production*, 210:804–810, 2019.